Sedimentary cycling and benthic fluxes of bio-essential trace metals in low-oxygen marine environments

---

Dissertation

zur Erlangung des Doktorgrades

der Mathematisch-Naturwissenschaftlichen Fakultät der

Christian-Albrechts-Universität zu Kiel

vorgelegt von

Anna Plaß

Kiel, 2021

Erster Gutachter: PD Dr. Florian Scholz

Zweiter Gutachter: Prof. Dr. Eric P. Achterberg

Tag der mündlichen Prüfung: 22.10.2021

Erklärung

Hiermit erkläre ich, dass ich die vorliegende Dissertation mit dem Titel „Sedimentary cycling and benthic fluxes of bio-essential trace metals in low-oxygen marine environments“, abgesehen von der Beratung durch meine Betreuer, nach Inhalt und Form eigenständig erarbeitet habe und keine anderen als die von mir aufgeführten Quellen und Hilfsmittel verwendet wurden. Diese Arbeit ist unter Einhaltung der Regeln guter wissenschaftlicher Praxis der Deutschen Forschungsgemeinschaft entstanden und wurde weder in Auszügen noch in ganzer Form an einer anderen Stelle im Rahmen eines Prüfungsverfahrens eingereicht. Teile dieser Arbeit wurden in Fachzeitschriften veröffentlicht oder zur Veröffentlichung eingereicht und sind entsprechend gekennzeichnet. Mir wurde kein akademischer Grad entzogen.

Kiel, Oktober 2021

Anna Plaß

Abstract

Trace metals are essential micronutrients required for marine life. They are indispensable components of phytoplankton enzymes which catalyse important biological functions. Due to their scarcity in the ocean, trace metals can (co-)limit primary productivity and thus affect the efficiency of the biological pump. Marine sediments are an important source and sink for trace metals to the ocean, especially in low-oxygen environments. However, the key processes and parameters that lead to trace metal release from or to fixation and burial within the sediments are not fully understood for most trace metals and the corresponding fluxes are not well quantified. As the oceans are losing oxygen, oxygen minimum zones serve as a present-day example to study how benthic trace metal cycles will respond to future ocean conditions. In order to investigate environmental controls on benthic trace metal exchange and pathways from or to the sediment, this study combines sediment, pore water, bottom water and benthic flux data. The main study site is the Peruvian margin, where one of the largest and most intense oxygen minimum zones is located. Additional data stems from a seasonally anoxic fjord in the Baltic Sea.

In the first scientific chapter of this thesis, Chapter II, the benthic cycling of the two trace metals iron (Fe) and cadmium (Cd), which have a contrasting sulphide solubility (Fe > Cd), is compared. Hydrogen sulphide concentrations exert an important control on the benthic fluxes of both trace metals at the Peruvian margin. Temporal magnitude changes of diffusive Fe effluxes into near-bottom waters are related to Fe retention via sulphide precipitation in the sediment due to high hydrogen sulphide concentrations. Further, benthic chamber incubation data indicated that Fe accumulation in anoxic near-bottom waters coincided with the depletion of nitrate and nitrite preventing Fe oxidation and subsequent (oxyhydr)oxide precipitation. Cadmium has one of the lowest sulphide solubilities among trace metals. The removal of Cd from near-bottom waters during benthic chamber incubations covaried with hydrogen sulphide concentrations in the surface sediment. This suggest that Cd accumulation in the sediment is mediated by precipitation of cadmium sulphide at the sediment-water interface or within the water column.

Oxygen minimum zone sediments are a source for manganese (Mn) and cobalt (Co) and a sink for nickel (Ni), cupper (Cu), zinc (Zn) and Cd. Chapter III, deals with the different mechanisms and pathways which lead to the enrichment or depletion of

trace metals in sediments at the Peruvian margin. Even though Mn and Co are both depleted in Peru margin sediments, the results of this thesis suggest that their cycling is partly decoupled. At least half of the Mn depletion in shelf sediments can be attributed to benthic diffusive efflux. In contrast, Co dissolution chiefly takes place in the water column as benthic diffusive Co effluxes are much lower compared to the rate of Co loss from the sediments. The majority of Ni accumulation in Peruvian shelf sediments can be explained by direct phytoplankton uptake in the photic zone and delivery with organic matter. For Cu, Zn and Cd however, this transport mechanism is rather of minor importance. Therefore, a covariation in sediments of Cu with particulate organic carbon suggests that the Cu accumulation may be primarily caused by scavenging by downward sinking organic matter. In addition, similar to Cd, the Cu delivery with sulphide minerals precipitated from the water column or near-bottom water likely contributes to the accumulation. The enrichment of Zn is driven by diffusive benthic fluxes from the near-bottom water into the sediment pore water, which matched the excess Zn accumulation. This is likely followed by sulphide precipitation, causing Zn retention in the sediment.

Chapter IV presents a novel device that was developed to sample dissolved and particulate trace metals in the layer of water above the seafloor, the benthic boundary layer. So far this has not been able to conduct with conventional trace metal sampling methods. The new device overcomes the existing limitations. Successful testing demonstrated that it enables simultaneous, uncontaminating and oxygen-free sampling of suspended particles and near-bottom water in high-resolution within the first few meters above the seafloor. The novel device will be an important tool for future studies on dissolved-particulate interactions at the ocean's lower boundary. It will help to solve remaining questions on how benthic trace metal fluxes are modified in this reactive interface layer and on trace metal particle association.

The results of this thesis demonstrate that trace metal behaviour in the ocean is very diverse and future ocean conditions, with declining oxygen and increasing hydrogen sulphide concentrations, may modify benthic trace metal fluxes individually. The differing trace metal fluxes at the seafloor may change trace metal stoichiometry in upwelling water masses and the future ocean, which can impact marine ecosystems in the surface ocean.

Kurzfassung

Spurenmetalle sind essentielle Mikronährstoffe für das Leben im Meer. Sie sind unentbehrliche Komponenten von Phytoplanktonenzymen, welche wichtige biologische Funktionen katalysieren. Aufgrund ihrer Knappheit im Ozean können Spurenmetalle die Primärproduktion (ko-)limitieren und dadurch die Effizienz der biologischen Pumpe beeinflussen. Marine Sedimente sind eine wichtige Quelle und Senke für Spurenmetalle im Ozean, vor allem in sauerstoffarmen Gebieten. Die Schlüsselprozesse und Parameter, welche zur Freisetzung vom oder zum Eintrag und zur Fixierung im Sediment führen, sind jedoch für die meisten Spurenmetalle noch nicht vollständig verstanden. Ebenso sind die entsprechenden Flüsse nicht ausreichend quantifiziert. Da die Ozeane Sauerstoff verlieren, stellen Sauerstoffminimumzonen ein gegenwärtiges Beispiel dar, wie sich zukünftige Bedingungen auf die benthischen Spurenmetallkreisläufe auswirken. Um zu untersuchen wie der Spurenmetallaustausch zwischen dem marinen Sediment und dem Meerwasser von diesen Umweltbedingungen beeinflusst wird, kombiniert diese Arbeit Sediment-, Porenwasser- und Bodenwasserdaten, sowie benthische Flüsse. Das Hauptuntersuchungsgebiet dieser Arbeit ist der Peruanischen Kontinentalrand, wo sich eine der weltweit größten und intensivsten Sauerstoffminimumzonen befindet. Zusätzliche Proben stammen aus einem saisonal anoxischen Fjord in der Ostsee.

Im ersten wissenschaftlichen Kapitel dieser Arbeit, Kapitel II, werden die benthischen Kreisläufe der Spurenmetalle Eisen (Fe) und Kadmium (Cd), welche eine gegensätzliche Sulfidlöslichkeit aufweisen (Fe > Cd), verglichen. Schwefelwasserstoffkonzentrationen steuern wesentlich die benthischen Flüsse beider Spurenmetalle auf dem Peruanischen Schelf. Zeitliche Veränderungen in der Magnitude von diffusen Fe Flüssen aus dem Sediment können auf Fe Zurückhaltung durch die Fällung von Sulfiden bei entsprechend hohen Schwefelwasserstoffkonzentrationen zurückgeführt werden. Des Weiteren weisen Inkubationen mittels benthischer Kammern eine Zunahme von Fe bei gleichzeitiger Abnahme von Nitrat und Nitrit im Bodenwasser auf, wodurch eine Fe-Oxidation und folgende Ausfällung von Fe-Hydroxid(oxid) verhindert wird. Kadmium hat eine der geringsten Sulfidlöslichkeiten unter den Spurenmetallen. Die Abnahme von Cd im bodennahen Wasser während Inkubationen mittels benthischer Kammern auf dem Peruanischen Schelf kovariierte mit Schwefelwasserstoffkonzentrationen im

Oberflächensediment. Dies deutet darauf hin, dass die Anreicherung von Cd im Sediment mittels Sulfidfällung an der Sediment-Wasser-Grenzschicht oder auch in der Wassersäule herbeigeführt wird.

Sedimente in Sauerstoffminimumzonen sind eine Quelle für Mangan (Mn) und Kobalt (Co) und eine Senke für Nickel (Ni), Kupfer (Cu), Zink (Zn) und Cd. Kapitel III beschäftigt sich mit den unterschiedlichen (Transport-)Mechanismen, welche zur An- oder Abreicherung von Spurenmetallen in Sedimenten am Peruanischen Kontinentalrand führen. Obwohl Mn und Co beide in den Sedimenten abgereichert sind, deuten die Ergebnisse dieser Arbeit darauf hin, dass ihre Kreisläufe teilweise entkoppelt sind. Mindestens die Hälfte der Abreicherung von Mn kann auf den diffusiven Fluss aus dem Sediment zurückgeführt werden. Im Gegensatz dazu findet die Lösung von Co größtenteils bereits in der Wassersäule statt, da die diffusive Freisetzung von Co aus dem Sediment wesentlich geringer als dessen Abreicherung ist. Ein Großteil der sedimentären Anreicherung von Ni in Peruanischen Schelfsedimenten kann auf die direkte Aufnahme von Phytoplankton in der photischen Zone und den Eintrag mittels organischer Materie zum Sediment erklärt werden. Hingegen spielt dieser Transportmechanismus für Cu, Zn und Cd eher eine geringe Rolle. Eine Kovariation von Cu und partikulärem organischen Kohlenstoff weist daher auf eine Anreicherung von Cu hauptsächlich mittels Bindung an absinkendes organisches Material hin. Zusätzlich, ähnlich wie Cd, kann Sulfidfällung im Bodenwasser oder in der Wassersäule zur Anreicherung von Cu beitragen. Die Anreicherung von Zn wird durch den diffusiven benthischen Fluss vom Bodenwasser ins Sedimentporenwasser gesteuert, welcher mit der Anreicherung von Zn übereinstimmt. Die anschließende Fixierung von Zn im Sediment ist höchstwahrscheinlich auf Sulfidfällung zurückzuführen.

Kapitel IV stellt ein neuentwickeltes Gerät zur Beprobung von gelösten und partikulären Spurenmetallen in der Wasserschicht oberhalb des Meeresbodens, der benthischen Grenzschicht, vor. Bisher konnte dies nicht mittels konventioneller Methoden zur Spurenmetallbeprobung durchgeführt werden. Das neue Beprobungsgerät überwindet die bestehenden Einschränkungen. Erfolgreiche Tests beweisen, dass eine gleichzeitige, spurenmetallreine und sauerstofffreie Beprobung von suspendierten Partikeln und Bodenwasser in hoher Auflösung in den ersten Metern oberhalb des Meeresbodens ermöglicht wird. Dieses neuartige Gerät wird ein

wichtiges Werkzeug für zukünftige Studien über Wechselwirkungen zwischen gelösten und partikulären Spurenmetallen an der unteren Grenze des Meeresbodens sein. Noch bestehende Fragen, wie Flüsse von Spurenmetallen in dieser reaktiven Grenzschicht modifiziert werden und auch in welcher Art partikuläre Spurenmetalle vorhanden sind, können hiermit geklärt werden.

Die Ergebnisse dieser Arbeit zeigen ein sehr diverses Verhalten der unterschiedlichen Spurenmetalle auf. Zukünftige Bedingungen in den Ozeanen, mit geringeren Sauerstoff- und höheren Schwefelwasserstoffkonzentrationen, können benthische Spurenmetallflüsse individuell verändern. Dies hat zur Folge, dass die unterschiedlichen Spurenmetallflüsse am Meeresboden die Stöchiometrie von Spurenmetallen in Auftriebswassermassen und im Ozean verändern können, was sich wiederum auf marine Ökosysteme im Oberflächenozean auswirken kann.

Contents

I. General introduction

I.1 Oxygen minimum zones

Oxygen minimum zones (OMZs) are oceanic regions with layers of water where oxygen concentrations are low or virtually zero. Oxygen minimum zones can be found throughout the world's oceans, typically in eastern boundary upwelling systems e.g. in the eastern Pacific and Atlantic Ocean but also in the northern Indian Ocean. Oxygen minimum zones develop through a coupling of biogeochemical and physical processes. Ekman-driven boundary upwelling supplies nutrient-rich subsurface waters to the euphotic zone, which fuels primary productivity and thus leads to high oxygen consumption through the respiration of organic matter. In addition the supply with oxygen is limited by weak ocean ventilation (Helly and Levin, 2004; Pennington et al., 2006; Karstensen et al., 2008; Paulmier and Ruiz-Pino, 2009; Brandt et al., 2015). Not only in open marine upwelling systems, also in continental seas as the Black Sea and the Baltic Sea anoxic conditions prevail, which is closely linked to stratification and eutrophication (Diaz and Rosenberg, 2008; Breitburg et al., 2018). Figure I.1 displays the dissolved oxygen concentrations of the world's oceans. Especially a large area off the western coast of North and South America is depleted in oxygen, where concentrations are below 20 µmol kg^{-1}. In particular in the eastern tropical South Pacific off the coast of Peru one of the most intense and dynamic OMZs prevails, which is the main study area of this thesis.

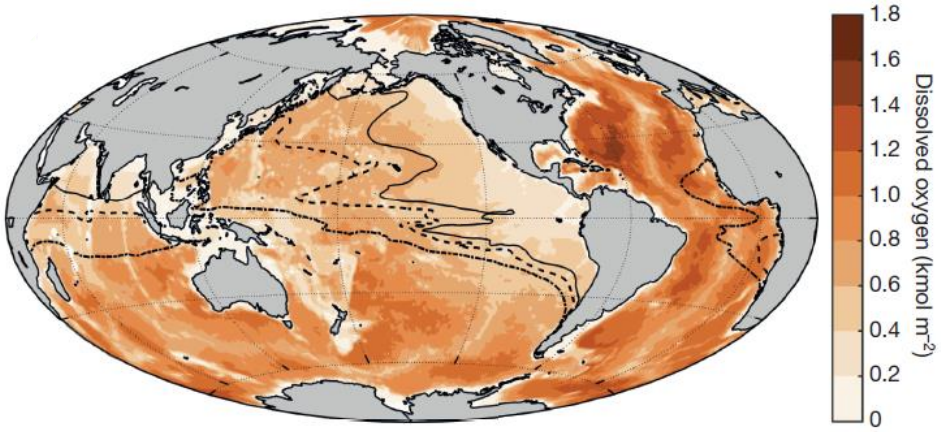

Figure I.1: Global oxygen inventory (dissolved oxygen, colour coded). Lines indicate boundaries of oxygen-minimum zones (OMZs): dashed-dotted, regions with less than 80 µ mol kg^{-1} oxygen anywhere within the water column; dashed lines and solid lines similarly represent regions with less than 40 µ mol kg^{-1} oxygen and 20 µ mol kg^{-1} oxygen, respectively. (Schmidtko et al., 2017)

Off Peru equatorward winds favour coastal upwelling throughout the year. The main source water for the upwelling is the southward subsurface flowing Peru-Chile Undercurrent, which is rich in nutrients and low in oxygen (Pizarro, 2002; Penven, 2005). The supply of this nutrient-rich water to the euphotic zone leads to the formation of one of the most productive regions worldwide (Pennington et al., 2006). The intensity of phytoplankton blooms follows a seasonality and reaches its maximum in austral summer (Echevin et al., 2008). The OMZ with complete oxygen depletion typically extends between 100 and 400 m water depth. Within the OMZ microbial processes as denitrification (the reduction of nitrate via nitrite and finally to nitrogen gas) and anaerobic ammonium oxidation (where nitrogen gas is produced from ammonia and nitrite) take place (Karstensen et al., 2008; Lam et al., 2009; Thamdrup et al., 2012; Dalsgaard et al., 2012). However, the Peruvian system is very dynamic and can show strong temporal changes of biogeochemical water column conditions. During (coastal) El Niño events, the Peruvian shelf can become oxygenated (Levin et al., 2002a; Gutiérrez et al., 2008). In contrast, during phases of stagnation (or supported by La Niña events), when quantitative chemolithoautotrophic hydrogen sulphide oxidation is inhibited due to nitrate and nitrite depletion, hydrogen sulphide produced in the sediments by sulphide-reducing bacteria can accumulate in the water column (Schunck et al., 2013; Ohde, 2018).

El Niño and La Niña events, which impact temperature, salinity and oxygen in surface waters off Peru, are phases of El Niño Southern Oscillation, a coupled ocean-atmosphere system. During the neutral phase trade winds pile up warm surface water in the western Pacific and favour the upwelling of cold water in the eastern Pacific. La Niña is an intensification of the neutral phase with unusual cold sea surface temperatures in the eastern Pacific and often follows El Niño events. El Niño events develop due to weak trade winds and are marked by unusual warm sea surface temperatures in the eastern Pacific and heavy rainfall. At the same time the thermocline deepens and the upwelling of cold and nutrient-rich water is reduced. The periodic oscillations of warm and cold phases occur every 2 to 7 years (McPhaden et al., 2006; Stramma et al., 2016; Echevin et al., 2018; Peng et al., 2019).

Throughout the past decades the world’s oceans have lost around 2 % of their oxygen and OMZs have been expanding (Stramma et al., 2008; Stramma et al., 2010; Helm et al., 2011; Schmidtko et al., 2017). As a consequence of climate change,

modelling scenarios predict a continuation of ocean deoxygenation and an expansion of OMZs, which is driven by the following factors. First, ocean warming reduces the oxygen solubility. Second, increased stratification decreases ventilation and oxygen supply. And third, a potentially increased productivity, due to higher carbon dioxide concentrations, could result in higher oxygen consumption through respiration of organic matter (Bopp et al., 2002; Oschlies et al., 2008; Keeling et al., 2010). Considering this development, it is important to evaluate the impacts that will be caused by the environmental changes. Ocean anoxia threatens planktonic and benthic organisms, of which many are not tolerant to low-oxygen conditions. Further hydrogen sulphide is toxic for most multicellular organisms and the release into the water column leads to the mortality of these organisms, including fish. (Torrans and Clemens, 1982; Bagarinao, 1992; Hamukuaya et al., 1998; Diaz and Rosenberg, 2008; Levin et al., 2009). Oxygen does not only play a key role for marine ecosystems and major nutrient cycles (e.g. Bopp et al., 2002; Thamdrup et al., 2012), it is also an important parameter which controls the cycling of trace metals (TMs) (Sundby et al., 1986; Morford and Emerson, 1999; Tribovillard et al., 2006; Scholz et al., 2011; Rigaud et al., 2013; Homoky et al., 2016; Rapp et al., 2020).

I.2 Trace metal requirements of marine phytoplankton

Primary production is crucial for the uptake of carbon dioxide and almost half of the global net primary production takes place in the ocean. When phytoplankton takes up carbon dioxide and produces organic matter in the surface ocean, it can be either released through the respiration of this organic matter or exported to the seafloor and buried within the sediments, which is called the biological pump (Falkowski, 1998; Field, 1998; Geider et al., 2001). Besides the major elements and nutrients carbon, nitrogen and phosphorus, TMs are essential micronutrients required by marine phytoplankton. The TMs iron (Fe), manganese (Mn), cobalt (Co), nickel (Ni), cupper (Cu), zinc (Zn) and cadmium (Cd) are essential components of many phytoplankton enzymes that catalyse different important biological functions visualised in Figure I.2. Iron, Mn and Cu are required for photosynthesis, Co, Zn and Cd for carbon acquisition, Fe, Ni and Cu for nitrogen acquisition and Fe and Zn for phosphorous acquisition. Furthermore, Co is required for the biosynthesis of vitamin B12 (Morel and Price, 2003;

Morel et al., 2014; Lohan and Tagliabue, 2018). Following the Redfiled ratio (C_{120}:N_{16}:P_1) an extended ratio for TMs in phytoplankton is approximately $(C_{124})_{1000}$:$Fe_{7.5}$:Mn:$_{2.8}$:$Zn_{0.8}$:$Cu_{0.38}$:$Co_{0.29}$:$Cd_{0.21}$. However, this ratio is variable, dependent on differing nutrient requirements of different organisms and the nutrient availability (Ho et al., 2003; Moore et al., 2013).

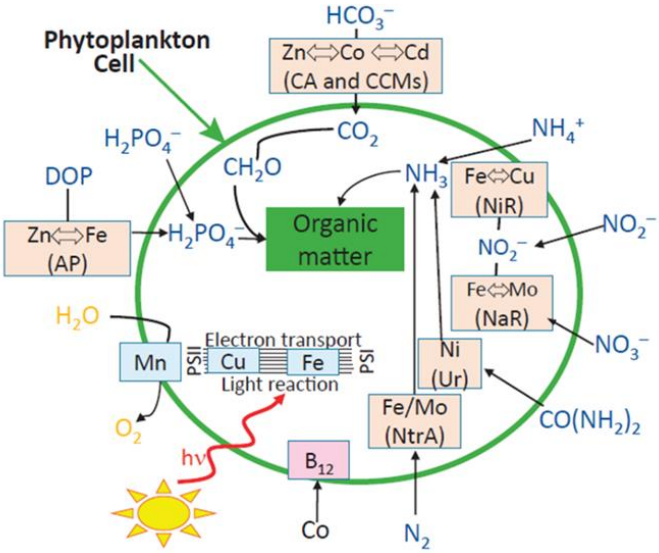

Figure I.2: A model phytoplankton cell (green circle) showing the uptake of carbon, nitrogen and phosphorus (blue) from seawater and the subsequent conversion of that carbon into organic matter. The uptake requires enzymes (orange boxes) which have essential trace-metal requirements (black). For photosynthesis, phytoplankton cells require manganese (Mn) to split water (H_2O) to produce oxygen (O_2) in photosystem II (PSII). Copper (Cu) and iron (Fe) are also essential for photosynthesis. Vitamins, such as B12 (purple box), require cobalt (Co). Abbreviations in alphabetical order: AP = alkaline phosphatase; CA = carbonic anhydrase; CCMs = carbon concentrating mechanisms; DOP = dissolved organic phosphorus; NaR = nitrate reductase; NiR = nitrite reductase; NtrA = nitrogenase; PSI = photosystem I; PSII = photosystem II; Ur = urease. (Lohan and Tagliabue, 2018)

Unlike their abundance in the continental crust, TM concentrations in the ocean are as low as nanomole or picomole per litre and the scarcity of TMs can (co-)limit marine primary production. Figure I.3 compares the intracellular phytoplankton and dissolved seawater stoichiometry of TMs normalised to carbon. It displays that the ratios of TMs in phytoplankton are lower than or close to the seawater ratio, indicating that all of the TMs Fe, Mn, Co, Ni, Cu, Zn and Cd can potentially limit phytoplankton growth. Experimental and in-situ nutrient addition studies demonstrate that in around 30 % of the surface ocean, phytoplankton growth is limited by Fe availability, especially

at high latitudes. In some regions Fe limitation is also accompanied by a co-limitation of Co (Moore et al., 2013 and references therein; Morel et al., 2014).

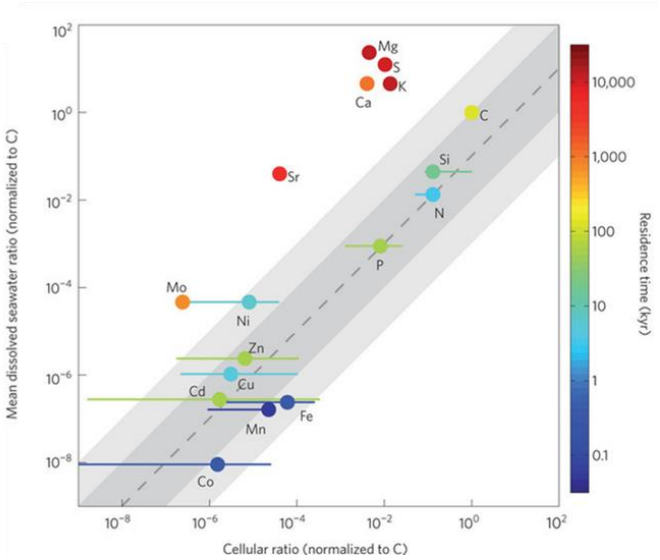

Figure I.3: Comparisons between intracellular and dissolved seawater elemental stoichiometry. Representative (circle) and observed range (bar) of elemental ratios in oceanic phytoplankton normalized to carbon (nutrient:C quotas), plotted against mean dissolved seawater ratios. Colours indicate oceanic residence times. Dark and light grey regions indicate <10-fold and <100-fold excesses and deficiencies relative to nitrogen, which is limiting over much of the ocean. Elements to the top left of the shaded area are thus in great excess in sea water, and biological processing has little influence on their distribution, whereas some of those in the shaded regions have the potential to become limiting. (Moore et al., 2013)

I.3 Trace metal fluxes and cycling in marine sediments

In general, the sources of TMs to the ocean are known. These are supply from continents by rivers, atmospheric dust, ice bergs, hydrothermalism or release from marine sediments (Fig. I.4, summarised by Scor Working Group, 2007; Homoky et al., 2016). More recently, the TM supply to the ocean from marine sediments, especially under low oxygen conditions, have become an important area of research. Several studies documented high concentrations of Fe, Mn and Co in oxygen depleted water columns and ascribed this to a sedimentary release of these TMs (Saito et al., 2004; Noble et al., 2012; Rapp et al., 2019a). Indeed, diffusive fluxes from the sediments into the water column are common for these TMs under low oxygen conditions (Heggie and Lewis, 1984; Sundby et al., 1986; Pakhomova et al., 2007; Scholz et al., 2011; Noffke et al., 2012; van de Velde et al., 2020). On the other side, TM enrichments of Ni, Cu,

Zn and Cd in OMZ sediments, compared to the lithogenic background sedimentation, demonstrate that TMs are being removed from the water column and transferred to the sediments in oxygen-depleted settings (Borchers et al., 2005; Böning et al., 2009; Little et al., 2015). Possible removal pathways for TMs from the ocean are diffusive fluxes, which depend on the concentration gradient between the water column and the sediment pore water. Furthermore, particulate input via scavenging by sinking organic or inorganic matter, mineral precipitation or direct uptake of TMs by phytoplankton in the photic zone and deposition via organic detritus can contribute to TM accumulation in marine sediments (Fig. I.4).

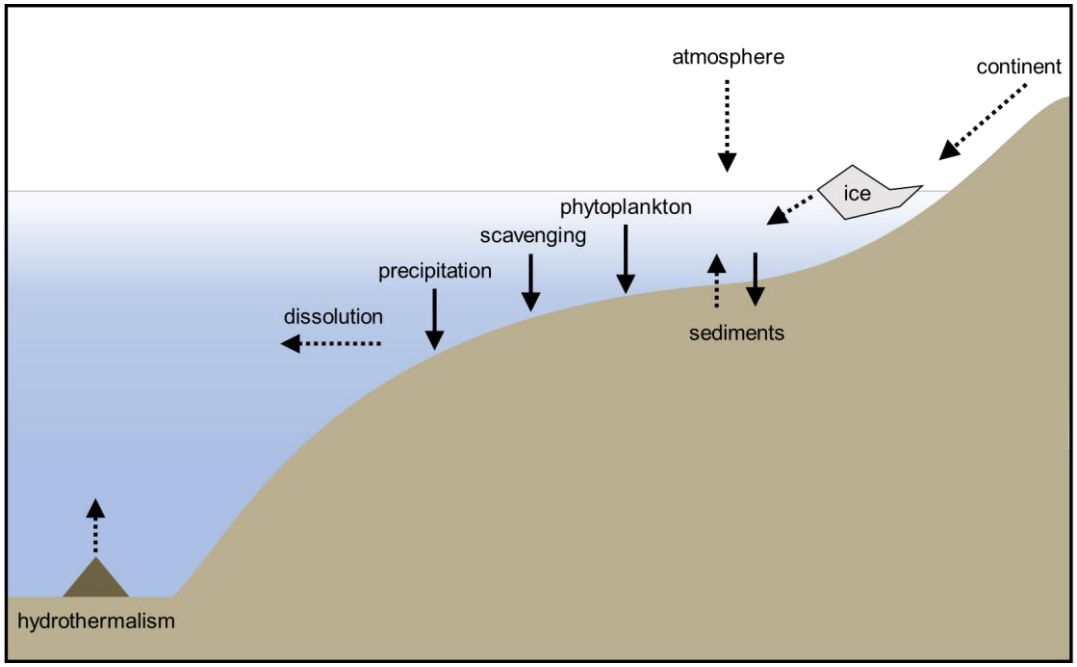

Figure I.4: Sources and sinks of trace metals in the ocean. Sources of trace metals to the water column are displayed by dashed arrows. Sink mechanisms and trace metal removal from the water column and deposition in the sediments are displayed by solid arrows.

Benthic fluxes and TM cycling in marine sediments are dependent on a range of (redox) reactions that can take place during early diagenesis. Within the sediments catabolic processes, the microbial respiration of organic matter, follows a sequence involving different electron acceptors, called the early diagenetic sequence. The consumption of the different electron acceptors or respiratory process follows the order of decreasing energy yield that is: aerobic respiration, nitrate reduction, Mn reduction,

Fe reduction, sulphate reduction and methanogenesis (Fig. I.5) (Froelich et al., 1979; Canfield and Thamdrup, 2009). The important diagenetic reactions that lead either to TM release or TM fixation within the sediments are summarised in Table I.1.

Table I.1: Important diagenetic reactions involving trace metals (TM). OM stands for organic matter. TM-FeS, TM-FeS_2, TM-$Fe(OH)_3$, TM-MnO_2, TM-CO_3 and TM-OM represent trace elements association on particulate phases by adsorption or coprecipitation without specifying the nature. (modified after Rigaud et al. (2013))

Description	**Reaction**
Primary redox reactions	
MnO_2 reduction	$OM + 2\ MnO_2 + CO_2 + H_2O \rightarrow 2\ Mn^{2+} + HCO_3^- + NH_4^+ HPO^{2-}$
$Fe(OH)_3$ reduction	$OM + 4\ Fe(OH)_3 + CH_2O + 8\ H^+ \rightarrow 4\ Fe^{2+} + 11\ H_2O + CO_2$
Secondary redox and precipitation reactions	
Mn oxidation by O_2	$Mn^{2+} + ½\ O_2 + 2\ HCO_3^- \rightarrow MnO_2 + 2\ CO_2 + H_2O$
Fe oxidation by O_2	$Fe^{2+} + ¼\ O_2 + 2\ HCO_3^- + ½\ H_2O \rightarrow Fe(OH)_3 + 2\ CO_2$
Fe oxidation by NO_3^-	$2\ Fe^{2+} + NO_3^- + 5\ H_2O \rightarrow 2\ Fe(OH)_3 + NO_2^- + 4\ H^+$
Fe oxidation by NO_2^-	$6\ Fe^{2+} + 2\ NO_2^- + 14\ H_2O \rightarrow 6\ Fe(OH)_3 + N_2 + 10\ H^+$
FeS precipitation	$Fe^{2+} + 2\ HCO_3^- + H_2S \rightarrow FeS + 2\ CO_2 + 2\ H_2O$
Pyrite precipitation	$FeS + H_2S \rightarrow FeS_2 + H_2$
Reactions involving trace metals (TM)	
TM sulphide precipitation	$TM^{2+} + H_2S \rightarrow TMS + 2\ H^+$
TM adsorption/coprecipitation on FeS/ FeS_2	$TM^{2+} + FeS \rightarrow$ TM-FeS or $TM^{2+} + FeS_2 \rightarrow$ TM-FeS_2
TM adsorption/coprecipitation on $Fe(OH)_3$	$TM^{2+} + Fe(OH)_3 \rightarrow$ TM-$Fe(OH)_3$
TM adsorption/coprecipitation on MnO_2	$TM^{2+} + MnO_2 \rightarrow$ TM-MnO_2
TM adsorption/coprecipitation on CO_3	$TM^{2+} + CO_3 \rightarrow$ TM-CO_3
adsorption on organic matter (OM)	$TM^{2+} + OM \rightarrow$ TM-OM

When Mn and Fe are released into the sediment pore water through microbial reduction, they can be (re)oxidised with oxygen, nitrate or nitrite, either in the sediment or after diffusion into the bottom water, depending on the prevailing redox conditions (Scholz et al., 2016; Heller et al., 2017). Iron- and Mn-oxide minerals can also incorporate other trace metals in particular Co and Ni, but also Cu, Zn and Cd. Conversely the reductive dissolution of these oxides leads to the release of the incorporated TMs (Finney et al., 1984; Shaw et al., 1990; Fernex et al., 1992; Tankéré et al., 2001; Audry et al., 2006; Peacock and Sherman, 2007; Olson et al., 2017). Furthermore the respiration of organic matter itself mobilises TMs which were incorporated into or scavenged by organic detritus, but dissolved TMs can also re(associate) with organic matter within the sediment (Audry et al., 2006; Rigaud et al., 2013). When hydrogen sulphide is present some TMs form mono-sulphides (TMS) while others are incorporated into pyrite (FeS_2) (Morse and Luther, 1999). Furthermore, TMs can be incorporated into or adsorbed onto carbonates precipitated in the water column or sediment (Middelburg et al., 1987; Kuleshov, 2017).

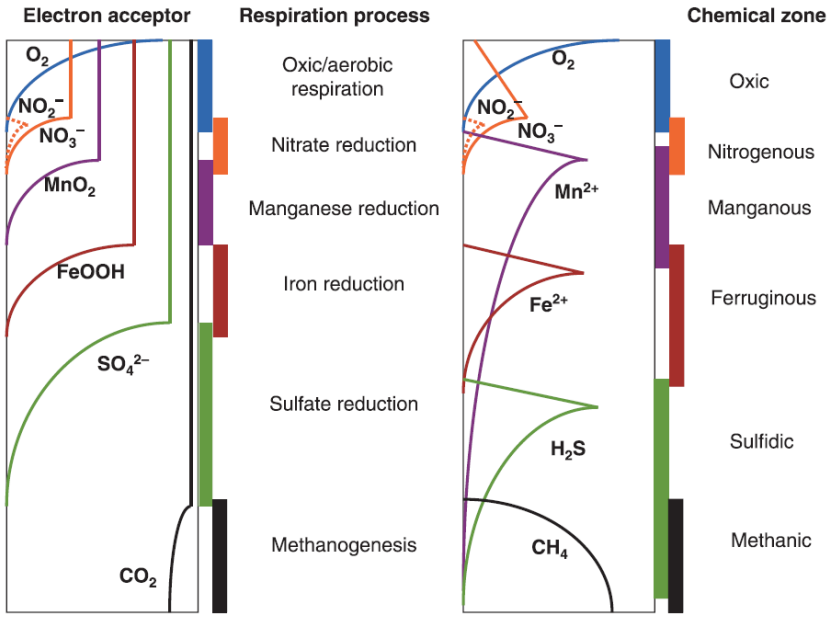

Figure I.5: On the left, a cartoon representing the depth distribution of common electron acceptors in the environment and the names used to represent the zones where these different electron acceptors are used. This is an abstraction of the real system and not necessarily an accurate representation of how these profiles would look in nature. On the right, a cartoon reflecting the chemical zonations, which typically accompany the respiration processes on the left. Note that there is considerable overlap between some of these chemical zones and that they do not necessarily reflect the depth distribution of the accompanying respiration process. (Canfield and Thamdrup, 2009)

I.4 Thesis objective and scientific key questions

The focus of this thesis lays on TM exchange processes between marine sediments and the bottom water/water column in low-oxygen environments. Due to ongoing ocean deoxygenation TM cycling in oxygen minimum zones serves as a present-day example for future ocean conditions. It is well known that sediments underlaying OMZs present a source for some TMs and a sink for others. However, the controlling processes, parameters and the location of sink and source mechanisms is poorly constrained for most TMs. Furthermore, a precise quantification of benthic TM fluxes is still missing. Therefore, the scientific key questions and goals of this thesis are:

1. Which are the important parameters and mechanisms involved in benthic TM cycling and under which environmental conditions do marine sediments represent either a source or a sink for TMs to the ocean?

2. A better quantification of TM fluxes associated with different pathways from or to the sediments.

3. How do sedimentary TM cycling and fluxes respond to ocean deoxygenation?

To gain an integrated picture of TM cycling under low-oxygen conditions, sediment, pore water and bottom water data, benthic fluxes, biological processes and oceanographic transport are considered in this thesis. The results of this thesis contribute to a better quantification of TM source and sink fluxes at the seafloor, which help reduce the existing uncertainties in oceanic TM mass balances. Further the results of this thesis can be used to refine the parameterisation of TM fluxes in global biogeochemical models and to improve the applicability of TMs as paleo-proxies for redox-conditions and biogeochemical cycling in the geological past.

This thesis consists of three stand-alone articles. Chapter II focuses on how hydrogen sulphide concentrations regulate benthic Fe and Cd fluxes in the OMZ off Peru. Chapter III deals with the different pathways of the TMs Mn, Co, Ni, Cu, Zn and Cd from or to the sediment in the Peruvian OMZ. Chapter IV introduces a novel method to sample dissolved and particulate TMs at the benthic boundary. Chapter II and Chapter III have been published in peer-reviewed scientific journals and Chapter IV was submitted to a peer-reviewed scientific journal. A summary of the main findings of the three individual chapters and an outlook is provided in Chapter V.

References

Audry S., Blanc G., Schäfer J., Chaillou G. and Robert S. (2006) Early diagenesis of trace metals (Cd, Cu, Co, Ni, U, Mo, and V) in the freshwater reaches of a macrotidal estuary. *Geochim. Cosmochim. Acta* **70**, 2264–2282. Available at: https://linkinghub.elsevier.com/retrieve/pii/S0016703706000718.

Bagarinao T. (1992) Sulfide as an environmental factor and toxicant: tolerance and adaptations in aquatic organisms. *Aquat. Toxicol.* **24**, 21–62. Available at: https://pdf.sciencedirectassets.com/271226/1-s2.0-S0166445X00X01397/1-s2.0-0166445X9290015F/main.pdf?x-amz-security-token=AgoJb3JpZ2luX2VjEAMaCXVzLWVhc3QtMSJHMEUCIQCYQuZVcR1FHzysAZIifXX3W08Nb3RtxZxvQM230hXqxgIgSkDtwodeaUtQDINwwPGCH2cMiSkqNOzt8SmAa%2F%2BX9.

Böning P., Brumsack H.-J., Schnetger B. and Grunwald M. (2009) Trace element signatures of Chilean upwelling sediments at ~36°S. *Mar. Geol.* **259**, 112–121. Available at: http://dx.doi.org/10.1016/j.margeo.2009.01.004.

Bopp L., Le Quéré C., Heimann M., Manning A. C. and Monfray P. (2002) Climate-induced oceanic oxygen fluxes: Implications for the contemporary carbon budget. *Global Biogeochem. Cycles* **16**, 6-1-6–13. Available at: http://doi.wiley.com/10.1029/2001GB001445.

Borchers S. L., Schnetger B., Böning P. and Brumsack H.-J. (2005) Geochemical signatures of the Namibian diatom belt: Perennial upwelling and intermittent anoxia. *Geochemistry, Geophys. Geosystems* **6**. Available at: http://doi.wiley.com/10.1029/2004GC000886.

Brandt P., Bange H. W., Banyte D., Dengler M., Didwischus S.-H., Fischer T., Greatbatch R. J., Hahn J., Kanzow T., Karstensen J., Körtzinger A., Krahmann G., Schmidtko S., Stramma L., Tanhua T. and Visbeck M. (2015) On the role of circulation and mixing in the ventilation of oxygen minimum zones with a focus on the eastern tropical North Atlantic. *Biogeosciences* **12**, 489–512. Available at: https://bg.copernicus.org/articles/12/489/2015/.

Breitburg D., Levin L. A., Oschlies A., Grégoire M., Chavez F. P., Conley D. J., Garçon V., Gilbert D., Gutiérrez D., Isensee K., Jacinto G. S., Limburg K. E., Montes I., Naqvi S. W. A., Pitcher G. C., Rabalais N. N., Roman M. R., Rose K.

A., Seibel B. A., Telszewski M., Yasuhara M. and Zhang J. (2018) Declining oxygen in the global ocean and coastal waters. *Science (80-.).* **359**, eaam7240. Available at: http://www.sciencemag.org/lookup/doi/10.1126/science.aam7240.

Canfield D. E. and Thamdrup B. (2009) Towards a consistent classification scheme for geochemical environments, or, why we wish the term 'suboxic' would go away. *Geobiology* **7**, 385–392. Available at: http://doi.wiley.com/10.1111/j.1472-4669.2009.00214.x.

Dalsgaard T., Thamdrup B., Farías L. and Revsbech N. P. (2012) Anammox and denitrification in the oxygen minimum zone of the eastern South Pacific. *Limnol. Oceanogr.* **57**, 1331–1346. Available at: http://doi.wiley.com/10.4319/lo.2012.57.5.1331.

Diaz R. J. and Rosenberg R. (2008) Spreading Dead Zones and Consequences for Marine Ecosystems. *Science (80-.).* **321**, 926–929. Available at: https://www.sciencemag.org/lookup/doi/10.1126/science.1156401.

Echevin V., Aumont O., Ledesma J. and Flores G. (2008) The seasonal cycle of surface chlorophyll in the Peruvian upwelling system: A modelling study. *Prog. Oceanogr.* **79**, 167–176. Available at: http://dx.doi.org/10.1016/j.pocean.2008.10.026.

Echevin V., Colas F., Espinoza-Morriberon D., Vasquez L., Anculle T. and Gutierrez D. (2018) Forcings and Evolution of the 2017 Coastal El Niño Off Northern Peru and Ecuador. *Front. Mar. Sci.* **5**, 1–16. Available at: https://www.frontiersin.org/article/10.3389/fmars.2018.00367/full.

Falkowski P. G. (1998) Biogeochemical Controls and Feedbacks on Ocean Primary Production. *Science (80-.).* **281**, 200–206. Available at: https://www.sciencemag.org/lookup/doi/10.1126/science.281.5374.200.

Fernex F., Février G., Bénaïm J. and Arnoux A. (1992) Copper, lead and zinc trapping in Mediterranean deep-sea sediments: probable coprecipitation with Mn and Fe. *Chem. Geol.* **98**, 293–306. Available at: https://linkinghub.elsevier.com/retrieve/pii/000925419290190G.

Field C. B. (1998) Primary Production of the Biosphere: Integrating Terrestrial and Oceanic Components. *Science (80-.).* **281**, 237–240. Available at:

https://www.sciencemag.org/lookup/doi/10.1126/science.281.5374.237.

Finney B., Heath G. R. and Lyle M. (1984) Growth rates of manganese-rich nodules at MANOP Site H (Eastern North Pacific). *Geochim. Cosmochim. Acta* **48**, 911–919. Available at: https://linkinghub.elsevier.com/retrieve/pii/0016703784901844.

Froelich P. N., Klinkhammer G. P., Bender M. L., Luedtke N. A., Heath G. R., Cullen D., Dauphin P., Hammond D., Hartman B. and Maynard V. (1979) Early oxidation of organic matter in pelagic sediments of the eastern equatorial Atlantic: suboxic diagenesis. *Geochim. Cosmochim. Acta* **43**, 1075–1090. Available at: https://linkinghub.elsevier.com/retrieve/pii/0016703779900954.

Geider R. J., Delucia E. H., Falkowski P. G., Finzi A. C., Grime J. P., Grace J., Kana T. M., La Roche J., Long S. P., Osborne B. A., Platt T., Prentice I. C., Raven J. A., Schlesinger W. H., Smetacek V., Stuart V., Sathyendranath S., Thomas R. B., Vogelmann T. C., Williams P. and Woodward F. I. (2001) Primary productivity of planet earth: biological determinants and physical constraints in terrestrial and aquatic habitats. *Glob. Chang. Biol.* **7**, 849–882. Available at: http://doi.wiley.com/10.1046/j.1365-2486.2001.00448.x.

Gutiérrez D., Enríquez E., Purca S., Quipúzcoa L., Marquina R., Flores G. and Graco M. (2008) Oxygenation episodes on the continental shelf of central Peru: Remote forcing and benthic ecosystem response. *Prog. Oceanogr.* **79**, 177–189.

Hamukuaya H., O'Toole M. J. and Woodhead P. M. J. (1998) Observations of severe hypoxia and offshore displacement of Cape hake over the Namibian shelf in 1994. *South African J. Mar. Sci.* **19**, 57–59. Available at: http://www.tandfonline.com/doi/abs/10.2989/025776198784126809.

Heggie D. and Lewis T. (1984) Cobalt in pore waters of marine sediments. *Nature* **311**, 453–455. Available at: http://www.nature.com/articles/311453a0.

Heller M. I., Lam P. J., Moffett J. W., Till C. P., Lee J. M., Toner B. M. and Marcus M. A. (2017) Accumulation of Fe oxyhydroxides in the Peruvian oxygen deficient zone implies non-oxygen dependent Fe oxidation. *Geochim. Cosmochim. Acta* **211**, 174–193. Available at: http://dx.doi.org/10.1016/j.gca.2017.05.019.

Helly J. J. and Levin L. A. (2004) Global distribution of naturally occurring marine hypoxia on continental margins. *Deep Sea Res. Part I Oceanogr. Res. Pap.* **51**,

1159–1168. Available at: https://linkinghub.elsevier.com/retrieve/pii/S0967063704000639.

Helm K. P., Bindoff N. L. and Church J. A. (2011) Observed decreases in oxygen content of the global ocean. *Geophys. Res. Lett.* **38**, 1–6.

Ho T.-Y., Quigg A., Finkel Z. V., Milligan A. J., Wyman K., Falkowski P. G. and Morel F. M. M. (2003) THE ELEMENTAL COMPOSITION OF SOME MARINE PHYTOPLANKTON1. *J. Phycol.* **39**, 1145–1159. Available at: http://doi.wiley.com/10.1111/j.0022-3646.2003.03-090.x.

Homoky W. B., Weber T., Berelson W. M., Conway T. M., Henderson G. M., van Hulten M., Jeandel C., Severmann S. and Tagliabue A. (2016) Quantifying trace element and isotope fluxes at the ocean–sediment boundary: a review. *Philos. Trans. R. Soc. A Math. Phys. Eng. Sci.* **374**, 20160246. Available at: https://royalsocietypublishing.org/doi/10.1098/rsta.2016.0246.

Karstensen J., Stramma L. and Visbeck M. (2008) Oxygen minimum zones in the eastern tropical Atlantic and Pacific oceans. *Prog. Oceanogr.* **77**, 331–350.

Keeling R. F., Körtzinger A. and Gruber N. (2010) Ocean Deoxygenation in a Warming World. *Ann. Rev. Mar. Sci.* **2**, 199–229. Available at: http://www.annualreviews.org/doi/10.1146/annurev.marine.010908.163855.

Kuleshov V. (2017) Manganese Carbonates in Modern Sediments. In *Isotope Geochemistry* Elsevier. pp. 5–62. Available at: http://dx.doi.org/10.1016/B978-0-12-803165-0.00002-1.

Lam P., Lavik G., Jensen M. M., van de Vossenberg J., Schmid M., Woebken D., Gutierrez D., Amann R., Jetten M. S. M. and Kuypers M. M. M. (2009) Revising the nitrogen cycle in the Peruvian oxygen minimum zone. *Proc. Natl. Acad. Sci.* **106**, 4752–4757. Available at: http://www.pnas.org/cgi/doi/10.1073/pnas.0812444106.

Levin L. A., Ekau W., Gooday A. J., Jorissen F., Middelburg J. J., Naqvi S. W. A., Neira C., Rabalais N. N. and Zhang J. (2009) Effects of natural and human-induced hypoxia on coastal benthos. *Biogeosciences* **6**, 2063–2098. Available at: https://bg.copernicus.org/articles/6/2063/2009/.

Levin L., Gutiérrez D., Rathburn A., Neira C., Sellanes J., Muñoz P., Gallardo V. and

Salamanca M. (2002) Benthic processes on the Peru margin: a transect across the oxygen minimum zone during the 1997–98 El Niño. *Prog. Oceanogr.* **53**, 1–27. Available at: https://linkinghub.elsevier.com/retrieve/pii/S0079661102000228.

Little S. H., Vance D., Lyons T. W. and McManus J. (2015) Controls on trace metal authigenic enrichment in reducing sediments: Insights from modern oxygen-deficient settings. *Am. J. Sci.* **315**, 77–119. Available at: http://www.ajsonline.org/cgi/doi/10.2475/02.2015.01.

Lohan M. C. and Tagliabue A. (2018) Oceanic Micronutrients: Trace Metals that are Essential for Marine Life. *Elements* **14**, 385–390. Available at: https://pubs.geoscienceworld.org/msa/elements/article/14/6/385/567322/Oceanic-Micronutrients-Trace-Metals-that-are.

McPhaden M. J., Zebiak S. E. and Glantz M. H. (2006) ENSO as an Integrating Concept in Earth Science. *Science (80-.).* **314**, 1740–1745. Available at: https://www.sciencemag.org/lookup/doi/10.1126/science.1132588.

Middelburg J. J., De Lange G. J. and van Der Weijden C. H. (1987) Manganese solubility control in marine pore waters. *Geochim. Cosmochim. Acta* **51**, 759–763. Available at: https://linkinghub.elsevier.com/retrieve/pii/001670378790086X.

Moore C. M., Mills M. M., Arrigo K. R., Berman-Frank I., Bopp L., Boyd P. W., Galbraith E. D., Geider R. J., Guieu C., Jaccard S. L., Jickells T. D., La Roche J., Lenton T. M., Mahowald N. M., Marañón E., Marinov I., Moore J. K., Nakatsuka T., Oschlies A., Saito M. A., Thingstad T. F., Tsuda A. and Ulloa O. (2013) Processes and patterns of oceanic nutrient limitation. *Nat. Geosci.* **6**, 701–710. Available at: http://dx.doi.org/10.1038/ngeo1765.

Morel F. M. M., Milligan A. J. and Saito M. A. (2014) Marine Bioinorganic Chemistry: The Role of Trace Metals in the Oceanic Cycles of Major Nutrients. In *Treatise on Geochemistry* Elsevier. pp. 123–150. Available at: https://linkinghub.elsevier.com/retrieve/pii/B9780080959757006057.

Morford J. L. and Emerson S. (1999) The geochemistry of redox sensitive trace metals in sediments. *Geochim. Cosmochim. Acta* **63**, 1735–1750. Available at:

https://linkinghub.elsevier.com/retrieve/pii/S001670379900126X.

Morse J. W. and Luther G. W. (1999) Chemical influences on trace metal-sulfide interactions in anoxic sediments. *Geochim. Cosmochim. Acta* **63**, 3373–3378. Available at: http://link.springer.com/10.1007/s10347-007-0115-3.

Noble A. E., Lamborg C. H., Ohnemus D. C., Lam P. J., Goepfert T. J., Measures C. I., Frame C. H., Casciotti K. L., DiTullio G. R., Jennings J. and Saito M. A. (2012) Basin-scale inputs of cobalt, iron, and manganese from the Benguela-Angola front to the South Atlantic Ocean. *Limnol. Oceanogr.* **57**, 989–1010.

Noffke A., Hensen C., Sommer S., Scholz F., Bohlen L., Mosch T., Graco M. and Wallmann K. (2012) Benthic iron and phosphorus fluxes across the Peruvian oxygen minimum zone. *Limnol. Oceanogr.* **57**, 851–867.

Ohde T. (2018) Coastal Sulfur Plumes off Peru During El Niño, La Niña, and Neutral Phases. *Geophys. Res. Lett.* **45**, 7075–7083.

Olson L., Quinn K. A., Siebecker M. G., Luther G. W., Hastings D. and Morford J. L. (2017) Trace metal diagenesis in sulfidic sediments: Insights from Chesapeake Bay. *Chem. Geol.* **452**, 47–59. Available at: http://dx.doi.org/10.1016/j.chemgeo.2017.01.018.

Oschlies A., Schulz K. G., Riebesell U. and Schmittner A. (2008) Simulated 21st century's increase in oceanic suboxia by CO 2-enhanced biotic carbon export. *Global Biogeochem. Cycles* **22**, 1–10.

Pakhomova S. V., Hall P. O. J., Kononets M. Y., Rozanov A. G., Tengberg A. and Vershinin A. V. (2007) Fluxes of iron and manganese across the sediment–water interface under various redox conditions. *Mar. Chem.* **107**, 319–331. Available at: https://linkinghub.elsevier.com/retrieve/pii/S0304420307001302.

Paulmier A. and Ruiz-Pino D. (2009) Oxygen minimum zones (OMZs) in the modern ocean. *Prog. Oceanogr.* **80**, 113–128. Available at: http://dx.doi.org/10.1016/j.pocean.2008.08.001.

Peacock C. L. and Sherman D. M. (2007) Sorption of Ni by birnessite: Equilibrium controls on Ni in seawater. *Chem. Geol.* **238**, 94–106. Available at: https://linkinghub.elsevier.com/retrieve/pii/S0009254106005006.

Peng Q., Xie S.-P., Wang D., Zheng X.-T. and Zhang H. (2019) Coupled ocean-atmosphere dynamics of the 2017 extreme coastal El Niño. *Nat. Commun.* **10**, 298. Available at: http://www.nature.com/articles/s41467-018-08258-8.

Pennington J. T., Mahoney K. L., Kuwahara V. S., Kolber D. D., Calienes R. and Chavez F. P. (2006) Primary production in the eastern tropical Pacific: A review. *Prog. Oceanogr.* **69**, 285–317.

Penven P. (2005) Average circulation, seasonal cycle, and mesoscale dynamics of the Peru Current System: A modeling approach. *J. Geophys. Res.* **110**, C10021. Available at: http://doi.wiley.com/10.1029/2005JC002945.

Pizarro O. (2002) Dynamics of seasonal and interannual variability of the Peru-Chile Undercurrent. *Geophys. Res. Lett.* **29**, 1581. Available at: http://doi.wiley.com/10.1029/2002GL014790.

Rapp I., Schlosser C., Browning T. J., Wolf F., Le Moigne F. A. C., Gledhill M. and Achterberg E. P. (2020) El Niño-Driven Oxygenation Impacts Peruvian Shelf Iron Supply to the South Pacific Ocean. *Geophys. Res. Lett.* **47**. Available at: https://onlinelibrary.wiley.com/doi/abs/10.1029/2019GL086631.

Rapp I., Schlosser C., Menzel Barraqueta J.-L., Wenzel B., Lüdke J., Scholten J., Gasser B., Reichert P., Gledhill M., Dengler M. and Achterberg E. P. (2019) Controls on redox-sensitive trace metals in the Mauritanian oxygen minimum zone. *Biogeosciences* **16**, 4157–4182. Available at: https://www.biogeosciences.net/16/4157/2019/.

Rigaud S., Radakovitch O., Couture R. M., Deflandre B., Cossa D., Garnier C. and Garnier J. M. (2013) Mobility and fluxes of trace elements and nutrients at the sediment-water interface of a lagoon under contrasting water column oxygenation conditions. *Appl. Geochemistry* **31**, 35–51. Available at: http://dx.doi.org/10.1016/j.apgeochem.2012.12.003.

Saito M. A., Moffett J. W. and DiTullio G. R. (2004) Cobalt and nickel in the Peru upwelling region: A major flux of labile cobalt utilized as a micronutrient. *Global Biogeochem. Cycles* **18**, 1–14.

Schmidtko S., Stramma L. and Visbeck M. (2017) Decline in global oceanic oxygen content during the past five decades. *Nature* **542**, 335–339. Available at:

http://dx.doi.org/10.1038/nature21399.

Scholz F., Hensen C., Noffke A., Rohde A., Liebetrau V. and Wallmann K. (2011) Early diagenesis of redox-sensitive trace metals in the Peru upwelling area - response to ENSO-related oxygen fluctuations in the water column. *Geochim. Cosmochim. Acta* **75**, 7257–7276. Available at: http://dx.doi.org/10.1016/j.gca.2011.08.007.

Scholz F., Löscher C. R., Fiskal A., Sommer S., Hensen C., Lomnitz U., Wuttig K., Göttlicher J., Kossel E., Steininger R. and Canfield D. E. (2016) Nitrate-dependent iron oxidation limits iron transport in anoxic ocean regions. *Earth Planet. Sci. Lett.* **454**, 272–281. Available at: http://dx.doi.org/10.1016/j.epsl.2016.09.025.

Schunck H., Lavik G., Desai D. K., Großkopf T., Kalvelage T., Löscher C. R., Paulmier A., Contreras S., Siegel H., Holtappels M., Rosenstiel P., Schilhabel M. B., Graco M., Schmitz R. A., Kuypers M. M. M. and LaRoche J. (2013) Giant Hydrogen Sulfide Plume in the Oxygen Minimum Zone off Peru Supports Chemolithoautotrophy. *PLoS One* **8**.

Scor Working Group (2007) GEOTRACES – An international study of the global marine biogeochemical cycles of trace elements and their isotopes. *Geochemistry* **67**, 85–131. Available at: https://linkinghub.elsevier.com/retrieve/pii/S0009281907000050.

Shaw T. J., Gieskes J. M. and Jahnke R. A. (1990) Early diagenesis in differing depositional environments: The response of transition metals in pore water. *Geochim. Cosmochim. Acta* **54**, 1233–1246.

Stramma L., Fischer T., Grundle D. S., Krahmann G., Bange H. W. and Marandino C. A. (2016) Observed El Niño conditions in the eastern tropical Pacific in October 2015. *Ocean Sci.* **12**, 861–873. Available at: https://os.copernicus.org/articles/12/861/2016/.

Stramma L., Johnson G. C., Sprintall J. and Mohrholz V. (2008) Expanding Oxygen-Minimum Zones in the Tropical Oceans. *Science (80-.).* **320**, 655–658. Available at: http://www.sciencemag.org/cgi/doi/10.1126/science.1153847.

Stramma L., Schmidtko S., Levin L. A. and Johnson G. C. (2010) Ocean oxygen

minima expansions and their biological impacts. *Deep. Res. Part I Oceanogr. Res. Pap.* **57**, 587–595.

Sundby B., Anderson L. G., Hall P. O. J., Iverfeldt Å., van der Loeff M. M. R. and Westerlund S. F. G. (1986) The effect of oxygen on release and uptake of cobalt, manganese, iron and phosphate at the sediment-water interface. *Geochim. Cosmochim. Acta* **50**, 1281–1288. Available at: https://linkinghub.elsevier.com/retrieve/pii/0016703786904114.

Tankéré S. P. ., Muller F. L. ., Burton J. ., Statham P. ., Guieu C. and Martin J.-M. (2001) Trace metal distributions in shelf waters of the northwestern Black Sea. *Cont. Shelf Res.* **21**, 1501–1532. Available at: https://linkinghub.elsevier.com/retrieve/pii/S0278434301000139.

Thamdrup B., Dalsgaard T. and Revsbech N. P. (2012) Widespread functional anoxia in the oxygen minimum zone of the Eastern South Pacific. *Deep Sea Res. Part I Oceanogr. Res. Pap.* **65**, 36–45. Available at: http://dx.doi.org/10.1016/j.dsr.2012.03.001.

Torrans E. L. and Clemens H. P. (1982) Physiological and biochemical effects of acute exposure of fish to hydrogen sulfide. *Comp. Biochem. Physiol. Part C Comp. Pharmacol.* **71**, 183–190. Available at: https://linkinghub.elsevier.com/retrieve/pii/030644928290034X.

Tribovillard N., Algeo T. J., Lyons T. and Riboulleau A. (2006) Trace metals as paleoredox and paleoproductivity proxies: An update. *Chem. Geol.* **232**, 12–32. Available at: https://linkinghub.elsevier.com/retrieve/pii/S000925410600132X.

van de Velde S. J., Hylén A., Kononets M., Marzocchi U., Leermakers M., Choumiline K., Hall P. O. J. and Meysman F. J. R. (2020) Elevated sedimentary removal of Fe, Mn, and trace elements following a transient oxygenation event in the Eastern Gotland Basin, central Baltic Sea. *Geochim. Cosmochim. Acta* **271**, 16–32. Available at: https://doi.org/10.1016/j.gca.2019.11.034.

II. The control of hydrogen sulfide on benthic iron and cadmium fluxes in the oxygen minimum zone off Peru

Anna Plass[1], Christian Schlosser[1], Stefan Sommer[1], Andrew W. Dale[1], Eric P. Achterberg[1], Florian Scholz[1]

[1]GEOMAR Helmholtz Centre for Ocean Research Kiel, Wischhofstraße 1-3, 24148 Kiel, Germany

Published in Biogeosciences, 17, 3685–3704, 2020

Abstract

Sediments in oxygen-depleted marine environments can be an important sink or source of bio-essential trace metals in the ocean. However, the key mechanisms controlling the release from or burial of trace metals in sediments are not exactly understood. Here, we investigate the benthic biogeochemical cycling of Fe and Cd in the oxygen minimum zone off Peru. We combine bottom water and pore water concentrations, as well as benthic fluxes determined from pore water profiles and in-situ from benthic chamber incubations, along a depth transect at 12° S. In agreement with previous studies, both concentration-depth profiles and in-situ benthic fluxes indicate a release of Fe from sediments to the bottom water. Diffusive Fe fluxes and Fe fluxes from benthic chamber incubations (-0.3 – -17.5 mmol m^{-2} y^{-1}) are broadly consistent at stations within the oxygen minimum zone, where the flux magnitude is highest, indicating that diffusion is the main transport mechanism of dissolved Fe across the sediment-water interface. The occurrence of mats of sulfur oxidizing bacteria on the seafloor represents an important control on the spatial distribution of Fe fluxes by regulating hydrogen sulfide (H_2S) concentrations and, potentially, Fe sulfide precipitation within the surface sediment. Rapid removal of dissolved Fe after its release to anoxic bottom waters hints to oxidative removal by nitrite and interactions

with particles in the near-bottom water column. Benthic flux estimates of Cd suggest a flux into the sediment within the oxygen minimum zone. Fluxes from benthic chamber incubations (up to 22.6 µmol m^{-2} y^{-1}) exceed diffusive fluxes (< 1 µmol m^{-2} y^{-1}) by a factor > 25, indicating that downward diffusion of Cd across the sediment-water interface is of subordinate importance for Cd removal from benthic chambers. As Cd removal in benthic chambers co-varies with H_2S concentrations in the pore water of surface sediments, we argue that Cd removal is mediated by precipitation of CdS within the chamber water or directly at the sediment-water interface. A mass balance approach, taking into account the contributions of diffusive and chamber fluxes as well as Cd delivery with organic material, suggests that CdS precipitation in the near-bottom water could make an important contribution to the overall Cd mass accumulation in the sediment solid phase. According to our results, the solubility of trace metal sulfide minerals (Cd << Fe) is a key-factor controlling trace metal removal and consequently the magnitude as well as the temporal and spatial heterogeneity of sedimentary fluxes. We argue that depending on their sulfide solubility, sedimentary source or sink fluxes of trace metals will change differentially as a result of declining oxygen concentrations and an associated expansion of sulfidic surface sediments. Such a trend could cause a change in the trace metal stoichiometry of upwelling water masses with potential consequences for marine ecosystems in the surface ocean.

II.1 Introduction

II.1.1 Scientific rationale

The world´s oceans are losing oxygen (e.g. Keeling et al. 2010; Stramma et al. 2010; Helm et al. 2011). In total around 2 % of oxygen has been lost over the past five decades (Schmidtko et al., 2017) and an expansion of oxygen minimum zones (OMZs) in the tropical oceans has been documented over the same timespan (Stramma et al., 2008). The biogeochemical cycling of several nutrient-type trace metals (TMs) is likely to be particularly susceptible to changing oxygen concentrations as they occur in different oxidation states (e.g. Fe, Mn, Co) and/or precipitate as sulfide mineral in anoxic-sulfidic environments (e.g. Fe, Zn, Cd; listed in the order of decreasing sulfide

solubility). However, with the exception of Fe (Dale et al., 2015a; Lohan and Bruland, 2008; Rapp et al., 2018; Schlosser et al., 2018; Scholz et al., 2014a), little information is available on how other TM fluxes will respond to ocean deoxygenation. As certain TMs are essential for the growth of marine organisms (e.g. Fe, Mn, Co, Ni, Zn, Cd), TM availability can (co-)limit primary productivity and therefore affect oceanic carbon sequestration through the biological pump (Saito et al., 2008; Moore et al., 2013; Morel et al., 2014). As a consequence, a better understanding of how TMs respond to low oxygen conditions is essential for predicting how marine ecosystems and the carbon cycle will evolve in the future ocean, with modelling scenarios predicting a continuation of ocean deoxygenation (Bopp et al., 2002; Oschlies et al., 2008; Keeling et al., 2010)

Marine sediments are an important source or sink of TMs to the ocean under low oxygen conditions (Böning et al., 2004; Brumsack, 2006; Scor Working Group, 2007; Severmann et al., 2010; Noble et al., 2012; Biller and Bruland, 2013; Conway and John, 2015a; Klar et al., 2018). In the OMZ off the coast of Peru, substantial fluxes of reduced Fe and other TMs across the sediment-bottom water interface have been documented (Noffke et al., 2012; Scholz et al., 2016) or inferred (Hawco et al., 2016). While a number of studies have addressed biogeochemical processes that lead to benthic Fe release, the key biogeochemical processes and conditions that control the sedimentary release or burial of other TMs in open marine systems are still poorly constrained. Moreover, a detailed picture of removal or stabilization processes and rates that take place in the highly dynamic water layer overlying the seafloor is lacking.

In this article, we compare the benthic biogeochemical cycling of Fe and Cd. It has been established that the Peruvian OMZ represents a source of dissolved Fe to the ocean (Noffke et al., 2012; Fitzsimmons et al., 2016; John et al., 2018a). In contrast, earlier studies have demonstrated that OMZs represent a sink for Cd (Janssen et al., 2014; Böning et al., 2004). Because of their contrasting tendency to form sulfide minerals and different supply pathways to the sediment, Fe and Cd can serve as prototypes to provide information about how sedimentary fluxes of different TMs may respond to declining oxygen concentrations. Under more reducing conditions the mobility of TMs can either be enhanced or diminished, e.g., through precipitation of sulfide minerals that are buried in the sediments (e.g. Westerlund et al., 1986; Rigaud et al., 2013; Olson et al., 2017). Increased burial or release of TMs at the seafloor can have an impact on the amplitude of primary productivity, especially at the

eastern ocean boundaries where the near-bottom water column is connected to the surface ocean via upwelling. Moreover, since the inventories of TMs in the ocean are generally dependent on the respective input and output fluxes, changes in the balance between trace metal recycling and burial can have an impact on oceanic TM reservoirs on longer timescales. By comparing the benthic biogeochemical cycling of Fe and Cd across spatial and temporal redox gradients, we aim to provide general constraints on how the stoichiometry of bio-essential TMs in seawater may be affected by ocean deoxygenation.

II.1.2 Marine biogeochemistry of iron

Iron is the most abundant TM in phytoplankton and part of a range of metalloenzymes that are involved in important biological functions, such as photosynthesis or nitrogen fixation (Twining and Baines, 2013). Despite Fe being highly abundant in the continental crust, its low availability limits primary productivity in up to 30 % of the surface ocean area (Moore et al., 2013). This limitation arises from the low solubility of its thermodynamically stable form in oxic waters, Fe(III). Concentrations can reach up to ~ 1 nM when Fe(III) is kept in solution through complexation with organic ligands (Rue and Bruland, 1997; Liu and Millero, 2002; Boyd and Ellwood, 2010; Raiswell and Canfield, 2012). The thermodynamically stable form of Fe under anoxic conditions, Fe(II), is more soluble and therefore anoxic waters are typically characterized by higher dissolved Fe concentrations (up to tens of nM) (Tim M. Conway and John, 2014; Vedamati et al., 2014b; Fitzsimmons et al., 2016; Schlosser et al., 2018).

Sediments within OMZs are considered an important source of dissolved Fe and some of the highest sedimentary Fe fluxes have been observed in these regions (Severmann et al., 2010; Noffke et al., 2012). Under anoxic conditions, Fe(II) can be liberated from the sediments into pore waters from Fe-(oxyhydr)oxides through reductive dissolution by microbes or abiotic reduction with H_2S (Canfield, 1989). In the absence of oxygen, dissolved Fe(II) escapes the rapid re-oxidation and subsequent (oxyhydr)oxide precipitation and can, therefore, diffuse from pore waters into bottom waters. However, in anoxic OMZs, where denitrification takes place, Fe(II) can also be re-oxidized with nitrate as a terminal electron acceptor, either mediated by nitrate-reducing microbes or abiotically through reaction with nitrite (Straub et al., 1996;

Carlson et al., 2013; Scholz et al., 2016; Heller et al., 2017). The solubility of Fe in sulfidic (i.e. NO_3^- and NO_2^- depleted) water is relatively high (Rickard et al., 2006) and during sulfidic events dissolved Fe can accumulate in the water column (up to hundreds of nM) because of decreased Fe oxidation (Scholz et al., 2016) and stabilization as aqueous Fe sulfide complexes and clusters (Schlosser et al., 2018). However, Fe fluxes across the benthic boundary have also been hypothesized to decrease under strongly sulfidic conditions in the surface sediments, when pore waters become oversaturated with respect to Fe monosulfide (Scholz et al., 2014a), which is the precursor for pyrite (FeS_2) (Raiswell and Canfield, 2012).

II.1.3 Marine biogeochemistry of cadmium

Cd is abundant in phytoplankton despite concentrations that are one order of magnitude lower than Fe (Moore et al., 2013; Twining and Baines, 2013). A function for Cd as a catalytic metal atom in the carbonic anhydrase protein has been found in diatoms (Lane and Morel, 2000) and it can also substitute Zn and enhance phytoplankton growth under Zn limitation in different phytoplankton species (Price and Morel, 1990; Lee and Morel, 1995; Sunda and Huntsman, 2000; Xu et al., 2008). In marine sediments Cd can be released from the solid phase to the pore waters through the remineralization of organic matter (Klinkhammer et al., 1982; Collier and Edmond, 1984; Gendron et al., 1986; Gerringa, 1990; Audry et al., 2006; Scholz and Neumann, 2007). After its release to the pore water, Cd can diffuse across the sediment-water interface. Under anoxic and sulfidic conditions, Cd is thought to be precipitated as CdS (Greenockite) and retained in the sediment (Westerlund et al., 1986; Gobeil et al., 1987; Rosenthal et al., 1995; Audry et al., 2006). Due to its low sulfide solubility, CdS can precipitate at much lower H_2S concentrations than FeS (mackinawite) (Morse and Luther, 1999).

Most previous studies have focused on the benthic cycling of Cd in near- and in-shore environments such as estuaries and lagoons (e.g. Westerlund et al., 1986; Colbert et al., 2001; Audry et al., 2006b; Metzger et al., 2007; Point et al., 2007; Scholz and Neumann, 2007). By contrast, little is known about Cd cycling in open-marine sedimentary environments, where the redox- and sediment-dynamics are different. Previous studies on sedimentary Cd cycling generally concluded that the flux of organic material and the presence of H_2S are the most important factors controlling the balance

between Cd recycling versus precipitation and burial (e.g. Westerlund et al., 1986; Colbert et al., 2001; Audry et al., 2006; Metzger et al., 2007; Scholz and Neumann, 2007). Low oxygen regions in the ocean are considered an important sink for Cd (Janssen et al., 2014; Conway and John, 2015b; Xie et al., 2019) and sediments below OMZs are highly enriched in Cd (Ragueneau et al., 2000; Böning et al., 2004; Borchers et al., 2005; Muñoz et al., 2012; Little et al., 2015). However, the respective contributions of different Cd removal mechanisms to Cd accumulation in the sediment have not been quantified.

II.1.4 Study area

Seasonal upwelling of nutrient-rich waters off the Peruvian coast in austral winter leads to high rates of primary productivity in the photic zone (~ 300 mmol C m^{-3} d^{-1}) (Pennington et al., 2006). The combination of oxygen consumption through the respiration of this organic matter and low oxygen concentrations in water masses that supply upwelling regions, leads to the formation of one of the world's most intense OMZs, with complete oxygen consumption in the OMZ core between ~ 100 m – 300 m water depth (Karstensen et al., 2008; Thamdrup et al., 2012). Upon oxygen depletion, NO_3^- can serve as an electron acceptor for respiration. Therefore, denitrification, dissimilatory reduction of NO_3^- to ammonium (DNRA) and anaerobic ammonium oxidation (anammox) with NO_2^- are important biogeochemical processes within the anoxic and nitrogenous water column (Lam et al., 2009; Lam and Kuypers, 2011; Dalsgaard et al., 2012). The OMZ overlying the Peruvian shelf is a temporally and spatially dynamic system where biogeochemical conditions can range from fully oxic to anoxic and sulfidic. Occasional shelf oxygenation events occur mostly during El Niño events and are linked to the propagation of coastal trapped waves (Gutiérrez et al., 2008). During such events, oxygenated water can be found on the upper slope to 200 – 300 m water depth (Levin et al., 2002b). By contrast, sulfidic events can occur during periods of stagnation, when oxygen, NO_3^- and NO_2^- become depleted in the water column due to sluggish ventilation. Once NO_3^- and NO_2^- are depleted, chemolithoautotrophic H_2S oxidation is impeded. Hydrogen sulfide produced by bacterial sulfate reduction in sediments can then be released to the water column (Schunck et al., 2013) at rates reaching several mmol m^{-2} d^{-1} (Sommer et al., 2016).

Our sampling campaign (cruises M136 and M137) took place in April and May 2017, during the decline of a coastal El Niño event. A coastal El Niño is a local phenomenon that refers to reduced upwelling and increased sea surface temperatures off the coasts of Peru and Ecuador, with typically heavy rainfall on land. During this event in austral summer, coastal waters off Peru showed a strong positive sea surface temperature anomaly of up to 2 – 4 °C (Garreaud, 2018; Echevin et al., 2018). The warming is proposed to be a result of strong local alongshore wind anomalies and equatorial Kelvin waves propagating towards the Peruvian coast (Echevin et al., 2018; Peng et al., 2019).

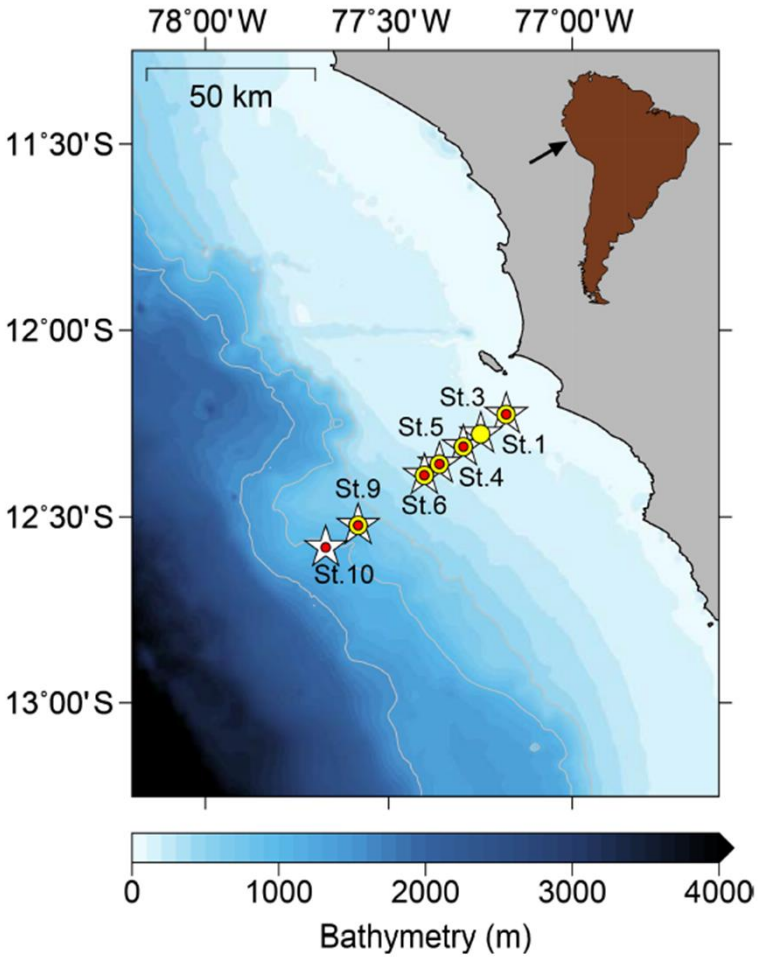

Figure II.1: Sampling stations on the Peruvian continental margin during cruises M136 & M137 along a latitudinal depth transect at 12° S. The sampling stations for pore waters are depicted by white stars, for bottom waters by yellow dots and for benthic chamber incubations by red dots.

II.2 Methods

II.2.1 Sampling and sample handling

In this study, data from three different types of samples were combined: (1) pore waters for the determination of benthic diffusive fluxes and to study TM cycling in sediments; (2) Benthic chamber incubations, to determine in-situ fluxes across the sediment-water interface; (3) Bottom water concentration-depth profiles to determine the fate of TMs in the particle-rich and dynamic near-bottom water column.

The sampling took place during RV Meteor cruises M136 and M137 in austral autumn between April and May 2017. We also compared our data to benthic diffusive Fe(II) fluxes from RV Meteor cruise M92 that took place in austral summer during January 2013. Our sampling stations covered the entire Peruvian shelf and slope across a transect at 12°S (Fig. II.1) with water depths from 75 – to 950 m, thus including stations above, inside and below the permanent OMZ. Our sampling of pore waters and sample collection from benthic chamber incubations generally followed the methodology described in Noffke et al. (2012).

Short sediment cores of 30 – 40 cm length were retrieved with a multiple corer (MUC). Upon recovery, the cores were directly transferred into the ship's cool room (4°C). The supernatant bottom water was instantly sampled and filtered through 0.2 µm cellulose acetate filters (Sartorius) and acidified to pH < 1 with subboiled distilled HNO_3. The sediment cores were subsequently sampled in vertical sections in a glove bag under Ar atmosphere to prevent any contact with oxygen. The sediment samples were centrifuged to separate the pore waters from the sediment solid phase. Pore waters were then filtered in another Ar-filled glove bag through 0.2 µm cellulose acetate filters (Sartorius). An 8 ml aliquot was acidified to pH < 1 with subboiled distilled HNO_3 and stored in acid cleaned low-density polyethylene (LDPE) bottles for TM analysis. Another aliquot was taken for analysis of H_2S concentrations. Additional sediment subsamples were collected in pre-weighed cups for water content and porosity determination as well as for Cd and organic C concentrations measurements in the solid phase.

Benthic landers, constructed from titanium frames, containing two circular benthic chambers for in-situ incubations, were deployed on the seafloor (see Sommer

et al. (2009) for details). After placement of the lander on the seafloor, the benthic chambers (internal diameter of 28.8 cm) were partially driven into the sediment, covering a sediment area of 651.4 cm^2. A volume between 12 – 18 l, overlying the first 20 – 30 cm of the seafloor, was enclosed in the chamber, depending on the insertion depth of the chamber into the sediment. Prior to the incubation, the seawater contained in the chamber was repeatedly replaced with ambient seawater to replace solutes and flush out particles that might have been mobilized during the insertion of the chamber into the sediment. Over the incubation time of around 32 hours, 8 consecutive samples of 12 ml were filtered in-situ through 0.2 µm cellulose acetate filters (Sartorius) via peristaltic pumps and collected in quartz glass tubes. All sampling tubes were acid cleaned prior to use to guarantee a TM clean sampling. After recovery of the lander, the quartz glass tubes were transferred to the laboratory and samples were stored in acid cleaned LDPE bottles and acidified to pH < 2 with subboiled distilled HNO_3. Other samples were collected simultaneously for analysis of nitrogen species. The incubated sediments within the benthic chamber were sampled after recovery of the lander and pore waters were extracted to analyze H_2S concentrations for comparison with pore water profiles from parallel MUCs.

To determine TM concentrations across the near-bottom water column, water samples were collected at 0.5, 1.0, 2.0, 3.0 and 4.0 m above the seafloor using sampling apparatus attached to the landers. Filter holders with 0.2 µm polyether sulfone filters (Supor) were attached at the various depths and connected to sampling tubes that went through peristaltic pumps into gas sampling bags (Tedlar). Sampling at 3.0 m and 4.0 m above the seafloor was realized by attaching the filter holders and tubing to an arm that was automatically unfolded upon placement of the lander at the seafloor. The peristaltic pumps transferred the seawater from the sampling depths into the sampling bags over the same time period as the lander incubations of around 32 hours. This resulted in an average sample volume of 1.5 l per depth. All filters, tubing and sampling bags were acid cleaned prior to deployment to guarantee a TM clean sampling. Directly after sample retrieval, a 60 ml aliquot was stored in acid cleaned LDPE bottles and acidified to pH < 2 for TM analysis. Another aliquot was taken for analysis of silicic acid ($Si(OH)_4$).

II.2.2 Analytical methods

Concentrations of Fe(II) in pore waters were measured on board directly after sample retrieval by photometry using the ferrozine method (Stookey, 1970). Other geochemical parameters in our different samples were also determined photometrical (U-2001 Hitachi spectrometer) using standard techniques (Grasshoff et al., 1999). Hydrogen sulfide concentrations were determined using the methylene blue method and $Si(OH)_4$ concentrations were determined using a heptamolybdate solution as reagent. Concentrations of nitrogen species were determined by an auto-analyzer (QuAAtro, SEAL Analytical) using sulfanilamide as reagent (Hydes et al., 2010).

For TM analysis of bottom water samples we followed the procedure described by Rapp et al. (2017), whereby the TMs were pre-concentrated by a fully automated device (SeaFAST). After raising the sample pH to 6.4 with an ammonium acetate buffer (1.5 M), 15 ml of sample was loaded onto a chelating resin column, where the seawater matrix was rinsed off, before the TMs were collected into 1ml elution acid (1 M subboiled HNO_3). Due to the smaller size of pore water samples and samples from benthic lander incubations, a half-automated device (Preblab) with a smaller sample loop and thus dead volume was used. On this device, sample loading and collection as well as the addition of buffer was done manually. For samples from benthic lander incubations and pore waters, an amount of 3 ml and 1 ml, respectively, was needed for pre-concentration. The samples were diluted with de-ionised water (MilliQ, Millipore) to increase the sample volume to 5 ml for samples from benthic chamber incubations and to 3 ml for pore waters. The pre-concentrated samples were measured by ICP-MS (HR-ICP-MS; Thermo Fisher Element XR) and TM concentrations were quantified by isotope dilution. The detection limits were 28.8 pM for Fe and 0.8 pM for Cd (Rapp et al., 2017). Accuracies for replicate measurements of reference seawater certified for TMs are listed in Table II.1.

For the calculation of sedimentary Cd enrichments (Cd_{xs}), Cd and Al contents in sediments were determined following total digestions of freeze dried and ground sediment samples. The sediment was digested in 40 % HF (suprapure), 65 % HNO3 (suprapure) and 60 % $HClO_4$ (suprapure). Concentrations were measured by ICP-OES (VARIAN 720-ES). The reference standard MESS was used to check the digestion procedure. The accuracy was ± 0.3 % for Cd and ± 1.3 % for Al (MESS-3 Cd: 0.24 ±

0.01 µg g^{-1}, recommended value 0.24 ± 0.01 µg g^{-1}, MESS-3 Al: 8.59 ± 0.11 µg g^{-1}, recommended value 8.59 ± 0.23 µg g^{-1}).

Organic carbon content in the sediment was determined using an Elemental Analyzer (Euro EA) after removal of inorganic carbon with 0.25 mM HCl. Precision of the measurement was ± 1 %.

Table II.1: Accuracy of replicate concentration measurements (n = 7) of certified reference seawater for trace metals NASS-7 and CASS-6 by ICP-MS.

	NASS-7 certified value	NASS-7 measured value	CASS-6 certified value	CASS-6 measured value
Fe (µg/L)	0.351 ± 0.026	0.352 ± 0.017	1.56 ± 0.12	1.56 ± 0.03
Cd (µg/L)	0.0161 ± 0.0016	0.0162 ± 0,0024	0.0217 ± 0.0018	0.0216 ± 0.0016

II.2.3 Diffusive flux calculations

Benthic diffusive fluxes (F_D) were determined using Fick's first law of diffusion using concentration gradients between the uppermost pore water sample (0 – 1 cm) and the overlying bottom water (dC/dx) (Boudreau, 1997):

$$F_D = -\Phi D_{sed}(\mathrm{dC/dx}) \quad \text{(Eq. II.1)}$$

The effective molecular diffusion coefficients of Fe and Cd for sediments (D_{sed}) were calculated from the molecular diffusion coefficient in seawater (D_{sw}) under standard conditions (Li and Gregory, 1974) by adjusting it to in-situ temperature, pressure and salinity applying the Stokes-Einstein Equation. We determined the diffusion coefficients for sediments as follows:

$$D_{sed} = D_{sw}/\theta^2 \quad \text{(Eq. II.2)}$$

Tortuosity (θ) was calculated from porosity (Φ) as follows (Boudreau, 1997):

$$\theta^2 = 1 - \ln(\phi^2) \quad \text{(Eq. II.3)}$$

Positive values represent a flux from the bottom water into the sediment pore water, negative values a flux from the sediment pore water into the bottom water. All input values for the diffusive flux calculations are listed in Tables II.S.1 and II.S.2 in the supplement.

Due to the coarse resolution of our pore water profiles and the steep gradients between the uppermost pore water and bottom water sample (see close-up profiles, Fig. II.S.1 and II.S.2 in the supplement), we chose to follow previous studies (Pakhomova et al., 2007; Noffke et al., 2012; Scholz et al., 2016; Lenstra et al., 2019; Scholz et al., 2019) and calculate diffusive benthic fluxes based on a two point concentration gradient. Including deeper samples into a linear regression or applying more advanced curve fitting methods would reduce the statistical uncertainty, but fail to capture the sharp concentration gradients at the sediment surface and thus lead to erroneous flux estimates (cf. Shibamoto and Harada, 2010).

The fluxes from benthic lander incubations were calculated by fitting a linear regression to the concentration change over time. The relevant equations are listed together with the coefficients of determination (R^2) in Table II.S.4 in the supplement. Concentration changes over time were converted to fluxes by taking into account the water volume enclosed in the benthic chamber, estimated for each deployment from the insertion depth of the benthic chamber into the sediment. The uncertainties of fluxes were estimated by propagating the uncertainties of the linear regressions. Following previous studies (e.g. Friedrich et al. (2002); Lenstra et al. (2019)), only fluxes where the linear regression has an $R^2 > 0.3$ are reported in Tables II.2 and II.3.

II.3 Results

II.3.1 Biogeochemical conditions in the water column

Due to the particular atmospheric and oceanographic conditions, the decline of a coastal El Niño during our sampling campaign (cruises M136 and M137), the water column overlying the Peruvian shelf was oxygenated. Oxygen concentrations were > 20 µM in the water column down to around 100 m water depth. However, bottom water oxygen concentrations directly above the seafloor, measured using optodes attached

to lander, were below the detection limit (> 1 µM) at the shallowest station (Station 1). The OMZ, with O_2 concentrations < 5 µM, extended from around 120 to 400 m water depth. The water column within the OMZ was nitrogenous (i.e. NO_3^- reducing) as indicated by the presence of NO_2^- (≥ 4 µM), an intermediate product of denitrification (Zumft, 1997). Oxygen gradually increased to > 50 µM below 400 m towards 950 m water depth (Fig. II.2). As we will compare some of our data to those of an earlier cruise (M92), the corresponding oxygen distribution across the Peruvian continental margin is shown for comparison (Fig. II.2).

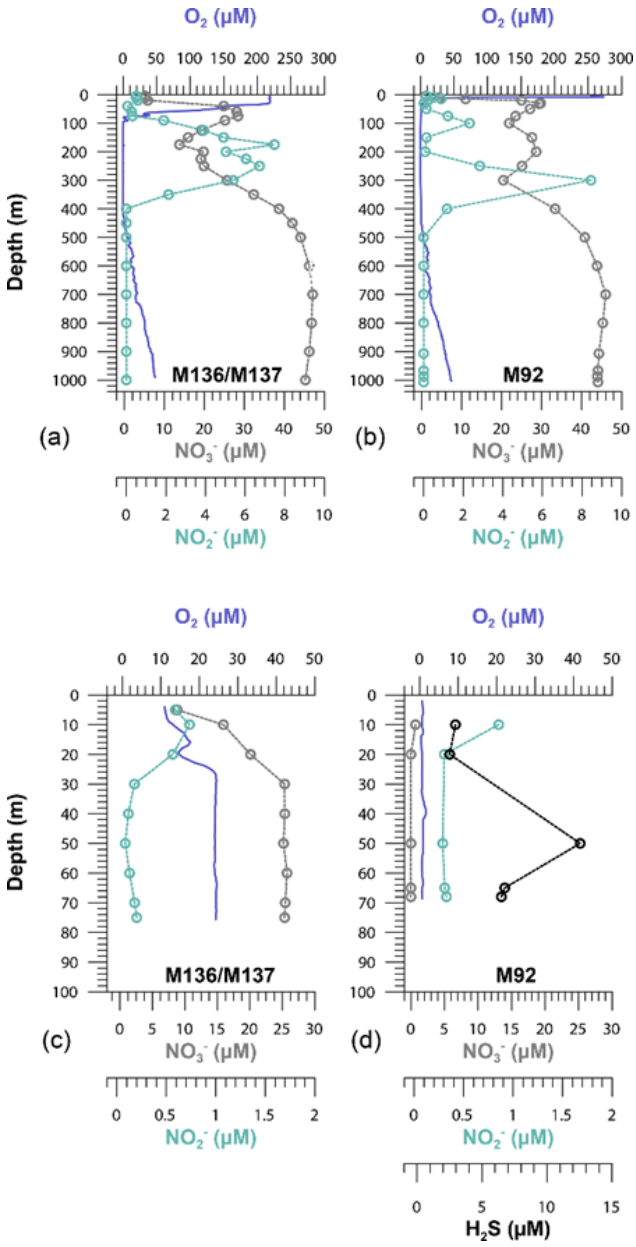

Figure II.2: Oxygen (O2), nitrate (NO_3^-), nitrite (NO_2^-) and hydrogen sulfide (H_2S) concentrations on the Peruvian slope (Station 10, 1000m depth), crossing the oxygen minimum zone (a, b), and the upper shelf (Station 1, 75m depth) (c, d) during cruises M136–M137 and M92 along the 12° S transect.

II.3.2 Bottom water, pore water and benthic flux data

II.3.2.1 Iron

Iron concentrations in near-bottom waters decreased from near-shore to off-shore stations, from > 100 nM at the shallowest shelf station at 75 m water depth (Station 1) to 6 nM at 750 m water depth (Station 9) (Fig. II.3a). At a number of stations within the OMZ (Station 3 and 4), vertical concentration gradients were observed. Here Fe concentrations decreased by 15 – 20 nM from 0.5 to 4 m above the seafloor. Multiple sampling at the shallowest shelf station (Station 1) revealed that Fe concentrations were temporally variable and ranged from ~ 100 nM at the end of April to < 60 nM at the end of May 2017.

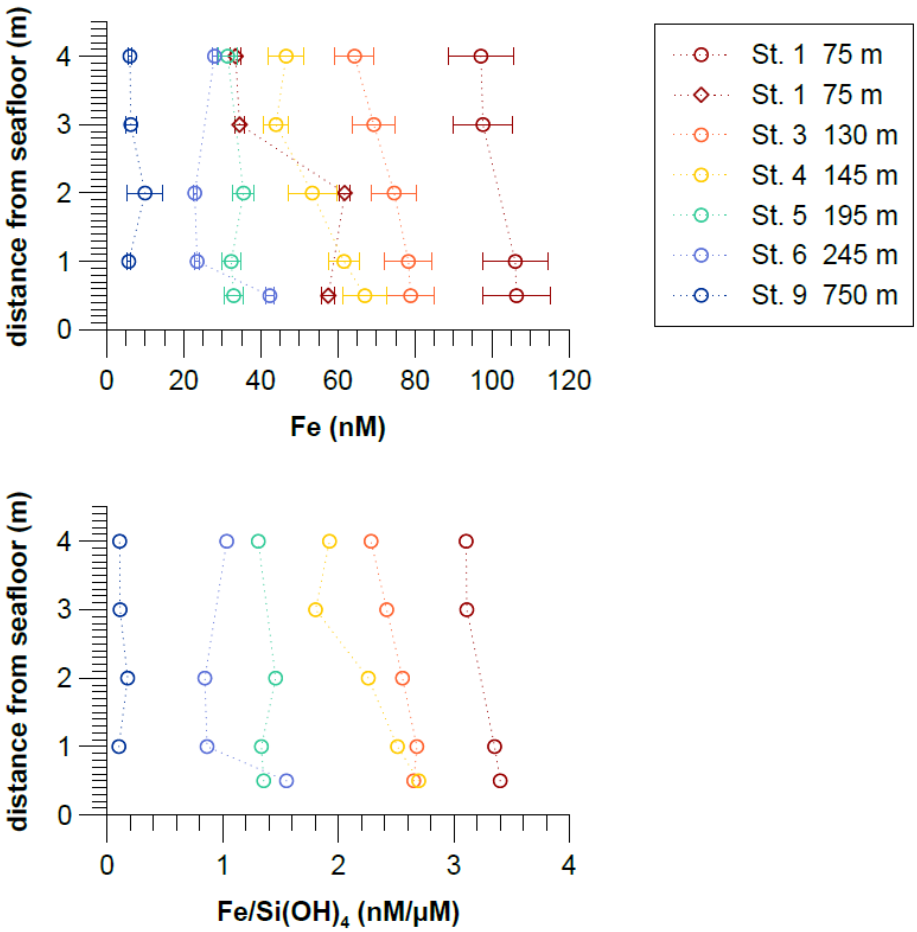

Figure II.3a: Near-bottom water concentrations of dissolved Fe and dissolved Fe to silicic acid ratios 0.5 m to 4 m above the seafloor across the 12° S transect. The red diamonds show results from a second sampling at Station 1 one month later. Concentrations of silicic acid are listed in Table II.S.3 in the supplement.

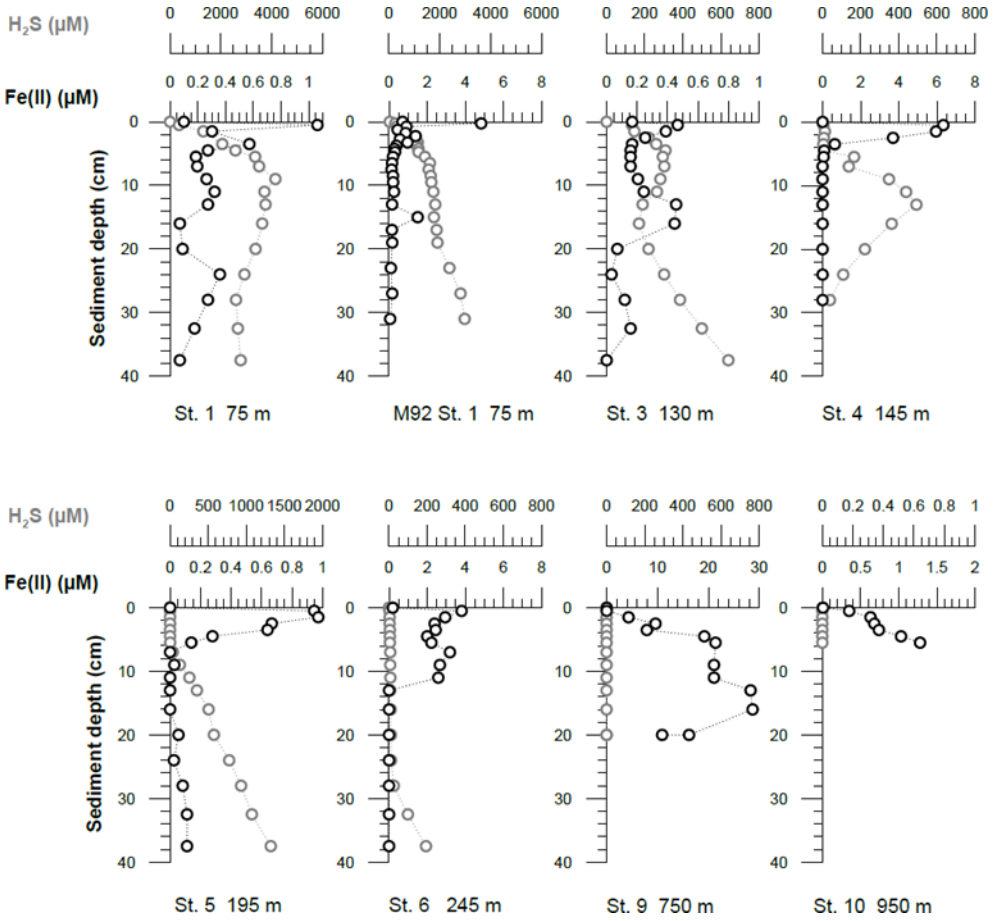

Figure II.4: Pore water dissolved Fe(II) and hydrogen sulfide concentrations. Data from an earlier cruise, M92, at Station 1 (75 m water depth) are displayed for comparison. The uppermost sample represents the bottom water concentration. The analytical error is smaller than the symbol size.

Concentrations of Fe(II) in pore waters were highest (up to a few µM) in the upper 5 – 10 cm of the sediment cores. Deeper in the sediment cores, concentrations decreased to > 0.2 µM (Fig. II.4). At all stations, sharp concentration gradients between the uppermost pore water and bottom water sample were observed, with higher concentrations in pore waters at the sediment surface (µM) than in the overlying bottom water (nM). This observation implies a diffusive flux from pore waters into bottom waters. The steepest concentration gradients across the sediment-water interface were observed within the OMZ. The highest Fe(II) concentrations at the sediment surface (> 6 µM) were observed at Station 4 (145 m water depth). At this station, the benthic diffusive flux into the bottom waters was also highest at -17.5 mmol m^{-2} y^{-1}.

The lowest diffusive fluxes of 0.0 (due to concentrations below the detection limit) and -0.3 mmol m^{-2} y^{-1} were observed on the upper slope below the OMZ at Stations 9 and 10 respectively (Table II.2). An accumulation of H_2S in pore waters coincided with a depletion of Fe(II) concentrations (Fig. II.4). At Station 1, we observed the highest H_2S concentrations throughout the core and in particular at the sediment surface, with maximum concentrations reaching > 4 mM. At Stations below the OMZ (Station 9 and 10), no H_2S was detected within pore waters (Fig. II.4).

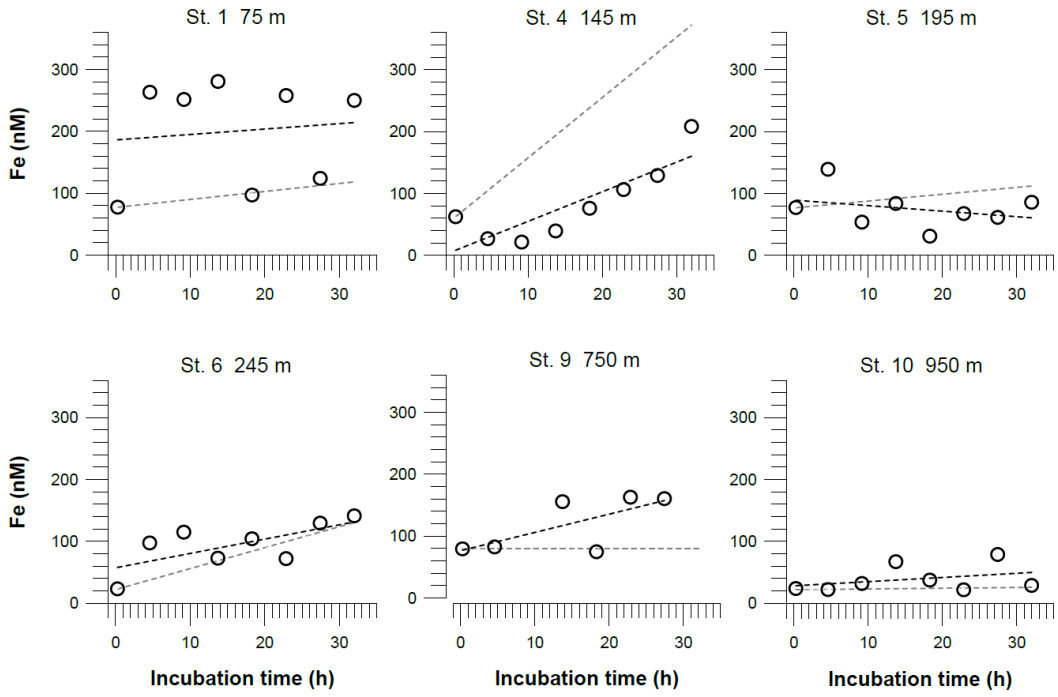

Figure II.5: Dissolved Fe concentrations in incubated bottom waters from benthic chamber incubations. The black dashed line represents the linear regressions of the concentration change over the incubation time. The equations for these linear regressions are listed together with the coefficients of determination (R^2) in Table II.S.4 in the supplement. The grey dashed line represents theoretical concentration gradients over the incubation time based on our benthic diffusive fluxes (Table II.2). The analytical error is smaller than the symbol size.

Iron concentrations inside the benthic chambers reached maximum values > 300 nM. At Station 4 and 6, located inside the OMZ, concentrations in the chambers increased in a linear way during the incubation. At stations above and below the OMZ, we did not observe a similar trend over time. For comparison with diffusive

fluxes, we estimated benthic Fe fluxes from linear regressions of Fe concentrations versus time (Table II.2). We also calculated the theoretical concentration gradients over time in the benthic chambers based on our diffusive flux estimates (Fig. II.5). At some stations the incubation data were largely consistent in direction and slope with the diffusive fluxes. In particular at Station 4 and 6 inside the OMZ, where the highest diffusive fluxes of -17.5 and -8.0 mmol m^{-2} y^{-1} were observed, expected and observed concentration gradients were in good agreement. At these stations also the highest R^2 for the linear regressions of the concentration change over the incubation time were calculated (Station 4: R^2 = 0.7, Station 6: R^2 = 0.5) (Table II.S.4). At stations below the OMZ, diffusive fluxes of < 1 mmol m^{-2} y^{-1} were too low to be detected over the incubation time of 32 hours.

II.3.2.2 Cadmium

In near-bottom waters Cd concentrations increased with distance from the coast, from 0.4 nM at the shallowest station at 75 m water depth (Station 1) to 1.1 nM below the OMZ at 750 m water depth (Station 9). Cadmium concentrations were constant at each station between 0.5 and 4 m above the seafloor (Fig. II.3b).

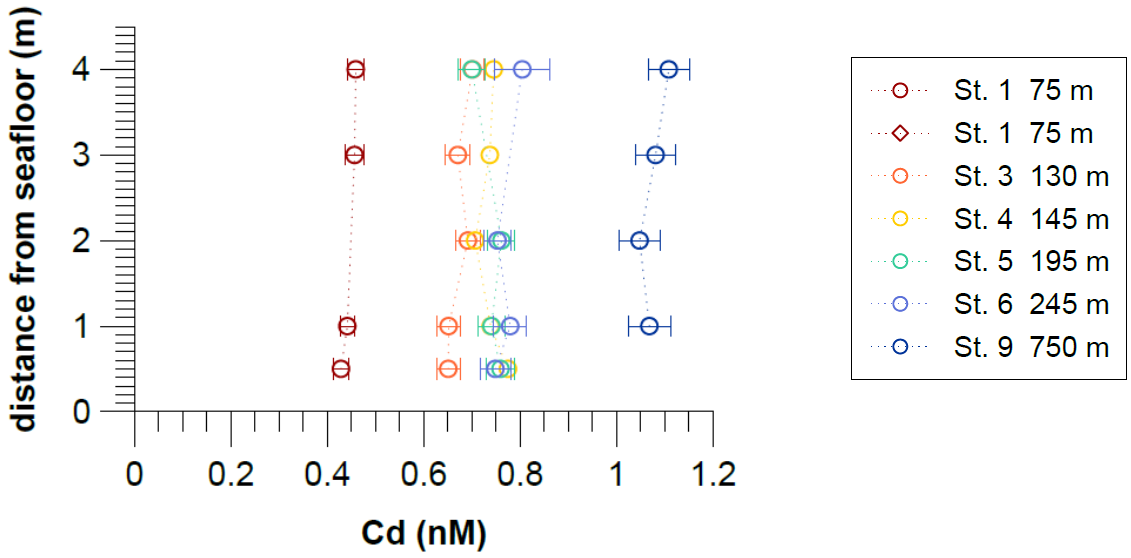

Figure II.3b: Near-bottom water concentrations of dissolved Cd 0.5 m to 4 m above the seafloor across the 12° S transect.

Cadmium concentrations in pore waters ranged between 0.1 – 2 nM (Fig. II.6). Within the OMZ, bottom water concentrations were higher than concentrations in pore water at the sediment surface (0 - 1 cm), indicating a downward diffusive flux into the sediments. The benthic diffusive fluxes inside the OMZ were on the order of 0.6 – 0.8 µmol m^{-2} y^{-1} (Table II.3). In contrast, at Stations 1 and 9 an upward-directed concentration gradient was observed, indicating a diffusive flux from the sediments into bottom waters. The upward diffusive flux was -1.9 µmol m^{-2} y^{-1} above the permanent OMZ and -0.2 µmol m^{-2} y^{-1} below the OMZ (Table II.3). Pore water Cd concentrations at greater sediment depths were mostly higher than bottom water concentrations. In some cases (Station 3 and 4), elevated pore water Cd concentrations (up to 2 nM) coincided with elevated H_2S concentrations (few hundred µM).

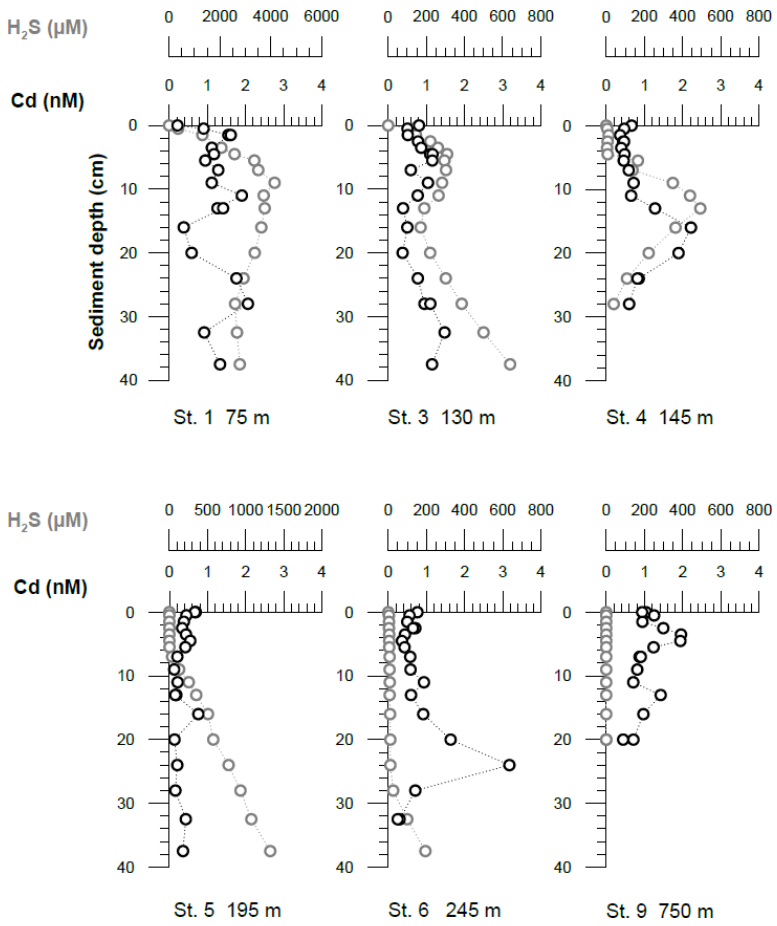

Figure II.6: Pore water dissolved Cd and hydrogen sulfide concentrations. The uppermost sample represents the bottom water concentrations. The analytical error is smaller than the symbol size.

In the benthic chambers three different Cd trends were observed (Fig. II.7). Above the permanent OMZ (Station 1), Cd concentrations in the chambers were low (< 0.2 nM) throughout the incubation period, indicating no Cd flux. At sites within the OMZ (Station 4, 5 and 6), concentrations decreased from ~ 0.6 – 0.3 nM over the course of the incubation. Below the OMZ (Stations 9 and 10), Cd concentrations in the chamber were high (~ 1 nM) and remained constant or increased slightly during the incubation. At sites within the OMZ, Cd removal within the chamber was near-linear (Station 4, 5 and 6: R^2 = ≥ 0.9) (Table II.S.4), which translates to a removal flux of 13 – 23 µmol m^{-2} y^{-1}. The Cd removal fluxes in benthic chambers were more than one order of magnitude higher than diffusive benthic fluxes (0.6 – 0.8 µmol m^{-2} y^{-1}) (Table II.3).

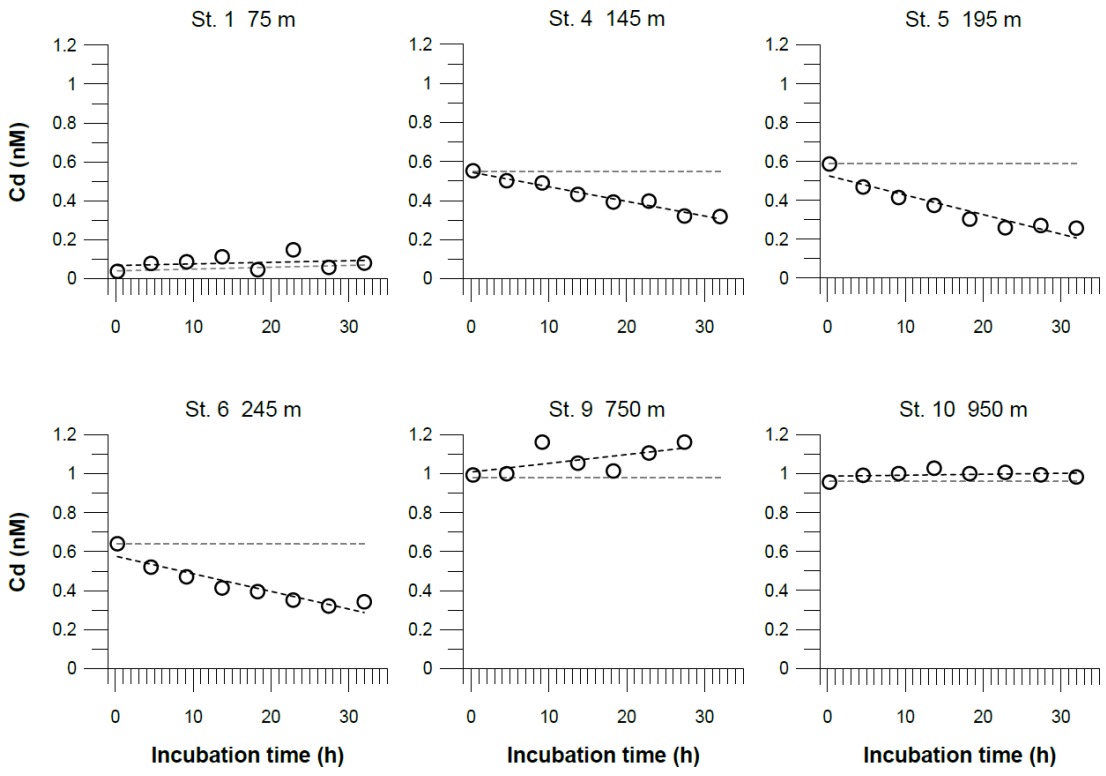

Figure II.7: Dissolved Cd concentrations in incubated bottom waters from benthic chamber incubations. The black dashed line represents the linear regressions of the concentration change over the incubation time. The equations for these linear regressions are listed together with the coefficients of determination (R2) in Table II.S.4 in the supplement. The grey dashed line represents theoretical concentration gradients over the incubation time based on our benthic diffusive fluxes (Table II.3). The analytical error is smaller than the symbol size.

II.4 Discussion

II.4.1 Benthic iron cycling

II.4.1.1 Comparison of diffusive and in-situ benthic chamber iron fluxes

Concentrations of Fe in bottom waters from benthic chamber incubations are mostly higher than in ambient bottom waters because of Fe release from the sediment and an accumulation in the enclosed water volume inside the benthic chamber. In the absence of oxygen and, thus, bottom-dwelling macrofauna at stations within the OMZ, bioturbation and bioirrigation are unlikely to exert an important control on sedimentary Fe release. Consistent with this notion, the slope calculated from benthic diffusive fluxes is in good agreement with the concentration gradients observed within the benthic chambers at two stations within the OMZ (Station 4 and 6) (Fig. II.5). Moreover, our fluxes from benthic chamber incubations and diffusive fluxes are of similar magnitude at these stations (Table II.2). Therefore, diffusive transport of dissolved Fe from the sediment into the bottom water seems to be the main control on the concentration evolution observed within the benthic chamber.

Some of the concentration gradients in benthic chambers are non-linear, indicating that the Fe flux was not constant during the incubations. This is a common observation in Fe flux data from benthic chamber incubations and higher Fe fluxes generally have higher R^2 values for the linear regressions (Friedrich et al., 2002; Turetta et al., 2005; Severmann et al., 2010; Lenstra et al., 2019). However, the non-linearity can be used to identify additional processes affecting Fe concentrations and fluxes within the benthic chamber, which may also affect fluxes under natural conditions. One possible process that can remove dissolved Fe(II) under anoxic conditions is Fe oxidation with NO_3^- as the terminal electron acceptor or oxidation with NO_2^- (Straub et al., 1996; Klueglein and Kappler, 2013; Carlson et al., 2013). The oxidation of reduced Fe in the absence of oxygen, either microbially mediated with NO_3^- or abiotically with NO_2^-, has been hypothesized to be important in the water column of the Peruvian OMZ (Scholz et al., 2016; Heller et al., 2017). During our incubation at Station 4 (Fig. II.8), we observed a decline in Fe concentrations during the first ten hours of the incubation time. Concurrently, NO_3^- concentrations were decreasing, while NO_2^- accumulated, presumably due to progressive denitrification and release from the sediments. Once NO_3^- and NO_2^- were depleted, Fe concentrations

started to rise again, resulting in the highest in-situ Fe flux observed throughout our sampling campaign (Table II.2). The coincidence in timing of Fe accumulation and NO_2^- decrease suggest that depletion of Fe at the beginning of the incubation was most likely caused by Fe oxidation with NO_2^-. The incubation at Station 4 was the only one where NO_3^- and NO_2^- were substantially removed during the incubation. However, the high Fe flux cannot be interpreted as a natural flux estimate at steady state. In general, we argue that bottom water NO_2^- concentrations exert a first order control on the intensity of Fe efflux at the absence of oxygen and, therefore, need to be considered in the evaluation of sedimentary Fe mobility in anoxic-nitrogenous OMZs.

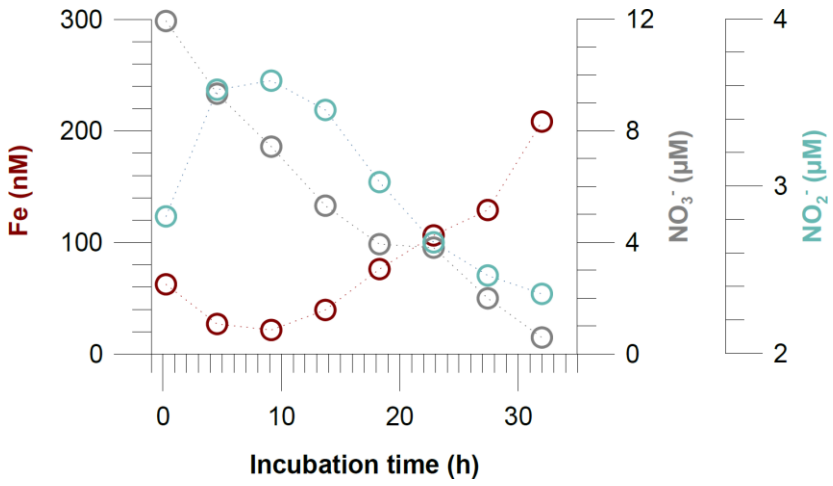

Figure II.8: Dissolved Fe, nitrate and nitrite concentrations in incubated bottom waters from the benthic chamber incubation at Station 4 (145 m water depth).

During the incubations at Station 1, 9 and 10, Fe concentrations did not continuously increase but fluctuated between high and low values. This observation could be explained by a combination of bioirrigation and bioturbation at stations where oxygen was present (Station 9 and 10), as well as rapid Fe oxidation and precipitation processes. Under oxic conditions, bottom-dwelling macrofauna is likely to increase the transfer of dissolved Fe from the sediments into the bottom water (Elrod et al., 2004; Lenstra et al., 2019). During episodes of oxygenation a population of macrofauna that can enhance bioturbation and bioirrigation was observed on the Peruvian shelf (Gutiérrez et al., 2008). However, under oxic conditions, any Fe delivered to the

chamber is prone to rapid oxidative removal. Moreover, ex-situ experiments have demonstrated a fast and efficient removal of up to 90% of dissolved Fe in incubated bottom waters due to particle resuspension (Homoky et al., 2012). Bioturbation and bioirrigation could also contribute to particle resuspension at oxic stations, thus leading to removal of dissolved Fe.

Furthermore, colloidal Fe could modify Fe concentrations within our samples and explain some of the fluctuations observed during the incubations. Colloids are quite reactive and much more soluble than larger particles. Therefore, they can be rapidly reduced and dissolved in anoxic environments, but they can also aggregate into larger particles (Raiswell and Canfield, 2012). The transfer of Fe between dissolved, colloidal and particulate pools is likely to affect the balance between Fe transport and re-precipitation and -deposition to some extent. However, since we did not differentiate between colloidal and truly dissolved fractions during our sampling, we cannot discuss this aspect further based on our data.

Oxidation processes and interactions with particles can efficiently remove Fe shortly after its transfer to bottom waters and this process is likely to be most intense close to the seafloor where the highest particle concentrations prevail. We argue that the same processes are reflected by declining Fe concentrations away from the seafloor in some of the bottom water profiles (Station 3 and 4) (Fig. II.3b).

II.4.1.2 Removal rates of dissolved iron in the near-bottom water column

We observed declining Fe concentrations in the first 4 m away from the seafloor at Station 3 and 4, which hints at removal of dissolved Fe in the near bottom waters after its release from the sediments. To differentiate between dilution with ambient bottom water (by currents) from Fe removal from the dissolved phase, Fe concentrations were normalized by $Si(OH)_4$ measured in the same samples (Fig. II.3a). Due to opal dissolution within Peru margin sediments, $Si(OH)_4$ is released into bottom waters (Ehlert et al., 2016). In contrast to Fe, we assume that $Si(OH)_4$ behaves conservatively and precipitation reactions within the bottom waters are of subordinate importance. The decreasing Fe to $Si(OH)_4$ ratios at Station 3 and 4 with distance from the seafloor indicate that there is Fe removal within the near-bottom water column that must be related to precipitation processes or scavenging.

We further constrained rates of dissolved Fe removal at stations with a discernable Fe to $Si(OH)_4$ gradient within the first 4 m distance from the seafloor. To this end, we first determined an eddy diffusion coefficient (K_y) using $Si(OH)_4$ fluxes from benthic chamber incubations (F_{Si}) (see chapter II.2.3 for methodology) and the known concentration gradient of dissolved $Si(OH)_4$ within the bottom water (d_{Si}/d_x), where x is the height above the seafloor. At the seafloor, the flux of $Si(OH)_4$ from the sediment is equal to the flux in the water column.

$$F_{Si} = -K_y(d_{Si}/d_x) \qquad \text{(Eq. II.4)}$$

This equation can be solved for the eddy diffusion coefficient.

Dissolved Fe in the bottom water (DFe) can be described by the solving the diffusion-reaction equation for DFe (ignoring advection and assuming a steady-state first-order consumption of dissolved Fe):

$$DFe = C_{BW} * exp.(-\sqrt{k_{Feox}}/\sqrt{K_y}) \qquad \text{(Eq. II.5)}$$

The equation can be fitted to the measured DFe concentrations in the bottom water by adjusting the Fe concentration directly above the seafloor (C_{BW}) and the Fe oxidation constant (k_{Feox}). From the fitted first-order rate constant $k_{Feox,}$ the half-life for dissolved Fe in bottom waters can be calculated.

The half-lifes of dissolved Fe in the first 4 m away from the seafloor are 2.5 min and 0.3 min at Station 3 and 4, respectively (Table II.4). Another study reported a dissolved Fe half-life of 17 hours under nitrogenous conditions in the first 10 – 20 m above the seafloor in the Peruvian OMZ (Scholz et al., 2016). Our calculations suggest that Fe removal in near-bottom waters is much faster. The approach assumes that $Si(OH)_4$ is transported vertically by eddy diffusion and oxidation controls the half-life of Fe in the first 4 m above the seafloor. It is possible that our assumption of solute transport by eddy diffusion is not correct. Alternatively, decreasing Fe and $Si(OH)_4$ concentration above the seafloor could be due to super-imposed water layers with different Fe and $Si(OH)_4$ concentrations but little vertical exchange. In this case our calculated half-life would be an underestimation.

Table II.4: Modelled half-lifes ($t_{1/2}$) of dissolved Fe within the first 4 m distance from the seafloor at Stations 3 and 4 and data used for determination of $t_{1/2}$ using Eq. II.4 and Eq. II.5.

station	water depth	$Si(OH)_4$ flux benthic chamber (F_{Si})	$Si(OH)_4$ concentration gradient (d_{Si})	eddy diffusion coefficient (K_y)	modelled Fe at sediment surface (C_{BW})	Fe oxidation constant (k_{Feox})	half-life in near-bottom water column ($t_{1/2}$)
	(m)	(μmol cm^{-2} d^{-1})	(μmol cm^{-3} cm^{-1})	(m^2 s^{-1})	(nM)	(d^{-1})	(min)
3	130	0.73	$-4.05*10^{-6}$	$1.55*10^{6}$	70	400	2.5
4	145	0.33	$-1.44*10^{-6}$	$1.96*10^{6}$	81	3500	0.3

As mentioned above (chapter II.4.1.1), in the absence of oxygen, removal processes of dissolved Fe could be related to oxidation of dissolved Fe with NO_2^- or to interactions with suspended particles, which are likely to be most abundant directly above the seafloor. Further research on dissolved-particulate interactions, including the role of colloidal Fe, in bottom waters is needed to better constrain how sedimentary Fe fluxes are modified in the near-bottom water column.

II.4.1.3 Controls on the temporal variability of benthic iron fluxes

The Peruvian OMZ is known to experience high-amplitude fluctuations in upwelling intensity as well as variability in bottom water oxygen, NO_3^-, NO_2^- and H_2S concentrations (Pennington et al., 2006; Gutiérrez et al., 2008; Graco et al., 2017; Ohde, 2018). To get an insight into how different biogeochemical conditions control benthic diffusive Fe(II) fluxes, we compared the fluxes from our recent cruise with fluxes from our earlier cruise M92 (Fig. II.9). Cruise M92 took place in austral autumn 2013 following the main upwelling season and during a period of intense primary productivity. Due to reduced upwelling and stable density stratification, the water column on the shallow shelf was not only depleted in oxygen but also in NO_3^- and NO_2^- during cruise M92 (Sommer et al., 2016). Under such conditions, chemolithoautotrophic H_2S oxidation with NO_3^- or NO_2^- was impeded so that pore water H_2S could be released from the sediment into the water column. As a result, the water

column during M92 was sulfidic between around 50 – 150 m water depth with the highest H_2S concentration of 13 µM observed at 50 m depth (Fig. II.2). While the biogeochemical conditions on the shallow shelf were fundamentally different to those during M136 and M137, below 150 m water depth the conditions were largely comparable (oxygen-depleted, NO_3^-: 20 – 30 µM, NO_2^- up to 9 µM between 150 – 300 m). At the stations with similar biogeochemical water column conditions, the Fe(II) fluxes during both sampling campaigns were remarkably similar (Fig. II.9). However, similar to the temporal variability of Fe concentrations in bottom waters at Station 1 (Fig. II.3a), we observed a pronounced difference in the diffusive flux magnitude on the shallow shelf where the biogeochemical conditions differed between both cruises. The highest diffusive flux during M92 in 2013 of -22.7 mmol m^{-2} y^{-1} was measured at Station 1. By contrast, during M136/137 in 2017 we determined a much lower flux of -2.6 mmol m^{-2} y^{-1} at this station. During M136 and M137 the highest flux of -17.5 mmol m^{-2} y^{-1} was measured at Station 4 at 145 m water depth.

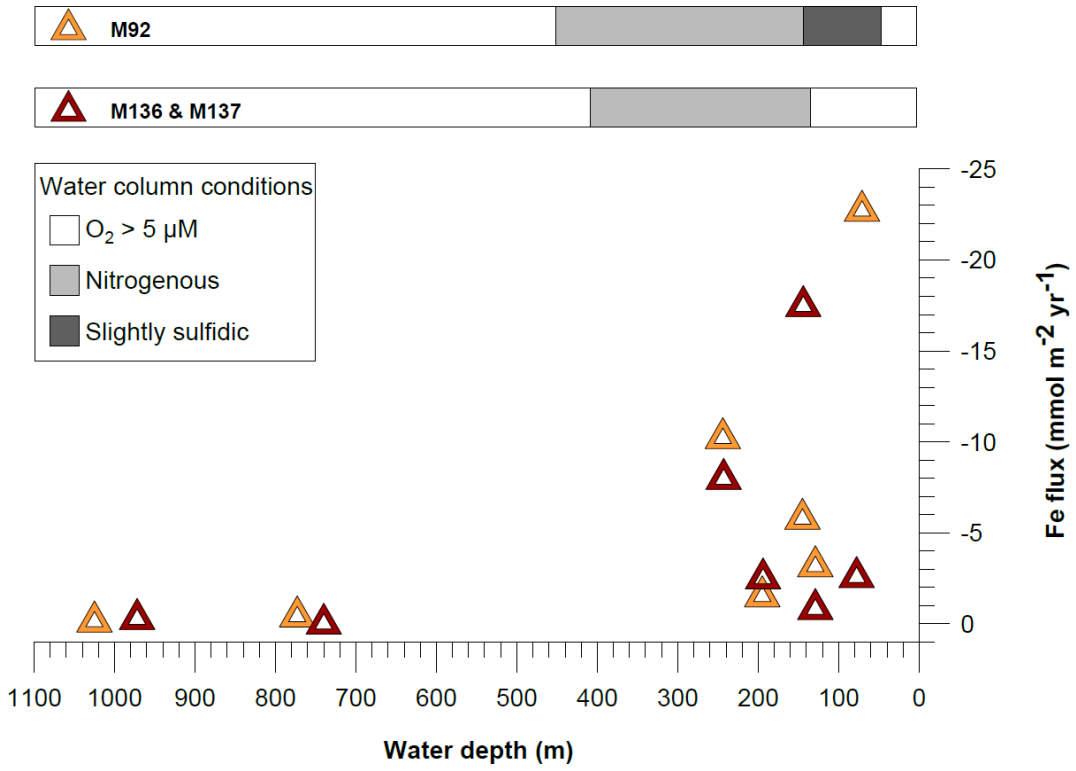

Figure II.9: Comparison of benthic diffusive Fe(II) fluxes between cruises M136 & M137 and M92 on the Peruvian shelf. Negative values represent fluxes from the sediment pore water into the bottom waters. Shaded bars on the upper panel display the geochemical conditions in the water column during the time of sampling.

Diffusive fluxes are a function of the concentration gradient between pore water and bottom water (Eq. II.1). As dissolved Fe concentrations in bottom waters are generally much lower (nM) compared to those observed in pore waters (µM), the flux magnitude is chiefly determined by differences in pore water Fe concentrations. During M92, pore waters at the sediment surface were characterized by high dissolved Fe concentrations (4.8 µM in the upper pore water sample), which resulted in a steep gradient and a comparably high Fe flux. Under the slightly sulfidic conditions that prevailed in the water column during M92, oxidative removal of dissolved Fe(II) with NO_3^- or NO_2^- was impeded (Scholz et al., 2016) and dissolved Fe(II) could be stabilized as aqueous iron sulfide (Schlosser et al., 2018). Therefore, the bottom water was characterized by high dissolved Fe concentrations (up to 0.7 µM in the supernatant bottom water of MUCs).

Despite oxic conditions in the water column during M136 and M137, we observed much higher H_2S concentrations in surface sediments at Station 1 compared to M92 (4100 µM during M136 and M137 versus 1800 µM during M92 within the first 8 cm of the core) (Fig. II.4). Because of higher H_2S concentrations, Fe concentrations were controlled by the solubility of Fe monosulfide minerals (FeS). It may seem counterintuitive that the surface sediment was highly sulfidic, while the overlying water column was oxygenated. In order to explain this observation, we need to consider the role of mats of filamentous sulfur oxidizing bacteria in controlling H_2S concentrations in surface sediments. (Gutiérrez et al., 2008; Noffke et al., 2012; Yücel et al., 2017). During M92 these mats were generally abundant on the shelf and upper slope (Sommer et al., 2016), thus limiting the extent of H_2S accumulation within surface sediments. Previous studies demonstrated that mats of sulfur oxidizing bacteria can disappear during periods of oxygenation (Gutiérrez et al., 2008). Consistent with this previous finding, visual inspection of the seafloor using the video-guided MUC revealed that the abundance of bacterial mats on the seafloor seemed greatly reduced, which is most probably related to oxic bottom water conditions on the shallow shelf during the coastal El Niño event. As these microaerophilic organisms tend to avoid high oxygen concentrations they probably started to die off or withdraw into the sediment once oxygen levels raised. We suggest that the disappearance of sulfide-oxidizing bacteria under oxic conditions created a situation where H_2S accumulation in the surface sediment and FeS precipitation limited the extent of Fe release into the bottom water.

Table II.2: Comparison of benthic diffusive Fe(II) fluxes out of the sediment and geochemical bottom water conditions between M136 & M137 and M92 on the Peruvian shelf. Fluxes during M92 correspond to similar depth (see Fig. II.9).

station	M136 & M137	M136 & M137	M136 & M137	M136 & M137	M136 & M137	M136 & M137	M92	M92
	water depth	latitude	longitude	water column condition	Fe(II) flux diffusive	Fe flux benthic chamber	water column condition	Fe(II) flux diffusive
	(m)	(S)	(W)		(mmol m^{-2} y^{-1})	(mmol m^{-2} y^{-1})		(mmol m^{-2} y^{-1})
1	75	12°13.52	77°10.93	O_2 < 5 µM	-2.56	–	slightly sulfidic	-22.69
3	130	12°16.68	77°14.95	nitrogenous	-0.81	–	slightly sulfidic	-3.16
4	145	12°18.71	77°17.80	nitrogenous	-17.45	-8.57 ± 2.18	nitrogenous	-5.77
5	195	12°21.50	77°21.70	nitrogenous	-2.49	–	nitrogenous	-1.51
6	245	12°23.30	77°24.82	nitrogenous	-7.96	-5.43 ± 2.36	nitrogenous	-10.20
9	750	12°31.35	77°35.01	O_2 > 5 µM	0.00	-6.11 ± 3.12	O_2 > 5 µM	0.00
10	950	12°34.90	77°40.32	O_2 > 5 µM	-0.26	–	O_2 > 5 µM	-0.12

II.4.2 Benthic cadmium cycling

II.4.2.1 Comparison of diffusive and in-situ benthic chamber cadmium fluxes

At stations above and below the permanent OMZ (Station 1, 9 and 10), the slopes of Cd concentrations versus time during benthic chamber incubations were largely consistent with theoretical Cd concentration gradients over time based on our diffusive flux estimates (Fig. II.7). In contrast, the fluxes determined with benthic chambers at stations within the OMZ (Station 4, 5 and 6) were 25 to 40 times higher than the diffusive flux (Table II.3). This discrepancy demonstrates that diffusion cannot be the dominant process leading to the continuous decrease of dissolved Cd during benthic chamber incubations. Alternatively, Cd could be precipitated within the benthic chamber and removed through downward sinking of Cd-rich particles. Cadmium sulfide (greenockite) has a relatively low solubility compared to sulfide minerals of other

TMs (CdS << FeS). It is generally agreed that CdS precipitation can take place at trace amounts of H_2S (H_2S < 1 µM, i.e., below the detection limit of the method applied in this study) (Davies-Colley et al., 1985; Rosenthal et al., 1995). Previous studies using in-situ benthic flux chambers have concluded that production of H_2S in the sediment or the accumulation of H_2S in benthic chambers during incubations can switch the direction of the Cd flux or intensify Cd removal through CdS precipitation (Westerlund et al., 1986; Colbert et al., 2001). Precipitation of CdS during the incubation is, therefore, a viable explanation for the discrepancy between diffusive Cd flux and Cd fluxes in benthic chambers observed in our study. Furthermore, the three different trends of Cd concentrations observed in benthic chamber incubations can be related to H_2S concentrations in the surface sediment below the benthic chambers (Table II.3). At stations within the OMZ (Station 4, 5 and 6), pore water H_2S concentrations in surface sediments were moderate (few µM). It is likely that there was a continuous leakage of trace amounts of H_2S from the pore water into the bottom waters during the incubation, thus leading to CdS precipitation and declining Cd concentrations. On the shallowest shelf station (Station 1), where pore water H_2S concentrations in the surface sediment were high (hundreds of µM), a potentially large amount could have been released at the beginning of the incubation, thus explaining pronounced Cd depletion in the chamber compared to the surrounding bottom water (0.1 nM within the chamber compared to 0.4 nM outside the chamber). Below the OMZ (Station 9 and 10), where there was no H_2S present in surface sediments, there was no Cd depletion in the chamber during the incubation and, consistent with previous studies in oxic settings (Westerlund et al., 1986; Ciceri et al., 1992; Zago et al., 2000; Turetta et al., 2005), both diffusive and benthic chamber flux data were indicative of an upward-directed flux out of the sediment. Due to the absence of H_2S, dissolved Cd released from biogenic particles in the surface sediment could accumulate in the pore water thus driving a diffusive flux out of the sediment.

II.4.2.2 Quantification of the sedimentary cadmium sink

Consistent with our Cd flux data there is general consent that OMZs are a sink for Cd. Several water column studies have observed Cd depletion in water masses within the Peruvian and other OMZs, which was mostly attributed to Cd removal via CdS precipitation in sulfidic micro-niches within particles in the water column (Janssen

et al., 2014; Conway and John, 2015a). Sedimentary studies showed that Cd is highly enriched in OMZ sediments, which has mostly been attributed to the delivery of Cd with organic material and subsequent fixation as CdS within sulfidic sediments (Ragueneau et al., 2000; Böning et al., 2004; Borchers et al., 2005; Muñoz et al., 2012; Little et al., 2015). Based on our data, we can quantify the delivery of Cd to the sediments via three different pathways: (1) diffusion across the sediment-water interface and CdS precipitation within the sediment; (2) Cd incorporation by phytoplankton and delivery to the sediment with organic matter; (3) CdS precipitation in the water column and particulate delivery to the sediment (Table II.3).

The enrichment of Cd in the sediment relative to the lithogenic background (expressed as excess Cd concentration; Cd_{xs}) was calculated using the following equation (Brumsack, 2006):

$$Cd_{xs} = Cd_{sample} - Al_{sample} * (Cd/Al)_{crust} \quad \text{(Eq. II.6)}$$

The Cd/Al ratio of the upper continental crust ($1.22*10^{-6}$) was used as lithogenic background reference (Taylor and McLennan, 2009). To calculate the flux of Cd to the sediment, Cd_{xs} was multiplied with the mass accumulation rate (MAR) from published data for each individual site (Dale et al., 2015b). To approximate the amount of Cd delivered to the sediment with organic material, the average concentration ratio of Cd to C in phytoplankton (Moore et al., 2013) was multiplied by published particulate organic carbon rain rates (maximum estimate) or burial rates (minimum estimate) for each individual site (Dale et al., 2015b). The Cd delivery via precipitation in the water column was determined as the remainder of Cd_{xs} * MAR after subtraction of the two other sources (i.e., diffusive flux and minimum/maximum delivery by organic material).

Sediments at all stations on the Peruvian shelf and slope are enriched in Cd relative to the lithogenic background. The accumulation rate of Cd decreases with distance from the coast from 250 µmol m^{-2} y^{-1} at Station 1 to 4 µmol m^{-2} y^{-1} at Station 9 (Table II.3). These fluxes generally exceed the amount of Cd delivered to the sediments via diffusion and associated with organic material. Together these mechanisms of Cd delivery can only account for ~ 20 % of the Cd enrichment at stations above and inside the permanent OMZ, with the delivery with organic material being of greater importance. The remaining Cd enrichment in the sediment (~ 80 %), after subtraction of diffusive and minimum/maximum organic Cd sources, must be

related to CdS precipitation in the water column and delivery of Cd-rich particles to the sediment. This removal process can be a combination of CdS precipitation in sulfidic micro-niches around sinking particles (Janssen et al., 2014; Bianchi et al., 2018), CdS precipitation in sulfide plumes (Xie et al., 2019) when sedimentary H_2S can spread throughout the water column (Schunck et al., 2013; Ohde, 2018), and precipitation of CdS in the near-bottom water (this study). Our estimated CdS precipitation in the water column within the OMZ agrees with the Cd fluxes determined from benthic chamber incubations, where dissolved Cd removal takes place in the 20 – 30 cm of overlying water above the seafloor. These Cd removal fluxes from benthic chambers alone are sufficient to account for 41 % – 68 % of the estimated particulate Cd removal from the water column and 38 % – 60 % of total Cd enrichment in the sediment within the OMZ (Table II.3). Considering that Cd precipitation in near-bottom water is unlikely to be restricted to the 20 – 30 cm above the seafloor, covered by our benthic chambers, the removal flux associated with this process is likely to be even higher. At Station 1, where the surface sediment below the benthic chamber was highly sulfidic, the particulate Cd removal calculated from the concentration difference between the bottom water (0.5 m) and the first sample from the benthic chamber incubation (taken after 0.25 h) was high enough to explain the total Cd enrichment in the sediment. Below the OMZ, at Station 9, where the smallest Cd enrichment was observed, the relative contribution of Cd delivery with organic material increases. About half of the Cd enrichment can be attributed to organic material at this station.

Once Cd is delivered to the sediment, it can either stay fixed in the solid phase or be released to the pore waters. Cadmium concentrations in pore waters of subsurface sediments (> 10 cm sediment depth) were mostly higher than bottom water concentrations (Fig. II.6), indicating a transfer of Cd from the solid phase into pore waters during early diagenesis. Cadmium sulfides are considered highly insoluble and stable within sediments (Elderfield et al., 1981), even upon re-oxygenation (Rosenthal et al., 1995). Therefore, Cd release through re-dissolution of CdS is ruled out as a potential source of dissolved Cd. Alternatively, Cd liberation upon remineralization of organic material could explain elevated Cd concentrations in the pore water. Elevated Cd concentrations in sulfidic pore waters have been observed in previous studies and attributed to Cd stabilization through formation of organic and inorganic complexes (Gobeil et al., 1987; Sundby et al., 2004). Experimental data gave evidence for the presence of dissolved Cd bisulfide and polysulfide complexes in pore waters. An

increase of electrochemically active Cd after UV irradiation, was explained by the destruction of electrochemically inactive bisulfide and polysulfide complexes (Gobeil et al., 1987). At very high H_2S concentrations (> 10^{-3} M) the solubility of Cd may increase due to an increase in these bisulfide and polysulfide complexes. Under such highly sulfidic conditions, Cd solubility may even exceed the solubility in oxygenated waters and highly sulfidic sediment can eventually lead to a diffusive source of Cd to the bottom water (Davies-Colley et al., 1985). Such a scenario may explain the negative (i.e., upward-directed) diffusive Cd flux at Station 1, where the pore waters of surface sediments are highly sulfidic.

Table II.3: Comparison of sedimentary Cd excess compared to the lithogenic background and the contribution of Cd delivery to the sediment via different pathways: (1) diffusion across the sediment-water interface and Cd sulfide precipitation within the sediment; (2) Cd incorporation by phytoplankton and delivery to the sediment with organic matter; (3) Cd sulfide precipitation in the water column and particulate delivery to the sediment.

station	water depth	Cd excess sediment[1]	(1) Cd flux diffusive	Cd flux benthic chamber	H_2S in surface sediment below benthic chamber	(2) Cd from organic matter[2]	(3) CdS precipitation in water column[3]
	(m)	(µmol m^{-2} y^{-1})	(µmol m^{-2} y^{-1})	(µmol m^{-2} y^{-1})	(µM)	(µmol m^{-2} y^{-1})	(µmol m^{-2} y^{-1})
1	75	248.87	-1.85	– (3109.5)[4]	641.02	8.34 – 49.04	199.83 – 240.53
3	130	153.41	0.83	–	–	4.87 – 17.40	135.19 – 147.72
4	145	35.07	0.54	13.4 ± 1.05	1.30	1.55 – 6.48	28.07 – 32.99
5	195	44.76	0.63	22.6 ± 3.24	9.52	5.71 – 7.71	36.36 – 38.36
6	245	35.15	0.55	21.2 ± 3.31	0.40	3.60 – 6.54	28.06 – 31.00
9	750	4.44	-0.30	0.00 ± 0.02	0.00	1.48 – 3.21	1.23 – 2.96
10	950	–	–	–	0.00	–	–

[1] Calculated after Brumsack (2006) and multiplied by the mass accumulation rate for each site (Dale et al., 2015b). [2] Determined by multiplication of Cd/C ratio in average phytoplankton (Moore et al., 2013) with particulate organic carbon rain rates (maximum values) and organic carbon accumulation rates (minimum values) for each individual site (data from Dale et al., 2015b). [3] Remainder of Cd excess in sediment after subtraction of diffusive and minimum and maximum organic Cd sources. [4] Flux calculated from the concentration difference between the bottom water (0.5 m) and the first sample from the benthic chamber incubation (taken after 0.25 h).

II.5 Conclusions and implications for trace metal sources and sinks in the future ocean

Consistent with earlier work, our results demonstrate that that OMZ sediments are a source for Fe and a sink for Cd. Moreover, based on our findings, biogeochemical conditions and processes that control the benthic fluxes of these TMs across the Peruvian OMZ can be further constrained.

Within the OMZ, where bottom dwelling macrofauna is absent, diffusion is the main process that transports Fe from the sediment pore water into the bottom water. The accumulation of high levels of H_2S in pore waters, modulated by the abundance of sulfur oxidizing bacteria, can reduce diffusive Fe release through sulfide precipitation within pore waters. In anoxic bottom waters Fe can be rapidly removed, likely via oxidation with NO_2^- and/or interaction with particles. Benthic Cd fluxes are directed from the bottom water into the sediment within the OMZ. Diffusive fluxes and delivery of Cd via organic material cannot account for the sedimentary Cd enrichment. Instead CdS precipitation in near-bottom waters could be the most important pathway that delivers Cd to the sediments.

According to our results, H_2S concentrations in surface sediments exert a first order control on the magnitude and direction of Fe and Cd fluxes across the sediment-water interface. With generally decreasing oxygen concentrations in the ocean and an expansion of OMZs (Stramma et al., 2008; Schmidtko et al., 2017), sulfidic surface sediments will likely also expand. With regard to the solubility of their sulfide minerals, Fe and Cd represent two opposite end members. The solubility of sulfide minerals of other important nutrient-type TMs, such as Ni and Zn, is intermediate between those of Fe and Cd (Fe > Ni > Zn > Cd). An expansion of sulfidic surface sediments is thus likely to affect sedimentary TM fluxes in a differing manner. This notion is illustrated in Fig. II.10, showing saturation indices calculated based on the range of TM concentrations observed in the ocean and typical H_2S concentrations observed in anoxic marine environments (nM – µM concentrations represent sulfidic events in the water column; µM – mM concentrations are typical for pore waters). Cadmium sulfide minerals become oversaturated at nM to µM H_2S concentrations, which explains why Cd removal can take place in the bottom water in OMZs. By contrast, FeS is highly undersaturated under the typical biogeochemical conditions in the water column. Therefore, FeS precipitation is unlikely to take place in the water column, even under

somewhat more reducing conditions. Other sulfide-forming TMs have an intermediate sulfide solubility (e.g. Zn, Ni), which could imply that the direction and magnitude of their sedimentary fluxes is susceptible to expanding ocean anoxia. The differing response of TMs to an expansion of sulfidic conditions may cause a change in the TM stoichiometry of upwelling water masses with potential consequences for TM-dependent marine ecosystems in surface waters.

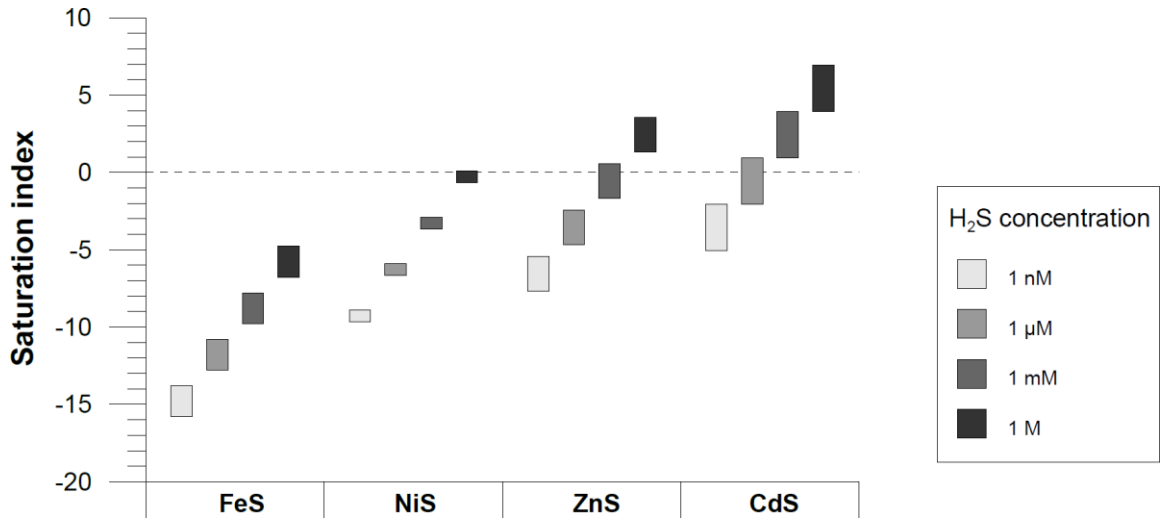

Figure II.10: Schematic overview of the possible mobility of different trace metal to an expansion of sulfidic conditions. Saturation indices (SI) were calculated for different H_2S concentrations and reported minimum and maximum concentrations of trace metals in the water column (data from Bruland and Lohan 2003). Equilibrium constants (log K under standard conditions) for Fe (FeS ppt: -3.92), Ni (millerite: -8.04), Zn (sphalerite: -11.62) and Cd (greenokite: -15.93) were taken from the PHREEQC WATEQ$_4$F database (Ball and Nordstrom, 1991).The results are approximate since concentrations instead of activities were used for calculations. A positive SI is indicative of oversaturation whereas a negative SI is indicative of undersaturation.

Acknowledgements

We are grateful for the support of the crew of RV Meteor during the fieldwork. For their technical and analytical assistance we thank A. Beck, A. Bleyer, B. Domeyer, D. Jasinski, A. Petersen, T. Steffens, R. Surberg and M. Türk. This study was supported by the German Research Foundation through the Emmy Noether

Nachwuchsforschergruppe ICONOX (Iron Cycling in Continental Margin Sediments and the Nutrient and Oxygen Balance of the Ocean) and Sonderforschungsbereich 754 (Climate-Biogeochemistry Interactions in the Tropical Ocean). We also would like to thank Edouard Metzger and Michael Staubwasser for their constructive reviews, as well as S. Wajih A. Naqvi for the editorial handling.

References

Audry, S., Blanc, G., Schäfer, J., Chaillou, G. and Robert, S.: Early diagenesis of trace metals (Cd, Cu, Co, Ni, U, Mo, and V) in the freshwater reaches of a macrotidal estuary, Geochim. Cosmochim. Acta, 70(9), 2264–2282, doi:10.1016/j.gca.2006.02.001, 2006.

Ball, J. W. and Nordstrom, D. K.: WATEQ4F -- User's manual with revised thermodynamic data base and test cases for calculating speciation of major, trace and redox elements in natural waters, US Geol. Surv., (Open-File Rep.), 91–183, doi:10.3133/ofr90129, 1991.

Bianchi, D., Weber, T. S., Kiko, R. and Deutsch, C.: Global niche of marine anaerobic metabolisms expanded by particle microenvironments, Nat. Geosci., 11(April), 1–6, doi:10.1038/s41561-018-0081-0, 2018.

Biller, D. V. and Bruland, K. W.: Sources and distributions of Mn, Fe, Co, Ni, Cu, Zn, and Cd relative to macronutrients along the central California coast during the spring and summer upwelling season, Mar. Chem., 155, 50–70, doi:10.1016/j.marchem.2013.06.003, 2013.

Böning, P., Brumsack, H. J., Böttcher, M. E., Schnetger, B., Kriete, C., Kallmeyer, J. and Borchers, S. L.: Geochemistry of Peruvian near-surface sediments, Geochim. Cosmochim. Acta, 68(21), 4429–4451, doi:10.1016/j.gca.2004.04.027, 2004.

Bopp, L., Le Quéré, C., Heimann, M., Manning, A. C. and Monfray, P.: Climate-induced oceanic oxygen fluxes: Implications for the contemporary carbon budget, Global Biogeochem. Cycles, 16(2), 6-1-6–13, doi:10.1029/2001GB001445, 2002.

Borchers, S. L., Schnetger, B., Böning, P. and Brumsack, H.-J.: Geochemical

signatures of the Namibian diatom belt: Perennial upwelling and intermittent anoxia, Geochemistry, Geophys. Geosystems, 6(6), doi:10.1029/2004GC000886, 2005.

Boudreau, B. P.: Diagenetic Models and Their Implementation, Springer., 1997.

Boyd, P. W. and Ellwood, M. J.: The biogeochemical cycle of iron in the ocean, Nat. Geosci., 3(10), 675–682, doi:10.1038/ngeo964, 2010.

Bruland, K. W. and Lohan, M. C.: Controls of Trace Metals in Seawater, in Treatise on Geochemistry, pp. 23–47, Elsevier., 2003.

Brumsack, H. J.: The trace metal content of recent organic carbon-rich sediments: Implications for Cretaceous black shale formation, Palaeogeogr. Palaeoclimatol. Palaeoecol., 232(2–4), 344–361, doi:10.1016/j.palaeo.2005.05.011, 2006.

Canfield, D. E.: Reactive iron in marine sediments, Geochim. Cosmochim. Acta, 53(3), 619–632, doi:10.1016/0016-7037(89)90005-7, 1989.

Carlson, H. K., Clark, I. C., Blazewicz, S. J., Iavarone, A. T. and Coates, J. D.: Fe(II) Oxidation Is an Innate Capability of Nitrate-Reducing Bacteria That Involves Abiotic and Biotic Reactions, J. Bacteriol., 195(14), 3260–3268, doi:10.1128/JB.00058-13, 2013.

Ciceri, G., Maran, C., Martinotti, W. and Queirazza, G.: Geochemical cycling of heavy metals in a marine coastal area: benthic flux determination from pore water profiles and in situ measurements using benthic chambers, Hydrobiologia, 235–236(1), 501–517, doi:10.1007/BF00026238, 1992.

Colbert, D., Coale, K. ., Berelson, W. . and Johnson, K. .: Cadmium Flux in Los Angeles/Long Beach Harbours and at Sites along the California Continental Margin, Estuar. Coast. Shelf Sci., 53(2), 169–180, doi:10.1006/ecss.2001.0802, 2001.

Collier, R. and Edmond, J.: The trace element geochemistry of marine biogenic particulate matter, Prog. Oceanogr., 13(2), 113–199, doi:10.1016/0079-6611(84)90008-9, 1984.

Conway, T. M. and John, S. G.: Quantification of dissolved iron sources to the North Atlantic Ocean, Nature, 511(7508), 212–215, doi:10.1038/nature13482, 2014.

Conway, T. M. and John, S. G.: Biogeochemical cycling of cadmium isotopes along a high-resolution section through the North Atlantic Ocean, Geochim. Cosmochim.

Acta, 148, 269–283, doi:10.1016/j.gca.2014.09.032, 2015a.

Conway, T. M. and John, S. G.: The cycling of iron, zinc and cadmium in the North East Pacific Ocean - Insights from stable isotopes, Geochim. Cosmochim. Acta, 164, 262–283, doi:10.1016/j.gca.2015.05.023, 2015b.

Dale, A. W., Nickelsen, L., Scholz, F., Hensen, C., Oschlies, A. and Wallmann, K.: A revised global estimate of dissolved iron fluxes from marine sediments, Global Biogeochem. Cycles, 29(5), 691–707, doi:10.1002/2014GB005017, 2015a.

Dale, A. W., Sommer, S., Lomnitz, U., Montes, I., Treude, T., Liebetrau, V., Gier, J., Hensen, C., Dengler, M., Stolpovsky, K., Bryant, L. D. and Wallmann, K.: Organic carbon production, mineralisation and preservation on the Peruvian margin, Biogeosciences, 12(5), 1537–1559, doi:10.5194/bg-12-1537-2015, 2015b.

Dalsgaard, T., Thamdrup, B., Farías, L. and Revsbech, N. P.: Anammox and denitrification in the oxygen minimum zone of the eastern South Pacific, Limnol. Oceanogr., 57(5), 1331–1346, doi:10.4319/lo.2012.57.5.1331, 2012.

Davies-Colley, R. J., Nelson, P. O. and Williamson, K. J.: Sulfide control of cadmium and copper concentrations in anaerobic estuarine sediments, Mar. Chem., 16(2), 173–186, doi:10.1016/0304-4203(85)90021-0, 1985.

Dengler, M.: Hydrochemistry of water samples during METEOR cruise M92. PANGAEA, https://doi.org/10.1594/PANGAEA.862046, 2016.

Echevin, V., Colas, F., Espinoza-Morriberon, D., Vasquez, L., Anculle, T. and Gutierrez, D.: Forcings and Evolution of the 2017 Coastal El Niño Off Northern Peru and Ecuador, Front. Mar. Sci., 5(October), 1–16, doi:10.3389/fmars.2018.00367, 2018.

Ehlert, C., Doering, K., Wallmann, K., Scholz, F., Sommer, S., Grasse, P., Geilert, S. and Frank, M.: Stable silicon isotope signatures of marine pore waters – Biogenic opal dissolution versus authigenic clay mineral formation, Geochim. Cosmochim. Acta, 191, 102–117, doi:10.1016/j.gca.2016.07.022, 2016.

Elderfield, H., McCaffrey, R. J., Luedtke, N., Bender, M. and Truesdale, V. W.: Chemical diagenesis in Narragansett Bay sediments, Am. J. Sci., 281(8), 1021–1055, doi:10.2475/ajs.281.8.1021, 1981.

Elrod, V. A., Berelson, W. M., Coale, K. H. and Johnson, K. S.: The flux of iron from continental shelf sediments: A missing source for global budgets, Geophys. Res. Lett., 31(12), n/a-n/a, doi:10.1029/2004GL020216, 2004.

Fitzsimmons, J. N., Conway, T. M., Lee, J.-M., Kayser, R., Thyng, K. M., John, S. G. and Boyle, E. A.: Dissolved iron and iron isotopes in the southeastern Pacific Ocean, Global Biogeochem. Cycles, 30(10), 1372–1395, doi:10.1002/2015GB005357, 2016.

Friedrich, J., Dinkel, C., Friedl, G., Pimenov, N., Wijsman, J., Gomoiu, M.-T., Cociasu, A., Popa, L. and Wehrli, B.: Benthic Nutrient Cycling and Diagenetic Pathways in the North-western Black Sea, Estuar. Coast. Shelf Sci., 54(3), 369–383, doi:10.1006/ecss.2000.0653, 2002.

Garreaud, R. D.: A plausible atmospheric trigger for the 2017 coastal El Niño, Int. J. Climatol., 38(January 2017), e1296–e1302, doi:10.1002/joc.5426, 2018.

Gendron, A., Silverberg, N., Sundby, B. and Lebel, J.: Early diagenesis of cadmium and cobalt in sediments of the Laurentian Trough, Geochim. Cosmochim. Acta, 50(5), 741–747, doi:10.1016/j.ijmachtools.2007.10.013, 1986.

Gerringa, L. J. A.: Aerobic degradation of organic matter and the mobility of Cu, Cd, Ni, Pb, Zn, Fe and Mn in marine sediment slurries, Mar. Chem., 29(C), 355–374, doi:10.1016/0304-4203(90)90023-6, 1990.

Gobeil, C., Silverberg, N., Sundby, B. and Cossa, D.: Cadmium diagenesis in Laurentian Trough sediments, Geochim. Cosmochim. Acta, 51(3), 589–596, doi:10.1016/0016-7037(87)90071-8, 1987.

Graco, M. I., Purca, S., Dewitte, B., Castro, C. G., Morón, O., Ledesma, J., Flores, G. and Gutiérrez, D.: The OMZ and nutrient features as a signature of interannual and low-frequency variability in the Peruvian upwelling system, Biogeosciences, 14(20), 4601–4617, doi:10.5194/bg-14-4601-2017, 2017.

Grasshoff, M., Erhardt, M. and Kremling, K.: Methods of seawater analysis., Wiley-VCH, Weinheim, doi:10.1002/ange.19770890738, 1999.

Gutiérrez, D., Enríquez, E., Purca, S., Quipúzcoa, L., Marquina, R., Flores, G. and Graco, M.: Oxygenation episodes on the continental shelf of central Peru: Remote forcing and benthic ecosystem response, Prog. Oceanogr., 79(2–4), 177–189, doi:10.1016/j.pocean.2008.10.025, 2008.

Hawco, N. J., Ohnemus, D. C., Resing, J. A., Twining, B. S. and Saito, M. A.: A dissolved cobalt plume in the oxygen minimum zone of the eastern tropical South Pacific, Biogeosciences, 13(20), 5697–5717, doi:10.5194/bg-13-5697-2016, 2016.

Heller, M. I., Lam, P. J., Moffett, J. W., Till, C. P., Lee, J. M., Toner, B. M. and Marcus, M. A.: Accumulation of Fe oxyhydroxides in the Peruvian oxygen deficient zone implies non-oxygen dependent Fe oxidation, Geochim. Cosmochim. Acta, 211, 174–193, doi:10.1016/j.gca.2017.05.019, 2017.

Helm, K. P., Bindoff, N. L. and Church, J. A.: Observed decreases in oxygen content of the global ocean, Geophys. Res. Lett., 38(23), 1–6, doi:10.1029/2011GL049513, 2011.

Homoky, W. B., Severmann, S., McManus, J., Berelson, W. M., Riedel, T. E., Statham, P. J. and Mills, R. A.: Dissolved oxygen and suspended particles regulate the benthic flux of iron from continental margins, Mar. Chem., 134–135, 59–70, doi:10.1016/j.marchem.2012.03.003, 2012.

Hydes, D., Aoyama, M., Aminot, A., Bakker, K., Becker, S., Coverly, S., Daniel, A., Dickson, A. G., Grosso, O., Kerouel, R., van Ooijen, J., Sato, K., Tanhua, T., Woodward, E. M. S. and Zhang, J. Z.: Determination of dissolved nutrients (N, P, Si) in seawater with high precision and inter-comparability using gas-segmented continuous flow analysers, Go-sh. Repeat Hydrogr. Man. IOCCP Rep. A Collect. Expert Reports Guidel., 134(14), 1–87 [online] Available from: http://archimer.ifremer.fr/doc/00020/13141/, 2010.

Janssen, D. J., Conway, T. M., John, S. G., Christian, J. R., Kramer, D. I., Pedersen, T. F. and Cullen, J. T.: Undocumented water column sink for cadmium in open ocean oxygen-deficient zones, Proc. Natl. Acad. Sci., 111(19), 6888–6893, doi:10.1073/pnas.1402388111, 2014.

John, S. G., Helgoe, J., Townsend, E., Weber, T., DeVries, T., Tagliabue, A., Moore, K., Lam, P., Marsay, C. M. and Till, C.: Biogeochemical cycling of Fe and Fe stable isotopes in the Eastern Tropical South Pacific, Mar. Chem., 201(March), 66–76, doi:10.1016/j.marchem.2017.06.003, 2018.

Karstensen, J., Stramma, L. and Visbeck, M.: Oxygen minimum zones in the eastern tropical Atlantic and Pacific oceans, Prog. Oceanogr., 77(4), 331–350,

doi:10.1016/j.pocean.2007.05.009, 2008.

Keeling, R. F., Körtzinger, A. and Gruber, N.: Ocean Deoxygenation in a Warming World, Ann. Rev. Mar. Sci., 2(1), 199–229, doi:10.1146/annurev.marine.010908.163855, 2010.

Klar, J. K., Schlosser, C., Milton, J. A., Woodward, E. M. S., Lacan, F., Parkinson, I. J., Achterberg, E. P. and James, R. H.: Sources of dissolved iron to oxygen minimum zone waters on the Senegalese continental margin in the tropical North Atlantic Ocean: Insights from iron isotopes, Geochim. Cosmochim. Acta, 236, 60–78, doi:10.1016/j.gca.2018.02.031, 2018.

Klinkhammer, G., Heggie, D. T. and Graham, D. W.: Metal diagenesis in oxic marine sediments, Earth Planet. Sci. Lett., 61(2), 211–219, doi:10.1016/0012-821X(82)90054-1, 1982.

Klueglein, N. and Kappler, A.: Abiotic oxidation of Fe(II) by reactive nitrogen species in cultures of the nitrate-reducing Fe(II) oxidizer Acidovorax sp. BoFeN1 - questioning the existence of enzymatic Fe(II) oxidation, Geobiology, 11(2), 180–190, doi:10.1111/gbi.12019, 2013.

Lam, P. and Kuypers, M. M. M.: Microbial Nitrogen Cycling Processes in Oxygen Minimum Zones, Ann. Rev. Mar. Sci., 3(1), 317–345, doi:10.1146/annurev-marine-120709-142814, 2011.

Lam, P., Lavik, G., Jensen, M. M., van de Vossenberg, J., Schmid, M., Woebken, D., Gutierrez, D., Amann, R., Jetten, M. S. M. and Kuypers, M. M. M.: Revising the nitrogen cycle in the Peruvian oxygen minimum zone, Proc. Natl. Acad. Sci., 106(12), 4752–4757, doi:10.1073/pnas.0812444106, 2009.

Lane, T. W. and Morel, F. M. M.: A biological function for cadmium in marine diatoms, Proc. Natl. Acad. Sci., 97(9), 4627–4631, doi:10.1073/pnas.090091397, 2000.

Lee, J. and Morel, F.: Replacement of zinc by cadmium in marine phytoplankton, Mar. Ecol. Prog. Ser., 127(1–3), 305–309, doi:10.3354/meps127305, 1995.

Lenstra, W. K., Hermans, M., Séguret, M. J. M., Witbaard, R., Behrends, T., Dijkstra, N., van Helmond, N. A. G. M., Kraal, P., Laan, P., Rijkenberg, M. J. A., Severmann, S., Teacă, A. and Slomp, C. P.: The shelf-to-basin iron shuttle in the Black Sea revisited, Chem. Geol., 511(April), 314–341, doi:10.1016/j.chemgeo.2018.10.024,

2019.

Levin, L., Gutiérrez, D., Rathburn, A., Neira, C., Sellanes, J., Muñoz, P., Gallardo, V. and Salamanca, M.: Benthic processes on the Peru margin: a transect across the oxygen minimum zone during the 1997–98 El Niño, Prog. Oceanogr., 53(1), 1–27, doi:10.1016/S0079-6611(02)00022-8, 2002.

Li, Y.-H. and Gregory, S.: Diffusion of ions in sea water and in deep-sea sediments, Geochim. Cosmochim. Acta, 38(5), 703–714, doi:10.1016/0016-7037(74)90145-8, 1974.

Little, S. H., Vance, D., Lyons, T. W. and McManus, J.: Controls on trace metal authigenic enrichment in reducing sediments: Insights from modern oxygen-deficient settings, Am. J. Sci., 315(2), 77–119, doi:10.2475/02.2015.01, 2015.

Liu, X. and Millero, F. J.: The solubility of iron in seawater, Mar. Chem., 77(1), 43–54, doi:10.1016/S0304-4203(01)00074-3, 2002.

Lohan, M. C. and Bruland, K. W.: Elevated Fe(II) and dissolved Fe in hypoxic shelf waters off Oregon and Washington: An enhanced source of iron to coastal upwelling regimes, Environ. Sci. Technol., 42(17), 6462–6468, doi:10.1021/es800144j, 2008.

Metzger, E., Simonucci, C., Viollier, E., Sarazin, G., Prévot, F., Elbaz-Poulichet, F., Seidel, J.-L. and Jézéquel, D.: Influence of diagenetic processes in Thau lagoon on cadmium behavior and benthic fluxes, Estuar. Coast. Shelf Sci., 72(3), 497–510, doi:10.1016/j.ecss.2006.11.016, 2007.

Moore, C. M., Mills, M. M., Arrigo, K. R., Berman-Frank, I., Bopp, L., Boyd, P. W., Galbraith, E. D., Geider, R. J., Guieu, C., Jaccard, S. L., Jickells, T. D., La Roche, J., Lenton, T. M., Mahowald, N. M., Marañón, E., Marinov, I., Moore, J. K., Nakatsuka, T., Oschlies, A., Saito, M. A., Thingstad, T. F., Tsuda, A. and Ulloa, O.: Processes and patterns of oceanic nutrient limitation, Nat. Geosci., 6(9), 701–710, doi:10.1038/ngeo1765, 2013.

Morel, F. M. M., Milligan, A. J. and Saito, M. A.: Marine Bioinorganic Chemistry: The Role of Trace Metals in the Oceanic Cycles of Major Nutrients, in Treatise on Geochemistry, vol. 197, pp. 123–150, Elsevier., 2014.

Morse, J. W. and Luther, G. W.: Chemical influences on trace metal-sulfide interactions in anoxic sediments, Geochim. Cosmochim. Acta, 63(19–20), 3373–

3378, doi:10.1016/S0016-7037(99)00258-6, 1999.

Muñoz, P., Dezileau, L., Cardenas, L., Sellanes, J., Lange, C. B., Inostroza, J., Muratli, J. and Salamanca, M. A.: Geochemistry of trace metals in shelf sediments affected by seasonal and permanent low oxygen conditions off central Chile, SE Pacific (~36°S), Cont. Shelf Res., 33, 51–68, doi:10.1016/j.csr.2011.11.006, 2012.

Noble, A. E., Lamborg, C. H., Ohnemus, D. C., Lam, P. J., Goepfert, T. J., Measures, C. I., Frame, C. H., Casciotti, K. L., DiTullio, G. R., Jennings, J. and Saito, M. A.: Basin-scale inputs of cobalt, iron, and manganese from the Benguela-Angola front to the South Atlantic Ocean, Limnol. Oceanogr., 57(4), 989–1010, doi:10.4319/lo.2012.57.4.0989, 2012.

Noffke, A., Hensen, C., Sommer, S., Scholz, F., Bohlen, L., Mosch, T., Graco, M. and Wallmann, K.: Benthic iron and phosphorus fluxes across the Peruvian oxygen minimum zone, Limnol. Oceanogr., 57(3), 851–867, doi:10.4319/lo.2012.57.3.0851, 2012.

Ohde, T.: Coastal Sulfur Plumes off Peru During El Niño, La Niña, and Neutral Phases, Geophys. Res. Lett., 45(14), 7075–7083, doi:10.1029/2018GL077618, 2018.

Olson, L., Quinn, K. A., Siebecker, M. G., Luther, G. W., Hastings, D. and Morford, J. L.: Trace metal diagenesis in sulfidic sediments: Insights from Chesapeake Bay, Chem. Geol., 452, 47–59, doi:10.1016/j.chemgeo.2017.01.018, 2017.

Oschlies, A., Schulz, K. G., Riebesell, U. and Schmittner, A.: Simulated 21st century's increase in oceanic suboxia by CO 2-enhanced biotic carbon export, Global Biogeochem. Cycles, 22(4), 1–10, doi:10.1029/2007GB003147, 2008.

Pakhomova, S. V., Hall, P. O. J., Kononets, M. Y., Rozanov, A. G., Tengberg, A. and Vershinin, A. V.: Fluxes of iron and manganese across the sediment–water interface under various redox conditions, Mar. Chem., 107(3), 319–331, doi:10.1016/j.marchem.2007.06.001, 2007.

Peng, Q., Xie, S.-P., Wang, D., Zheng, X.-T. and Zhang, H.: Coupled ocean-atmosphere dynamics of the 2017 extreme coastal El Niño, Nat. Commun., 10(1), 298, doi:10.1038/s41467-018-08258-8, 2019.

Pennington, J. T., Mahoney, K. L., Kuwahara, V. S., Kolber, D. D., Calienes, R. and Chavez, F. P.: Primary production in the eastern tropical Pacific: A review, Prog.

Oceanogr., 69(2–4), 285–317, doi:10.1016/j.pocean.2006.03.012, 2006.

Plass, A., Schlosser, C., Sommer, S., Dale, Achterberg, E. P., A., Scholz, F.: Iron, cadmium and hydrogen sulfide data from near-bottom water, sediment pore water and benthic chamber incubations during METEOR cruises M136 and M137. PANGEA, https://doi.pangaea.de/10.1594/PANGAEA.918805 (dataset in review), 2020.

Point, D., Monperrus, M., Tessier, E., Amouroux, D., Chauvaud, L., Thouzeau, G., Jean, F., Amice, E., Grall, J., Leynaert, A., Clavier, J. and Donard, O. F. X.: Biological control of trace metal and organometal benthic fluxes in a eutrophic lagoon (Thau Lagoon, Mediterranean Sea, France), Estuar. Coast. Shelf Sci., 72(3), 457–471, doi:10.1016/j.ecss.2006.11.013, 2007.

Price, N. M. and Morel, F. M. M.: Cadmium and cobalt substitution for zinc in a marine diatom, Nature, 344(6267), 658–660, doi:10.1038/344658a0, 1990.

Ragueneau, O., Tréguer, P., Leynaert, A., Anderson, R. F., Brzezinski, M. A., DeMaster, D. J., Dugdale, R. C., Dymond, J., Fischer, G., François, R., Heinze, C., Maier-Reimer, E., Martin-Jézéquel, V., Nelson, D. M. and Quéguiner, B.: A review of the Si cycle in the modern ocean: Recent progress and missing gaps in the application of biogenic opal as a paleoproductivity proxy, Glob. Planet. Change, 26(4), 317–365, doi:10.1016/S0921-8181(00)00052-7, 2000.

Raiswell, R. and Canfield, D. E.: The Iron Biogeochemical Cycle Past and Present, Geochemical Perspect., 1(1), 1–220, doi:10.7185/geochempersp.1.1, 2012.

Rapp, I., Schlosser, C., Rusiecka, D., Gledhill, M. and Achterberg, E. P.: Automated preconcentration of Fe, Zn, Cu, Ni, Cd, Pb, Co, and Mn in seawater with analysis using high-resolution sector field inductively-coupled plasma mass spectrometry, Anal. Chim. Acta, 976, 1–13, doi:10.1016/j.aca.2017.05.008, 2017.

Rapp, I., Schlosser, C., Menzel Barraqueta, J.-L., Wenzel, B., Lüdke, J., Scholten, J., Gasser, B., Reichert, P., Gledhill, M., Dengler, M. and Achterberg, E. P.: Controls on redox-sensitive trace metals in the Mauritanian oxygen minimum zone, Biogeosciences Discuss., (November), 1–49, doi:10.5194/bg-2018-472, 2018.

Rickard, D., Griffith, A., Oldroyd, A., Butler, I. B., Lopez-Capel, E., Manning, D. A. C. and Apperley, D. C.: The composition of nanoparticulate mackinawite, tetragonal

iron(II) monosulfide, Chem. Geol., 235(3–4), 286–298, doi:10.1016/j.chemgeo.2006.07.004, 2006.

Rigaud, S., Radakovitch, O., Couture, R. M., Deflandre, B., Cossa, D., Garnier, C. and Garnier, J. M.: Mobility and fluxes of trace elements and nutrients at the sediment-water interface of a lagoon under contrasting water column oxygenation conditions, Appl. Geochemistry, 31(April 2013), 35–51, doi:10.1016/j.apgeochem.2012.12.003, 2013.

Rosenthal, Y., Lam, P., Boyle, E. A. and Thomson, J.: Precipitation and postdepositional mobility, Earth Planet. Sci. Lett., 132, 99–111, doi:10.1016/0012-821X(95)00056-I, 1995.

Rue, E. L. and Bruland, K. W.: The role of organic complexation on ambient iron chemistry in the equatorial Pacific Ocean and the response of a mesoscale iron addition experiment, Limnol. Oceanogr., 42(5), 901–910, doi:10.4319/lo.1997.42.5.0901, 1997.

Saito, M. A., Goepfert, T. J. and Ritt, J. T.: Some thoughts on the concept of colimitation: Three definitions and the importance of bioavailability, Limnol. Oceanogr., 53(1), 276–290, doi:10.4319/lo.2008.53.1.0276, 2008.

Schlosser, C., Streu, P., Frank, M., Lavik, G., Croot, P. L., Dengler, M. and Achterberg, E. P.: H2S events in the Peruvian oxygen minimum zone facilitate enhanced dissolved Fe concentrations, Sci. Rep., 8(1), 1–8, doi:10.1038/s41598-018-30580-w, 2018.

Schmidtko, S., Stramma, L. and Visbeck, M.: Decline in global oceanic oxygen content during the past five decades, Nature, 542(7641), 335–339, doi:10.1038/nature21399, 2017.

Scholz, F. and Neumann, T.: Trace element diagenesis in pyrite-rich sediments of the Achterwasser lagoon, SW Baltic Sea, Mar. Chem., 107(4), 516–532, doi:10.1016/j.marchem.2007.08.005, 2007.

Scholz, F., Mcmanus, J., Mix, A. C., Hensen, C. and Schneider, R. R.: The impact of ocean deoxygenation on iron release from continental margin sediments, Nat. Geosci., 7(6), 433–437, doi:10.1038/ngeo2162, 2014.

Scholz, F., Löscher, C. R., Fiskal, A., Sommer, S., Hensen, C., Lomnitz, U., Wuttig,

K., Göttlicher, J., Kossel, E., Steininger, R. and Canfield, D. E.: Nitrate-dependent iron oxidation limits iron transport in anoxic ocean regions, Earth Planet. Sci. Lett., 454, 272–281, doi:10.1016/j.epsl.2016.09.025, 2016.

Scholz, F., Schmidt, M., Hensen, C., Eroglu, S., Geilert, S., Gutjahr, M. and Liebetrau, V.: Shelf-to-basin iron shuttle in the Guaymas Basin, Gulf of California, Geochim. Cosmochim. Acta, 261, 76–92, doi:10.1016/j.gca.2019.07.006, 2019.

Schunck, H., Lavik, G., Desai, D. K., Großkopf, T., Kalvelage, T., Löscher, C. R., Paulmier, A., Contreras, S., Siegel, H., Holtappels, M., Rosenstiel, P., Schilhabel, M. B., Graco, M., Schmitz, R. A., Kuypers, M. M. M. and LaRoche, J.: Giant Hydrogen Sulfide Plume in the Oxygen Minimum Zone off Peru Supports Chemolithoautotrophy, PLoS One, 8(8), doi:10.1371/journal.pone.0068661, 2013.

Scor Working Group: GEOTRACES – An international study of the global marine biogeochemical cycles of trace elements and their isotopes, Geochemistry, 67(2), 85–131, doi:10.1016/j.chemer.2007.02.001, 2007.

Severmann, S., McManus, J., Berelson, W. M. and Hammond, D. E.: The continental shelf benthic iron flux and its isotope composition, Geochim. Cosmochim. Acta, 74(14), 3984–4004, doi:10.1016/j.gca.2010.04.022, 2010.

Sommer, S., Linke, P., Pfannkuche, O., Schleicher, T., Schneider v. D, D., Reitz, A., Haeckel, M., Flögel, S. and Hensen, C.: Seabed methane emissions and the habitat of frenulate tubeworms on the Captain Arutyunov mud volcano (Gulf of Cadiz), Mar. Ecol. Prog. Ser., 382, 69–86, doi:10.3354/meps07956, 2009.

Sommer, S., Gier, J., Treude, T., Lomnitz, U., Dengler, M., Cardich, J. and Dale, A. W.: Depletion of oxygen, nitrate and nitrite in the Peruvian oxygen minimum zone cause an imbalance of benthic nitrogen fluxes, Deep. Res. Part I Oceanogr. Res. Pap., 112(3), 113–122, doi:10.1016/j.dsr.2016.03.001, 2016.

Sommer, S., Dengler, M.: Hydrochemistry of water samples during METEOR cruise M136. PANGAEA, https://doi.pangaea.de/10.1594/PANGAEA.904404 (dataset in review), 2019a.

Sommer, S., Dengler, M.: Hydrochemistry of water samples during METEOR cruise M137. PANGAEA, https://doi.pangaea.de/10.1594/PANGAEA.904405 (dataset in review), 2019b.

Stookey, L. L.: Ferrozine---a new spectrophotometric reagent for iron, Anal. Chem., 42(7), 779–781, doi:10.1021/ac60289a016, 1970.

Stramma, L., Johnson, G. C., Sprintall, J. and Mohrholz, V.: Expanding Oxygen-Minimum Zones in the Tropical Oceans, Science (80-.)., 320(5876), 655–658, doi:10.1126/science.1153847, 2008.

Stramma, L., Schmidtko, S., Levin, L. A. and Johnson, G. C.: Ocean oxygen minima expansions and their biological impacts, Deep. Res. Part I Oceanogr. Res. Pap., 57(4), 587–595, doi:10.1016/j.dsr.2010.01.005, 2010.

Straub, K. L., Benz, M., Schink, B. and Widdel, F.: Anaerobic, nitrate-dependent microbial oxidation of ferrous iron. Appl Environ Microbiol, Appl. Environ. Microbiol., 62(4), 1458–60, 1996.

Sunda, W. G. and Huntsman, S. A.: Effect of Zn, Mn, and Fe on Cd accumulation in phytoplankton: Implications for oceanic Cd cycling, Limnol. Oceanogr., 45(7), 1501–1516, doi:10.4319/lo.2000.45.7.1501, 2000.

Sundby, B., Martinez, P. and Gobeil, C.: Comparative geochemistry of cadmium, rhenium, uranium, and molybdenum in continental margin sediments, Geochim. Cosmochim. Acta, 68(11), 2485–2493, doi:10.1016/j.gca.2003.08.011, 2004.

Taylor, S. R. and McLennan, S. M.: Planetary crusts: Their composition, origin and evolution , by Stuart Ross Taylor and Scott M. McLennan, Meteorit. Planet. Sci., 44(3), 465–466, doi:10.1111/j.1945-5100.2009.tb00744.x, 2009.

Thamdrup, B., Dalsgaard, T. and Revsbech, N. P.: Widespread functional anoxia in the oxygen minimum zone of the Eastern South Pacific, Deep Sea Res. Part I Oceanogr. Res. Pap., 65, 36–45, doi:10.1016/j.dsr.2012.03.001, 2012.

Turetta, C., Capodaglio, G., Cairns, W., Rabar, S. and Cescon, P.: Benthic fluxes of trace metals in the lagoon of Venice, Microchem. J., 79(1–2), 149–158, doi:10.1016/j.microc.2004.06.003, 2005.

Twining, B. S. and Baines, S. B.: The Trace Metal Composition of Marine Phytoplankton, Ann. Rev. Mar. Sci., 5(1), 191–215, doi:10.1146/annurev-marine-121211-172322, 2013.

Vedamati, J., Goepfert, T. and Moffett, J. W.: Iron speciation in the eastern tropical

south pacific oxygen minimum zone off peru, Limnol. Oceanogr., 59(6), 1945–1957, doi:10.4319/lo.2014.59.6.1945, 2014.

Westerlund, S. F. G., Anderson, L. G., Hall, P. O. J., Iverfeldt, Å., Van Der Loeff, M. M. R. and Sundby, B.: Benthic fluxes of cadmium, copper, nickel, zinc and lead in the coastal environment, Geochim. Cosmochim. Acta, 50(6), 1289–1296, doi:10.1016/0016-7037(86)90412-6, 1986.

Xie, R. C., Rehkämper, M., Grasse, P., van de Flierdt, T., Frank, M. and Xue, Z.: Isotopic evidence for complex biogeochemical cycling of Cd in the eastern tropical South Pacific, Earth Planet. Sci. Lett., 512, 134–146, doi:10.1016/j.epsl.2019.02.001, 2019.

Xu, Y., Feng, L., Jeffrey, P. D., Shi, Y. and Morel, F. M. M.: Structure and metal exchange in the cadmium carbonic anhydrase of marine diatoms, Nature, 452(7183), 56–61, doi:10.1038/nature06636, 2008.

Yücel, M., Sommer, S., Dale, A. W. and Pfannkuche, O.: Microbial sulfide filter along a benthic redox gradient in the Eastern Gotland Basin, Baltic Sea, Front. Microbiol., 8(FEB), 1–16, doi:10.3389/fmicb.2017.00169, 2017.

Zago, C., Capodaglio, G., Ceradini, S., Ciceri, G., Abelmoschi, L., Soggia, F., Cescon, P. and Scarponi, G.: Benthic fluxes of cadmium, lead, copper and nitrogen species in the northern Adriatic Sea in front of the River Po outflow, Italy, Sci. Total Environ., 246(2–3), 121–137, doi:10.1016/S0048-9697(99)00421-0, 2000.

Zumft, W. G.: Cell biology and molecular basis of denitrification., Microbiol. Mol. Biol. Rev., 61(4), 533–616 [online] Available from: http://www.ncbi.nlm.nih.gov/pubmed/9409151

Supplement

Table II.S.1: Input data from M136 & M137 for diffusive flux calculations.

station	Fe(II) concentration bottom water	Fe(II) concentration in pore water at sediment surface	Cd concentration bottom water	Cd concentration in pore water at sediment surface	porosity	temperature	pressure	salinity
	(µM)	(µM)	(nM)	(nM)		(C°)	(bar)	
1	0.10	1.06	0.22	0.90	0.93	16.17	8.77	35.06
3	0.17	0.47	0.81	0.65	0.95	13.96	13.90	34.97
4	0.00	6.34	0.66	0.47	0.96	13.96	15.40	34.97
5	0.00	0.59	0.68	0.44	0.96	13.21	20.40	34.92
6	0.06	3.14	0.76	0.55	0.95	13.33	25.60	34.94
9	0.00	0.00	0.99	1.25	0.74	6.28	75.00	34.55
10	0.01	0.37	-	-	0.61	4.36	98.20	34.55

Table II.S.2: Input data from M92 for diffusive flux calculations.

station	Fe(II) concentration in bottom water	Fe(II) concentration in pore water sediment surface	porosity	temperature	pressure	salinity
	(µM)	(µM)		(C°)	(bar)	
1	0.70	4.83	0.96	13.99	8.1	34.98
3	0.21	0.77	0.98	13.84	13.90	34.98
4	1.15	1.80	0.96	13.77	15.50	34.96
5	0.03	0.31	0.96	13.16	20.50	34.94
6	0.20	2.13	0.96	13.16	25.40	34.94
9	0.03	0.03	0.84	5.17	78.30	34.54
10	0.00	0.06	0.74	4.62	103.4	34.55

Table II.S.3: Silicic acid ($Si(OH)_4$) concentrations in the near-bottom water column.

	Station 1	Station 3	Station 4	Station 5	Station 6	Station 9
distance from seafloor	$Si(OH)_4$ concentration	$Si(OH)_4$ concentration	$Si(OH)_4$ concentration	$Si(OH)_4$ concentration	$Si(OH)_4$ concentration	$Si(OH)_4$ concentration
(m)	(µM)	(µM)	(µM)	(µM)	(µM)	(µM)
0.5	31.28	29.74	24.86	24.32	27.28	-
1	31.63	29.22	24.51	24.20	27.14	56.22
2	-	29.2	23.61	24.35	27.02	56.04
3	31.38	28.66	24.36	-	-	55.96
4	31.27	28.17	24.20	24.00	27.04	55.44

Table II.S.4: Equations for linear regressions from benthic chamber incubation data (Y = concentration, X = incubation time) and coefficients of determination (R^2).

station	Fe	Fe	Cd	Cd
	linear regression	R^2	linear regression	R^2
1	Y = 0.88 * X + 186.18	0.01	Y= 0.00 * X + 0.068	0.06
4	Y = 4.78 * X + 7.07	0.72	Y = -0.01 * X + 0.55	0.96
5	Y = -0.89 * X + 89.28	0.1	Y = -0.01 * X + 0.53	0.89
6	Y = 2.32 * X + 57.34	0.47	Y = -0.01 * X + 0.58	0.87
9	Y = 2.95 * X + 76.38	0.49	Y = 0.00 * X + 1.01	0.36
10	Y = 0.67 * X + 28.20	0.12	Y = 0.00 * X + 0.99	0.07

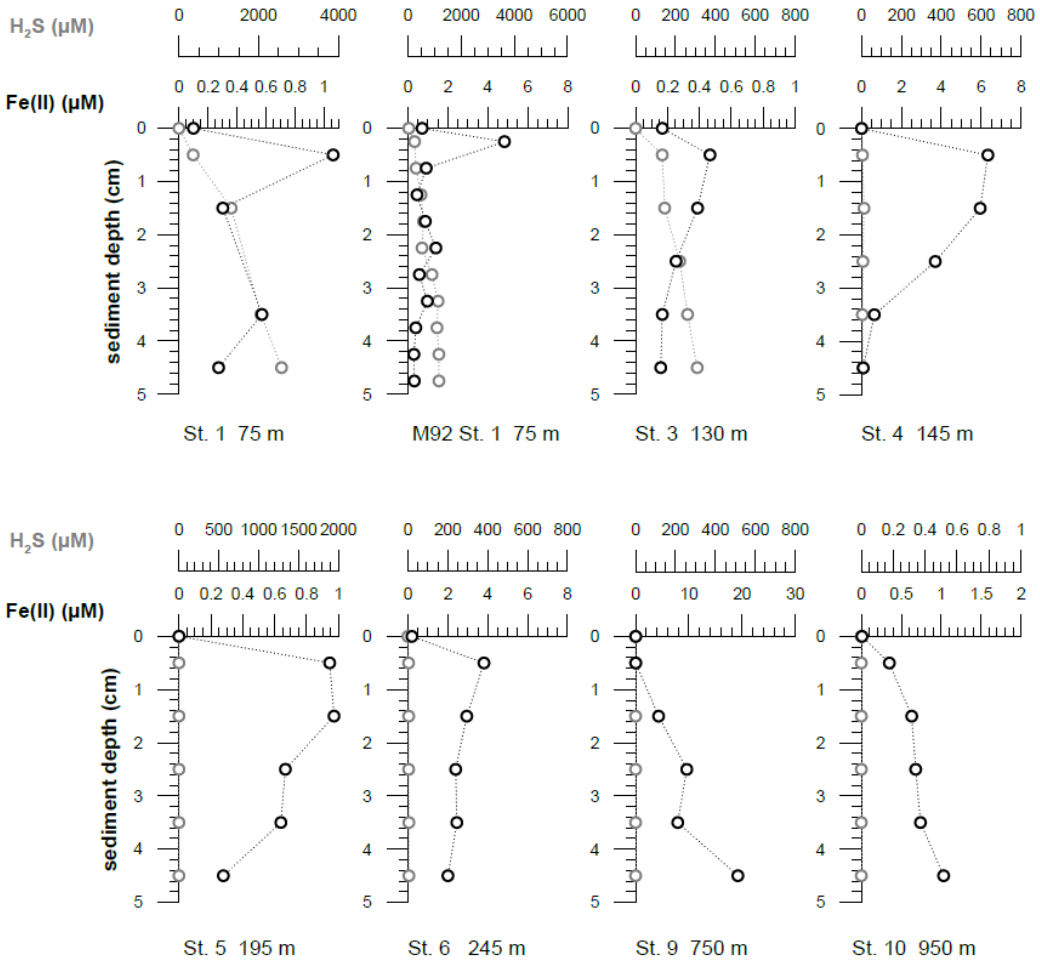

Figure II.S.1: Close up of pore water dissolved Fe(II) and hydrogen sulfide concentrations in the first 5 cm of the surface sediment. Data from an earlier cruise, M92, at Station 1 (75 m water depth) are displayed for comparison. The uppermost sample represents the bottom water concentration. The analytical error is smaller than the symbol size.

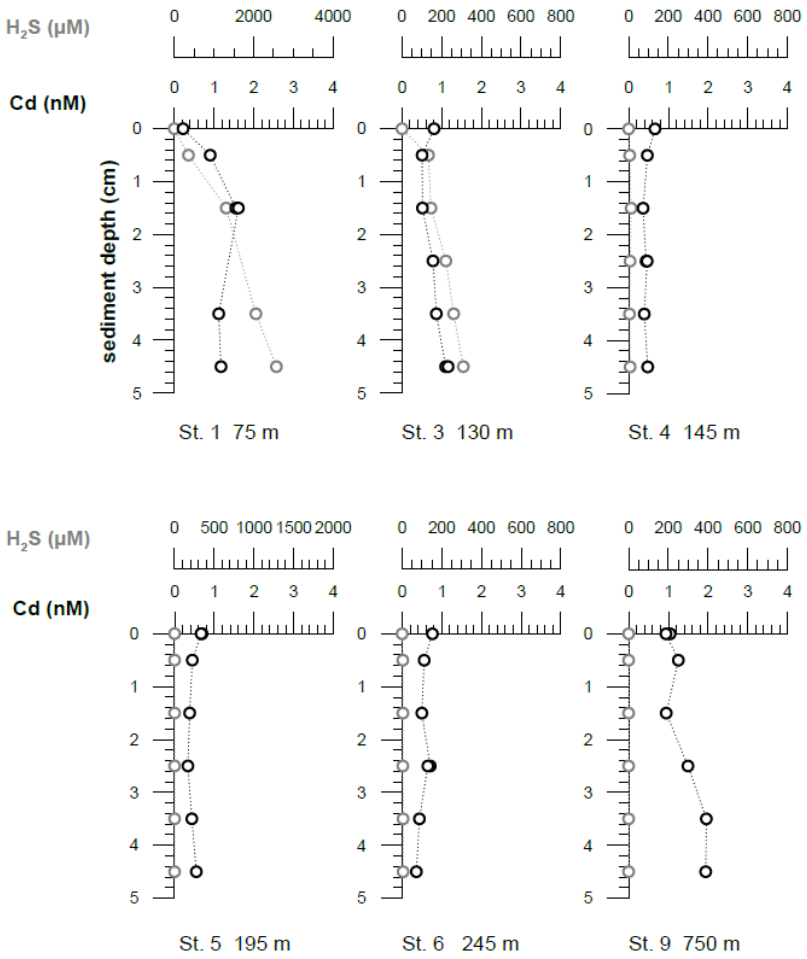

Figure II.S.2: Close up of pore water dissolved Cd and hydrogen sulfide concentrations in the first 5 cm of the surface sediment. The uppermost sample represents the bottom water concentrations. The analytical error is smaller than the symbol size.

III. Sedimentary cycling and benthic fluxes of manganese, cobalt, nickel, copper, zinc and cadmium in the Peruvian oxygen minimum zone

Anna Plass[1], Andrew W. Dale[1], Florian Scholz[1]

[1]GEOMAR Helmholtz Centre for Ocean Research Kiel, Wischhofstraße 1-3, 24148 Kiel, Germany

Published in Marine Chemistry, 233, 103982, 2021

Abstract

Marine sediments are an important source and sink of bio-essential trace metals to the ocean. However, the different mechanisms leading to trace metal release or burial are not fully understood and the associated fluxes are not well quantified. Here, we present sediment, pore water, sequential extraction and benthic flux data of Mn, Co, Ni, Cu, Zn and Cd along a latitudinal depth transect across the Peruvian oxygen minimum zone at 12°S. Sediments are depleted in Mn and Co compared to the lithogenic background. Diffusive Mn fluxes from the sediments into the bottom water (-26 to -550 µmol m^{-2} y^{-1}) are largely consistent with the rate of Mn loss from the solid phase (-100 to -1160 µmol m^{-2} yr^{-1}) suggesting that 50 % or more of the sedimentary Mn depletion is attributed to benthic efflux. In contrast, benthic Co fluxes (~ -3 µmol m^{-2} yr^{-1}) are lower than the rate of Co loss from the solid phase (up to -120 µmol m^{-2} yr^{-1}), implying Co dissolution in the water column. The trace metals Ni, Cu, Zn and Cd are enriched within the sediments with respect to the lithogenic background. Uptake of Ni by phytoplankton in the photic zone and delivery with organic matter to the sediment surface can account for up to 100 % of the excess Ni accumulation (87 to 180 µmol m^{-2} y^{-1}) in shelf sediments near the coast, whereas at greater water depth additional

scavenging by Mn- and Fe-oxides may contribute to Ni accumulation. Up to 20 % of excess Cu (33 to 590 µmol m^{-2} y^{-1}) and generally less than 20 % of excess Zn (58 to 2170 µmol m^{-2} y^{-1}) and Cd (6 to 260 µmol m^{-2} y^{-1}) can be explained by delivery with fresh organic matter. Sequential extraction data suggest that the discrepancies between the known sources of Cd (and Cu) and their excess accumulation may be driven by the delivery of allochthonous sulphide minerals precipitated from the water column. Additionally, Cu may be scavenged by downward sinking organic material. In contrast, precipitation of Zn sulphide chiefly takes place in the sediment. Diffusive Zn fluxes into the sediment (21 to 1990 µmol m^{-2} y^{-1}) match the excess Zn accumulation suggesting that Zn delivery is mediated by molecular diffusion from bottom waters. Considering the diverse behavioural pattern of trace metals observed in this study, we argue that declining oxygen and increasing hydrogen sulphide concentrations in a future ocean will modify trace metal fluxes at the seafloor and the trace metal stoichiometry of seawater.

III.1 Introduction

Trace metals (TM) are involved in many biogeochemical processes in the ocean For example, they are an essential component of enzymes that catalyse photosynthesis (Mn, Cu) as well as carbon (Co, Zn, Cd), nitrogen (Ni, Cu) and phosphorous (Zn) acquisition (Morel, 2003; Morel et al., 2014; Lohan and Tagliabue, 2018). Unlike their abundance in the continental crust, TMs are often scarce in seawater, with concentrations in the range of nano- to picomoles per liter (Bruland and Lohan, 2006). Because of their limited availability, TMs can (co-)limit primary productivity in the ocean and limit the efficiency of the biological pump (Saito et al., 2008; Moore et al., 2013; Morel et al., 2014).

In paleoceanographic studies, TM concentrations in sediments have been used to infer past biogeochemical conditions in the water column and sediments (Brumsack, 2006). Certain TM enrichments (Ni, Cu) are indicative of high organic matter rain rates to the seafloor as well as sulphidic conditions within the sediments as a result of TM retention and burial as sulphide minerals (Tribovillard et al., 2006; Algeo and Liu, 2020). In contrast, sedimentary enrichments of Mn and Co may be indicative of

hydrographically restricted conditions (Sweere et al., 2016) under which these elements become trapped within basin sediments.

A meaningful application of TM concentrations as paleo-redox or biogeochemical proxies requires a mechanistic understanding of their sources and sinks in the ocean, especially in low-oxygen environments. Temporal or permanent depletion of oxygen in the water column above the seafloor can affect the extent to which TMs are removed from the water column and sequestered in the sediment because TM mobility is redox-dependent (Sundby et al., 1986; Morford and Emerson, 1999; Tribovillard et al., 2006; Scholz and Neumann, 2007; Scholz et al., 2011; Rigaud et al., 2013; Rapp et al., 2020). For example, sediments in the oxygen minimum zone (OMZ) off Peru are enriched in some TMs (Ni, Cu, Zn, Cd) whereas others are depleted (Mn, Co) compared to the lithogenic background (Böning et al., 2004; Little et al., 2015). Similar patterns have been observed in the OMZs offshore Chile and Namibia (Borchers et al., 2005; Böning et al., 2009). These enrichment or depletion patterns are reflected in TM concentrations in the water column. High Mn and Co concentrations in the water column of oxygen-deficient regions (e.g. Namibia, Peru, Mauretania, Mexico, California) were ascribed to reductive dissolution or remineralisation in anoxic waters or release from anoxic sediments (Johnson et al., 1996; Nameroff et al., 2002; Noble et al., 2012; Hawco et al., 2016; Rapp et al., 2019b). Several studies have reported a quantitative removal of dissolved Cu, Zn and Cd within anoxic water columns of semi-restricted anoxic basins (e.g. Framvaren Fjord, Black Sea) and depletion in open-marine OMZs (e.g., Peru, Mauritania, North-East Pacific) (Jacobs et al., 1985; Tankéré et al., 2001; Janssen et al., 2014; Conway and John, 2015b; Roshan and Wu, 2015; Janssen and Cullen, 2015; Vance et al., 2016; Xie et al., 2019). However, the actual processes by which TMs are removed from the water column and delivered to the sediment are, in many cases, poorly constrained.

Potential TM delivery mechanisms to the sediment include incorporation into organic matter in the surface ocean by phytoplankton, scavenging by sinking organic material or Mn- and Fe-oxides, and sulphide precipitation. After deposition at the seafloor, TMs originally associated with fresh organic material or Mn- and Fe-oxides can be released and/or transferred to other solid phases such as refractory organic matter or sulphide minerals (Gendron et al., 1986; Shaw et al., 1990; Sheng et al., 2004; Böning et al., 2004; Vijayaraghavan et al., 2005; Audry et al., 2006; Rigaud et

al., 2013; Little et al., 2015; Olson et al., 2017). Trace metal precipitation within sediments can also induce a downward-directed TM flux across the sediment-water interface. These different delivery mechanisms are difficult to distinguish based on water column or sediment solid phase data alone, because dissolution, transformation and fixation is likely to take place during early diagenesis. Collectively, these processes determine the extent of TM accumulation in the sediment and, ultimately, the oceanic dissolved TM inventory.

In this manuscript, we aim to identify and quantify mechanisms that lead to the release or sequestration of Mn, Co, Ni, Cu, Zn and Cd in sediments in the OMZ off Peru. Our analysis is based on porewater and solid phase data for surface sediments along a sampling transect at 12°S (six stations) (Fig. III.1). We assign individual delivery pathways to each of these TMs by comparing diffusive benthic fluxes and accumulation rates due to organic matter burial and TM speciation data from sequential extractions. Our findings may help to reduce uncertainties that are associated with oceanic TM mass balances (e.g. Homoky et al., 2016; Little et al., 2016; Archer et al., 2020) and to parameterize TM fluxes in global biogeochemical models (Dale et al., 2015a; Homoky et al., 2016; Tagliabue et al., 2018).

III.2 Methods

III.2.1 Study area

The upwelling region in the Eastern Tropical South Pacific off the coast of Peru is characterised by one of the most intense OMZs in the ocean. The OMZ forms through a combination of seasonal upwelling of nutrient-rich water, high rates of primary productivity and subsequent oxygen consumption in subsurface waters. Waters with near-complete oxygen depletion are generally located between 100 and 500 m water depth (Pennington et al., 2006; Karstensen et al., 2008; Thamdrup et al., 2012). The biogeochemical conditions in the water column at our study sites are spatially highly variable and, at the shallower stations, also temporally variable. During phases of water stagnation on the shelf the water column can become anoxic and

depleted in nitrate (NO_3^-) and nitrite (NO_2^-) following intense denitrification (Sommer et al., 2016). Hydrogen sulphide (H_2S) generated in the sediments by microbial sulphate reduction can then be released to the water column and accumulate to micromolar levels (Schunck et al., 2013; Scholz et al., 2016; Ohde, 2018). In contrast. oxygenation events on the upper slope (down to 200 - 300 m) are linked to the passage of coastal trapped waves. The passage of these poleward waves often occurs during (coastal) El Niño phases and is associated with the deepening of the nutricline and upper oxycline (Ulloa et al., 2001; Levin et al., 2002b; Gutiérrez et al., 2008; Echevin et al., 2008; Ohde, 2018). A tracer release experiment that was carried out in our study area revealed that nutrients released into bottom waters at the Peruvian shelf (≤ 250 m depth) can potentially reach the surface ocean via transport and mixing processes (Freund, 2020). This observation highlights the relevance of benthic trace metal fluxes for biological processes in the surface ocean.

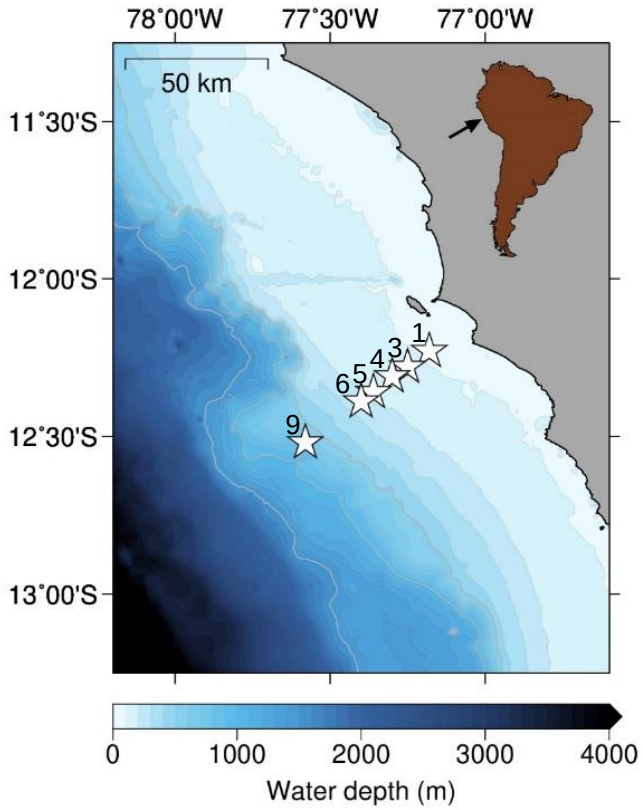

Figure III.1: Sampling locations (stars) and station numbers on the Peruvian continental margin during cruises M136 and M137. Water depths and station coordinates are summarised in Tab. III.S.1.

The sediments at our study sites on the Peruvian shelf (< 200 m) consist of fine grained diatomaceous and organic carbon-rich hemipelagic muds (Reimers and Suess, 1983; Suess et al., 1987; Froelich et al., 1988). The sediments on the slope consist of a mixture of phosphoritic sand, foraminiferal sand, and olive green mud (Muñoz et al., 2004). Sedimentation rates are highest on the inner shelf (75 m) at 0.47 cm y^{-1} and decrease on the outer shelf and slope to 0.14 to 0.05 cm y^{-1} (130 to 750 m) (Dale et al., 2020). The high productivity in surface waters leads to high particulate organic carbon (POC) rain rates, which reach 955 mg m^{-2} d^{-1} at 75 m and decrease offshore to 62 mg m^{-2} d^{-1} at 750 m (Dale et al., 2015b). The POC content in sediments ranges between 30 and 200 mg g^{-1}, with highest values found underneath anoxic bottom waters (Suits and Arthur, 2000; Böning et al., 2004; Dale et al., 2015b). Hydrogen sulphide in sediment pore waters reaches several tens to thousands of micromoles per litre (Suits and Arthur, 2000; Scholz et al., 2011; Noffke et al., 2012; Plass et al., 2020). The contents of sulphur bound to pyrite within the OMZ sediments are between 1 and 18 mg g^{-1}, and the contents of sulphur bound to organic matter are between 0.7 and 3.3 mg g^{-1}, with the highest values in the centre of the OMZ (Suits and Arthur, 2000; Scholz et al., 2014b).

III.2.2 Sampling and analytical methods

The sampling took place between April and May 2017 during RV Meteor cruises M136 and M137 at six stations across the Peruvian shelf and slope between 75 m and 750 m water depth (Fig. III.1). The station numbering was taken from Dale et al. (2015b) with the geographical coordinates listed in the supplement (Table III.S.1). Short sediment cores (ca. 30 cm) were retrieved with a multiple corer and immediately transferred to the onboard cool room (4 °C). The supernatant bottom water above the sediment core was then sampled and filtered through 0.2 µm cellulose acetate filters (Sartorius). Subsequently, the sediment cores were sliced in vertical sections in a glove bag under Ar-atmosphere. The samples were then centrifuged, and the supernatant was filtered as before under Ar-atmosphere and transferred to acid cleaned low-density polyethylene (LDPE) bottles. Pore water and supernatant samples were acidified to pH < 1 with subboiled distilled HNO_3. Hydrogen sulphide concentrations were measured photometrically (U-2001 Hitachi spectrometer) on separate non

acidified pore water samples using standard spectrophotometric techniques (Grasshoff et al., 1999). The centrifuged sediments were stored in the centrifuge tubes under Ar-atmosphere for TM analysis at the home laboratory. Separate uncentrifuged sediment samples were collected for determination of POC and total sulphur (TS) content as well as water content and porosity. All sediment and porewater samples that were not analysed on board were maintained at 4 °C.

To determine TM concentrations in the pore water, we generally followed the pre-concentration method described by Rapp et al. (2017) but with a half-automated device (Preplab). The acidified pore water samples (1 ml) were diluted with 2 ml of de-ionised water (MilliQ, Millipore) and irradiated with UV by light for 4 hours to destroy organic ligands that affect the recovery of Co and Cu. Before preconcentration the pH value of the sample was raised to 6.4 with an ammonium acetate buffer (1.5 M). Subsequently, the sample was loaded onto a chelating resin column where the seawater matrix was rinsed off. Then the column was rinsed with 1 ml of elution acid (1 M subboiled HNO_3) to collect the TMs. Trace metal concentrations in the pre-concentrated samples were measured by high resolution inductively coupled plasma mass spectrometry (HR-ICP-MS; Thermo Fisher Element XR). Trace metal concentrations were quantified by standard addition (Mn, Co) and isotope dilution (Ni, Cu, Zn, Cd). Accuracies for replicate measurements of reference seawater certified for TMs (NASS-7 and CASS-6) are listed in Table III.S.2. The pore water Cd data has been previously published along with benthic chamber data in Plass et al. (2020). These data are shown again here to explore the full range of TM behaviour on the Peruvian shelf.

Solid phase TM analyses was targeted at eight sampling depths per core (0.5 cm, 2.5 cm, 4.5 cm, 7cm, 11 cm, 16 cm, and 20 cm). Total digestions were used to determine total TM contents. Exactly 0.1 g of freeze dried and ground sediment was digested in 2 ml concentrated HF (suprapure) (40 %), 2 ml concentrated HNO_3 (suprapure) (65 %) and 3 ml concentrated $HClO_4$ (suprapure) (60 %) for 8 hours at 185 °C. The sample was then dried and re-dissolved with 1 ml concentrated HNO_3 (suprapure) and 5 ml deionized water (Milli-Q, Millipore) at 145 °C for 2 hours. The reference standard MESS-3 was treated in the same way to monitor the recovery of the digestion procedure.

A modified version of the four-step sequential extraction scheme of Huerta-Diaz and Morse (1990) was applied to determine host phases of TMs within the sediment. We opted to use unaltered wet sediment because drying can shift TMs from less mobile to more mobile phases and thus distort the results from the sequential extractions (Baeyens et al., 2003). For each extraction 0.5 g of wet sediment was used. To check the long-term reproducibility of the sequential extraction protocol, we included our in-house standard OMZ-2 (sediments from the Peruvian margin) into each extraction run (relative standard deviation ± 2 %, for Zn ± 9 %). The reference standard MESS-3 was also extracted along with the samples. All samples were constantly mixed on a shaking table during the extraction. After each extraction step the sample was centrifuged and the supernatant collected. The residual sediment was used for the subsequent extraction step. A full description of the extraction procedure follows:

Sequential extraction step 1, $HCl_{0.5M}$-fraction: The sediment was extracted in 20 ml of 0.5 M HCl (subboiled and distilled) and shaken for 1 hr. After centrifugation the supernatant was collected and stored for analysis. This extraction is operationally defined to dissolve TMs present as TM-monosulphides and TMs associated to amorphous (oxyhydr)oxides (Fe, Mn), carbonates and hydrous aluminosilicates (Kostka and Luther, 1994).

Sequential extraction step 2, HCl_{1M}-fraction: 15 ml of 1 M HCl (subboiled and distilled) were added to the residual sediment and shaken for 23 hr. After centrifugation and collection of the supernatant, the sediment was washed with 10 ml de-ionised water (MilliQ, Millipore) and centrifuged again. The supernatant was combined with the prior collected supernatant (1 M HCl) and stored for analysis. In principle, this extraction step is operationally defined to dissolve the same TM phases as step 1 plus more crystalline phases and some silicates minerals (Huerta-Diaz and Morse, 1990; Kostka and Luther, 1994).

Sequential extraction step 3, HF-fraction: During this step, 10 ml of 10 M HF (suprapure) was added to the residual sediment and shaken for 1 hr. The sample was centrifuged and the supernatant collected. Then, 10 ml of 10 M HF was added to the sediment and shaken for 16 hr, before 2 g of boric acid was added to dissolve any precipitated fluoride minerals. The shaking was then repeated for another 8 hr before centrifuging and collection of the supernatant. Subsequently, the sediment was washed with 10 ml boiling de-ionised water, centrifuged again and the supernatant

collected. All three supernatants collected during this extraction step were combined and stored for analysis. This extraction step is operationally defined to dissolve TMs associated with silicate minerals (Huerta-Diaz and Morse, 1990).

Sequential extraction step 4, HNO_3-fraction: For the last extraction step, 10 ml of concentrated HNO_3 (subboiled and distilled) was added to the remaining sample and shaken for 2 hr. Subsequently, the sample was centrifuged and the supernatant collected. The residual sediment was washed with 10 ml of concentrated HNO_3 (subboiled and distilled) and then with 10 ml of de-ionised water. After each washing step, the sample was centrifuged, the supernatant collected and combined with the prior collected supernatant and stored for TM analysis. This extraction step is operationally defined to dissolve TM associated with organic matter and pyrite (Huerta-Diaz and Morse, 1990).

Trace metals extracted in step 1, 2 and 4 are considered to be reactive and potentially mobile within the water column and surface sediment whereas TMs extracted in step 3 (silicate minerals) are considered to be of lithogenic origin and thus unreactive.

Concentrations of TMs (and also Al) in solutions from digestions and sequential extractions were measured by ICP-OES (VARIAN 720-ES). Due to its lower sedimentary content, Co concentrations were measured by ICP-MS (Agilent 7500). The recovery from replicate total digestions of the reference standard MESS-3 (n = 17, all within range) and the recovery from the sequential extraction method of our in-house standard OMZ-2 (n = 3, recovery > 90 % Mn, Co, Ni and Cd and > 80 % for Cu and Zn) are listed in Table III.S.3. Possible contamination during the extraction procedure was monitored using method blanks, which were treated in the same way as the samples.

Total sulphur and POC contents in freeze dried and ground sediment subsamples were determined by flash combustion in an Elemental Analyzer (Euro EA) after removal of inorganic carbon with 0.25 mM HCl (analytical grade). Precision and relative standard deviation of the measurement was ± 3 % for TS and ± 1 % for POC. Further sediment subsamples were freeze-dried for the determination of water content and porosity to convert the results from sequential extractions in mass units.

III.2.4 Flux calculations

To determine whether a TM is enriched or depleted relative to the lithogenic background (expressed as excess; TM_{xs}) we used the average TM and Al contents of each core and applied the following equation (Brumsack, 2006):

$$TM_{xs} = TM_{sample} - Al_{sample} * (TM/Al)_{crust} \quad \text{(Eq. III.1)}$$

Positive and negative TM_{xs} represent sedimentary enrichment and depletion, respectively. The TM:Al ratio of andesite was used as the lithogenic background reference, in line with the overall andesitic composition of Peru margin sediment (Böning et al., 2004). We applied the same reference values for Mn, Ni, Cu, Zn, Cd and Al from Peruvian andesite as Little et al. (2015) (taken from the GEOROC data base (Sarbas and Nohl, 2009)). The reference value for Co was taken from average andesite (Taylor and McLennan, 1995) which is nearly identical to the local andesite Co:Al ratio (Aguirre, 1988). To determine the excess TM flux/accumulation in the sediment, TM_{xs} was multiplied by the mass accumulation rate (MAR) for each individual site (taken from Dale et al. (2020)):

$$TM_{xs} * MAR = TM_{xs}MAR \quad \text{(Eq.III. 2)}$$

To quantity TM delivered to or removed from the sediments via diffusive transport (F_D) across the sediment water interface, we applied Fick's first law of diffusion (Boudreau, 1997):

$$\mathrm{F_D} = -\Phi \mathrm{D_{sed}}(\mathrm{dC/dx}) \quad \text{(Eq. III.3)}$$

In this equation, dC/dx is the concentration gradient between the uppermost pore water sample (0 – 1 cm sediment depth) and the bottom water. D_{sed} is the effective molecular diffusion coefficient of a TM in the sediment, which was determined as follows (Plass et al., 2020):

$$\mathrm{D_{sed}} = \mathrm{D_{sw}}/(1 - \ln(\phi^2)) \quad \text{(Eq. III.4)}$$

The molecular diffusion coefficients in seawater (D_{sw}) under standard conditions (Li and Gregory, 1974) were adjusted to in-situ temperature, pressure and salinity applying the Stokes-Einstein Equation. The denominator in Eq. III.4 represents tortuosity which is derived from porosity (Φ) (Boudreau, 1997). In this study, a positive F_D represents a flux from the bottom into the pore water and vice versa. All data for diffusive flux calculations are listed in Tables III.S.5.

Trace metals are also delivered to the sediment via incorporation into phytoplankton and deposition of organic detritus on the seafloor. We approximated this flux by multiplying the average TM to carbon (TM:C) ratio in average phytoplankton (Moore et al., 2013) with POC rain rates and POC burial rates (data from Dale et al. (2015b)) for each site. These give the maximum and minimum TM fluxes, respectively. Regional TM:C ratios from the equatorial Pacific in bulk phytoplankton and diatoms are available for some TMs from Twining et al. (2011) and for (mostly) zooplankton from Collier and Edmond (1984). Compared to average phytoplankton, regional ratios are generally slightly lower for Mn, similar for Ni and Cu, and slightly higher for Co, Zn and Cd. Available TM data for suspended particles within the OMZ off Peru show elevated TM to phosphorus (TM:P) ratios compared to average phytoplankton (Ohnemus et al., 2017; Lee et al., 2018). In this study, we converted this local particulate TM:P to TM:C ratio assuming a C:P ratio in phytoplankton of 124 (Ho et al., 2003; Moore et al., 2013). The uncertainties associated with variable TM:C ratios are discussed in Section III.4.2. The results of all flux calculations are listed in Table III.1 and displayed in Figure III.7.

III.3 Results

III.3.1 Biogeochemical conditions in the water column

The biogeochemical trends in the water column during our sampling campaign are presented in detail by Lüdke et al. (2020) and Plass et al. (2020). During the time of sampling, the bottom water above our sampling stations on the shelf was depleted in oxygen. The OMZ, with oxygen concentrations below the detection limit of the Winkler titration (3 to 5 µM), extended down to around 450 m water depth (Fig. III.2). Within the OMZ, nitrogenous conditions prevailed and concentrations of nitrite were in excess of 4 µM between 150 and 300 m water depth.

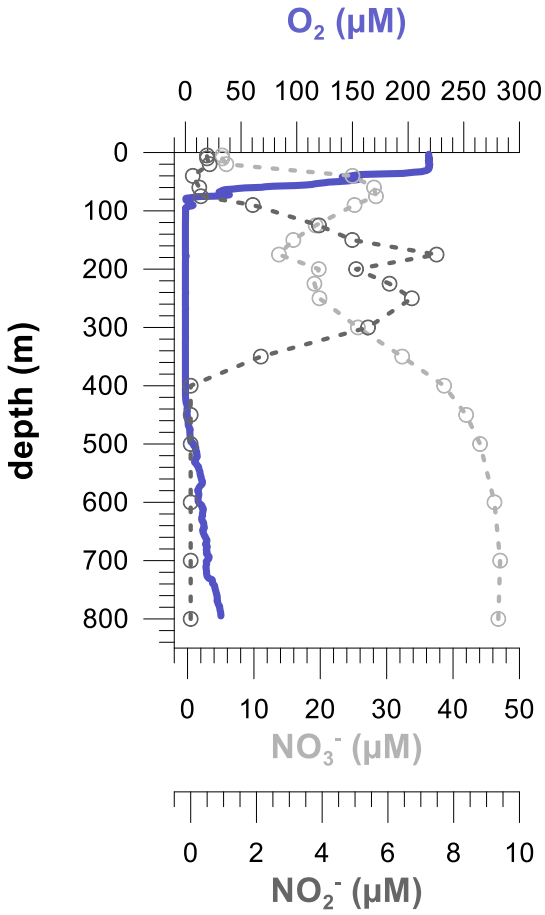

Figure III.2: Dissolved oxygen (O_2), nitrate (NO_3^-) and nitrite (NO_2^-) concentrations in the water column on the Peruvian shelf and slope during the time of sampling (from Plass et al. (2020)).

III.3.2 Pore water data

Pore water concentrations of Mn were highest in the upper 5 to 10 cm of the sediment at most stations, reaching several hundreds of nanomoles per litre. In deeper sediments Mn concentrations dropped below 100 nM at Stations 1, 3 and 5 (75, 130 and 195 m). At all stations, higher concentrations in pore waters than in the overlying bottom waters were observed. This implies an upward-directed diffusive flux of Mn to the bottom water. Particularly sharp concentration gradients at the sediment-water interface (up to 420 nM cm^{-1}) were measured at the shallow shelf stations, which result in the highest diffusive flux at St. 1 (75 m) (-550 µmol m^{-2} y^{-1}). Diffusive Mn fluxes decreased with increasing water depth and the lowest value was observed at Station 9 (750 m) (-26 µmol m^{-2} y^{-1}).

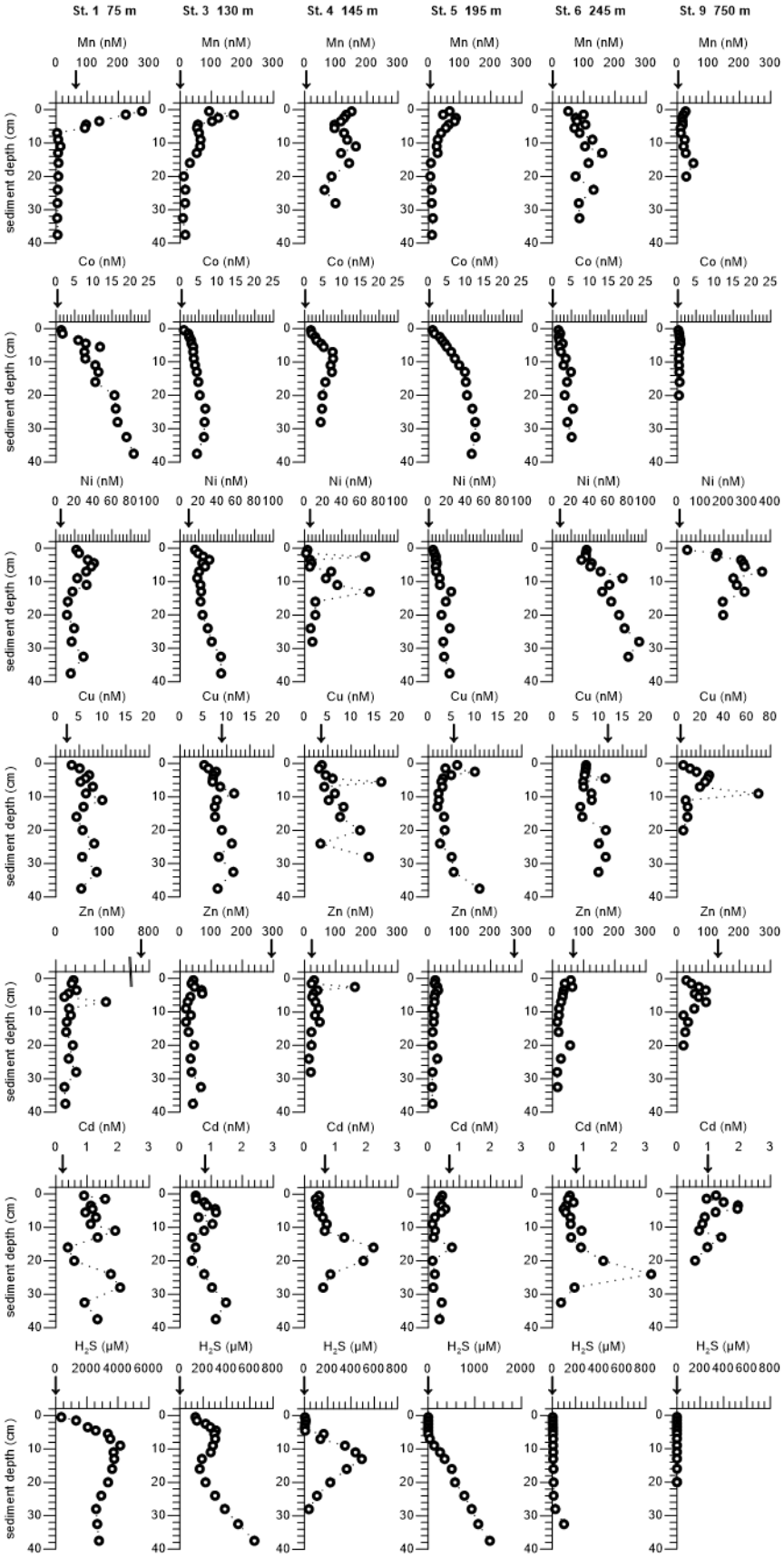

Figure III.3: Pore water dissolved trace metal concentrations. The arrow represents the bottom water concentration. Data for cadmium (Cd) and hydrogen sulphide (H_2S) are from Plass et al. (2020).

Concentrations of Co in pore waters increased from the sediment surface towards deeper sediments by several nanomoles per litre at stations within the OMZ. Concentrations in the uppermost pore water sample (~ 1 nM) were higher than in overlying bottom waters (< 1 nM), which again implies an upward diffusive flux from the pore water to the bottom water. Diffusive fluxes ranged between -4.1 and -1.7 µmol m^{-2} y^{-1} on the shelf, whereas at St. 9 (750 m) the flux was lowest with -0.13 µmol m^{-2} y^{-1}.

Pore water Ni concentrations generally increased with increasing sediment depth at most shelf stations, from a few nanomoles per litre at the sediment surface up to 92 nM in deeper sediments at St. 6 (245 m). The highest pore water Ni concentrations were observed at Station 9 (750 m) (up to 365 nM). With the exception of Station 4 (145 m), diffusive fluxes ranging from -12 to -71 µmol m^{-2} y^{-1} were directed from the pore water to the bottom water.

Copper concentrations were in the range of 2 to 26 nM and mostly varied around an average of 7 nM at stations within the OMZ. Concentration gradients across the sediment-water interface generally ranged between 2 and 10 nM cm^{-1} and diffusive fluxes were mostly directed out of the sediment (St. 1, 4, 5 and 9). The highest efflux of -3.5 µmol m^{-2} y^{-1} was observed at St. 9 (750 m). The highest flux into sediment was 13 µmol m^{-2} y^{-1} at St. 6.

The concentrations of dissolved Zn ranged between 20 and 40 nM at most stations and generally varied within a narrow range within the sediment cores. At a few stations, single values of maximum concentrations in the upper 10 cm reached close to or above 100 nM. Concentrations of Zn in bottom waters were of the order of several hundred nanomoles per litre. The high concentration gradients across the sediment-water interface imply downward diffusive fluxes of Zn into the sediment of up to 2000 µmol m^{-2} y^{-1} at St. 1 (75 m).

Concentrations of Cd in pore waters ranged between 0.1 and 2 nM. Bottom water concentrations were higher than concentrations in the surface pore water at most stations (St. 3, 4, 5 and 6) indicating a downward diffusive flux of 0.6 to 0.8 µmol m^{-2} y^{-1} into the sediment. Upward directed fluxes were observed at St. 1 (75 m) (-1.8 µmol m^{-2} y^{-1}) and St. 9 (750 m) (-0.3 µmol m^{-2} y^{-1}).

The sediment pore waters contained H_2S at all shelf stations. The highest concentrations (> 4000 µM) were measured at St. 1 (75 m). At St. 3 to 5 (130 to 195 m), concentrations reached up to 1000 µM. Hydrogen sulphide concentrations increased with sediment depth either from the sediment surface (St. 1 and 3) or from 5 cm depth (St. 4 and 5). At several stations, H_2S showed a peak between 5 and 15 cm (St. 1, 3, 4), whereas at St. 5 (195 m) the increase with depth was continuous. At the deepest station on the slope (St. 9), no H_2S was detected.

III.3.3 Total digestion data and trace metal excess

The total digestion data is presented together with the sequential extraction data in Fig. III.4. Total sedimentary contents of Mn, Co and Zn generally decreased with distance offshore, whereas contents of Ni and Cd increased, except at St. 9 where Ni contents decreased and Cd contents were lowest. Sedimentary Cu contents were rather constant along the sampling transect. There were no large variations in total TM contents with increasing sediment depth. Average station values for the different TMs were between the following; Mn: 133 to 382 µg g^{-1}, Co: 3 to 8 µg g^{-1}, Ni: 22 to 104 µg g^{-1}, Cu: 58 to 46 µg g^{-1}, Zn: 98 to 178, Cd: 2 to 52 µg g^{-1}.

The calculated enrichment or depletion of the different TMs compared to the lithogenic background sedimentation off Peru (TM_{xs}) is displayed in Fig. III.5. The negative TM_{xs} for Mn and Co illustrates that these TMs are depleted at all stations whereas Ni, Cu, Zn and Cd are enriched. These depletion and enrichment patterns as well as the ranges of TM_{xs} are similar to those observed in previous studies on the Peruvian margin (e.g. Böning et al., 2004; Little et al., 2015). Manganese showed the smallest depletion at the shallowest station St. 1 (75 m) (-56 µg g^{-1}) and the largest depletion at the deepest station St. 9 (750 m) (-138 µg g^{-1}). The depletion of Co (-4 to -6 µg g-1) varied across the transect and was smallest at St. 6 (245 m) and highest at St. 4 (145 m). Across the shelf, Ni_{xs} clearly increased (7 to 100 µg g^{-1}) whereas Cu_{xs} (33 to 40 µg g^{-1}) and Cd_{xs} (26 to 52 µg g^{-1}) increased only moderately with distance offshore. In contrast Zn_{xs} (74 to 124 µg g^{-1}) decreased across the shelf. The enrichment of Ni, Cu and Zn at the slope station (St. 9) was similar to those observed at the shelf stations, whereas Cd_{xs} was close to zero (2 µg g^{-1}).

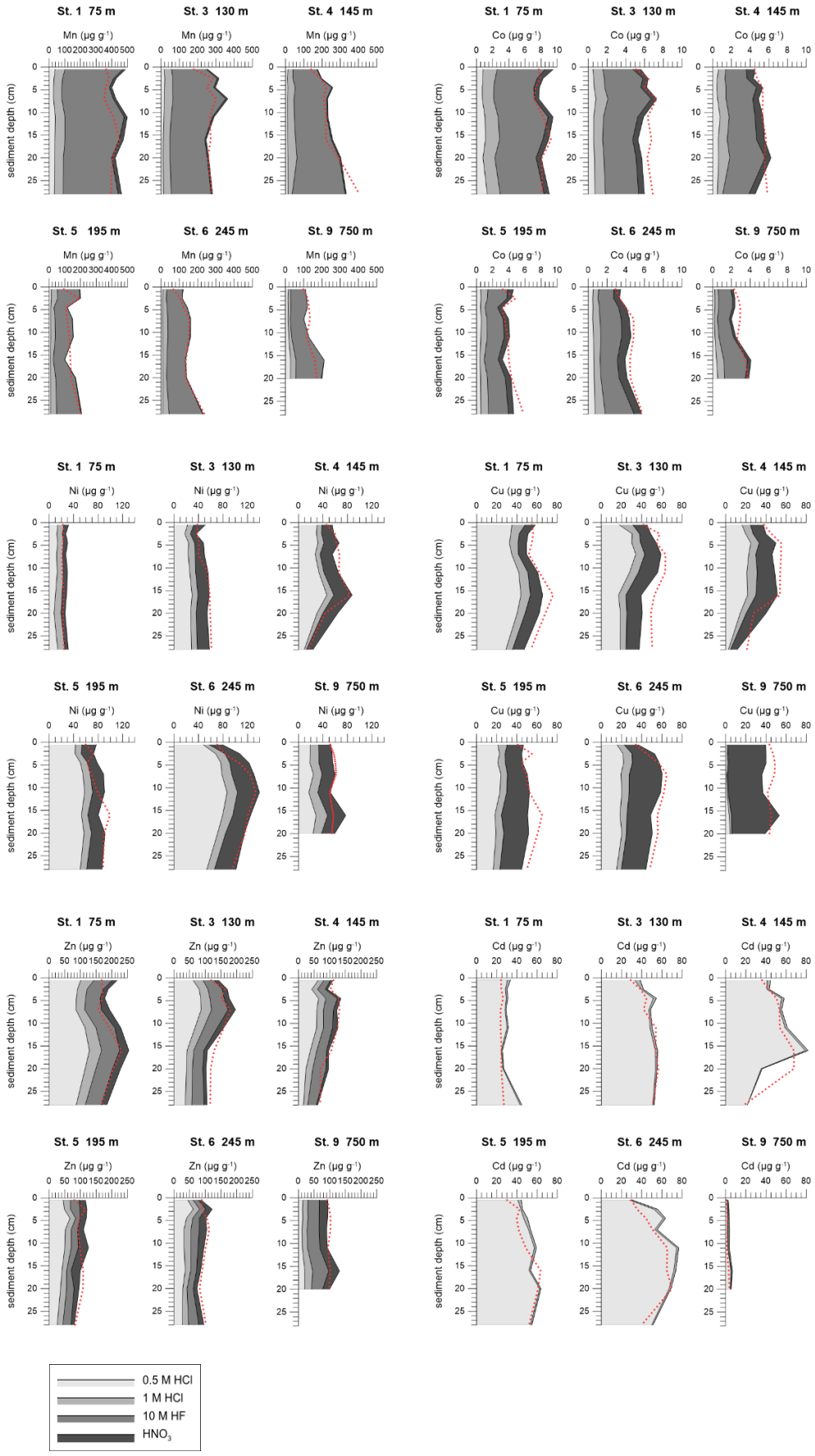

Figure III.4: Total trace metal contents in sediments determined from total digestions (red dashed line) and trace metal contents in different fractions determined from sequential extractions (HCl, HNO_3, HF).

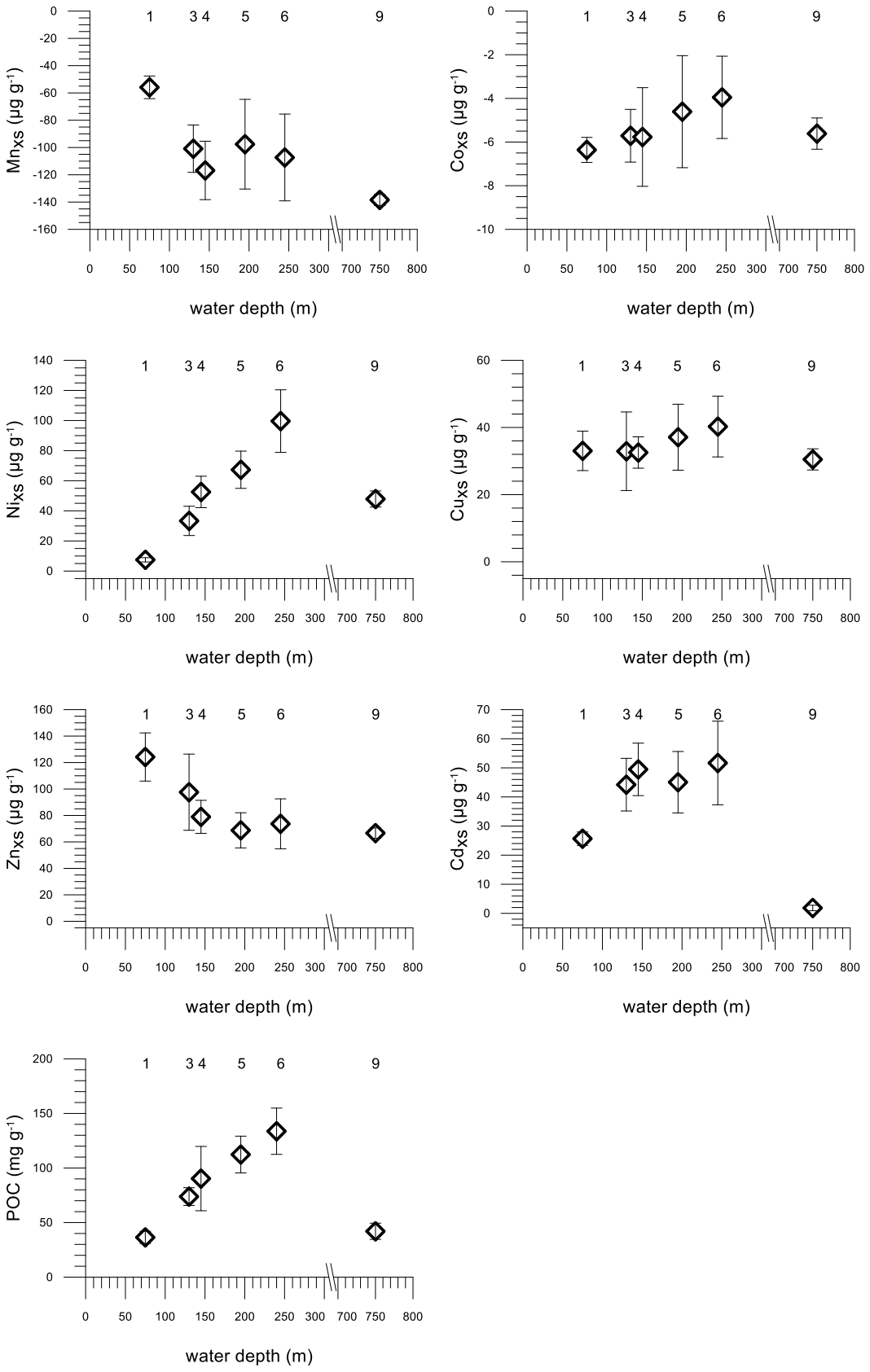

Figure III.5: Enrichment of trace metals (TM_{xs}) compared to the lithogenic background against water depth. The average particulate organic carbon content is also plotted. Numbers in the upper panel depict station numbers.

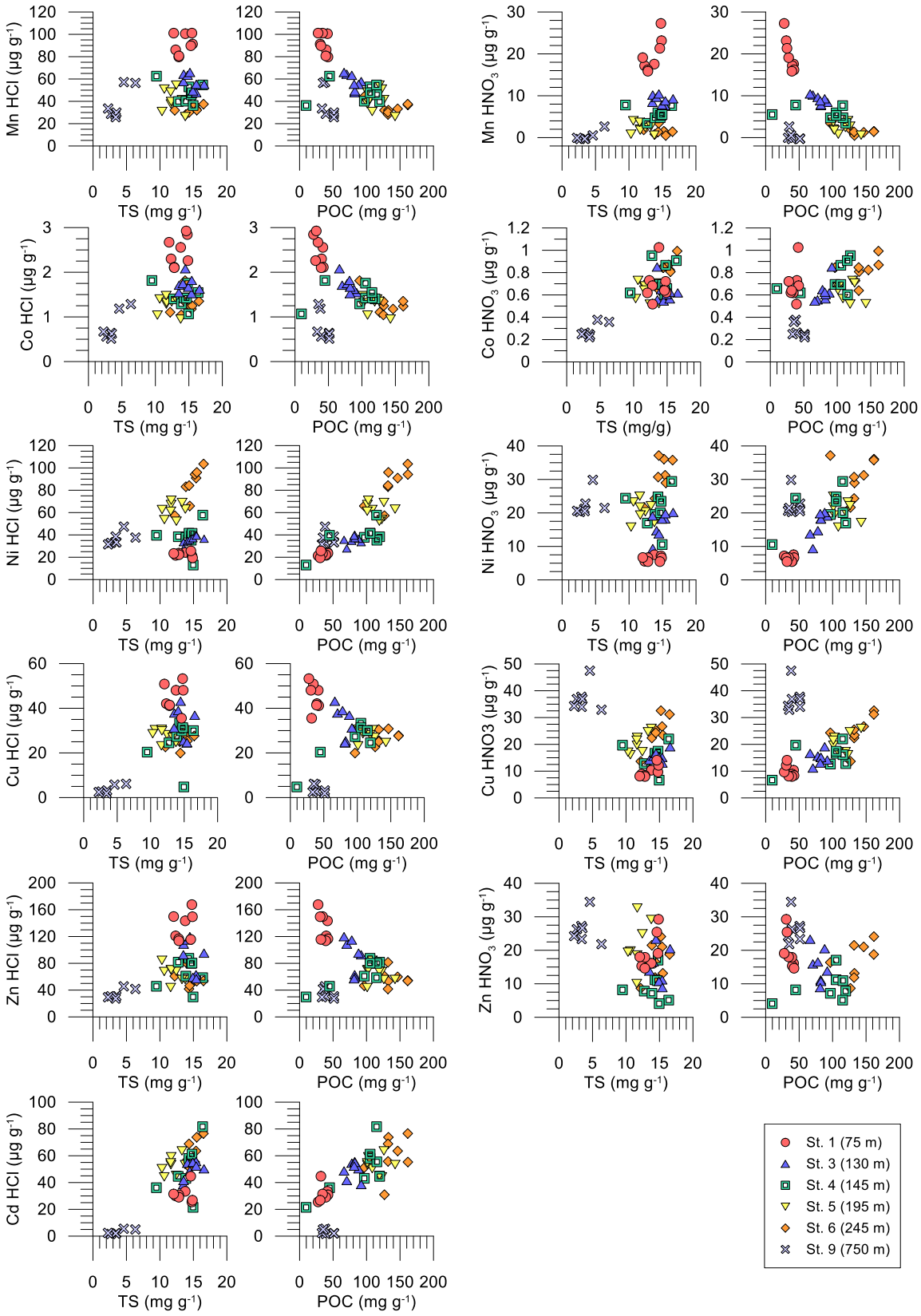

Figure III.6: Cross plots of trace metal contents in the combined HCl-fractions (TMs associated with monosulphides, (oxyhydr)oxides, carbonates and hydrous aluminosilicates) and HNO_3-fraction (TMs associated with pyrite and organic matter) from sequential extractions versus total sulphur (TS) and particulate organic carbon (POC) contents. Since no Cd was present in the HNO_3-fraction it is not shown.

III.3.4 Sequential extraction data

As pointed out in Section 2.2, multiple TM host phases may be dissolved in each step of the sequential extraction procedure (Huerta-Diaz and Morse, 1990; Zimmerman and Weindorf, 2010). Therefore, we refer to the extraction medium rather than specific target phases hereafter. The distribution of each TM across the different fractions was similar at all stations. The sum of the TM fractions mostly matched well with total TM contents obtained by total digestion (Fig. III.4).

At all stations, the largest proportion (> 60 %) of sedimentary Mn and Co was present in the HF-fraction (i.e. as silicates). Most of the remaining Mn and Co was present in the combined HCl-fractions (i.e. as monosulphides, (oxyhydr)oxides, carbonates). Compared to Mn (2 to 6 %), a larger amount of Co (7 to 21 %) was present in the HNO_3-fraction (i.e. as pyrite or organic matter). Approximately half of the total sediment contents of Ni and Cu were present in the $HCl_{0.5M}$-fraction. The remaining Ni was contained in the HNO_3-fraction (30 %) and HCl_{1M}-fraction (20 %). The main host phase of Cu switched from the $HCl_{0.5M}$-fraction towards the HNO_3-fraction with increasing water depth. Similar to Ni and Cu, half of the total Zn content at the shelf stations was present in the $HCl_{0.5M}$-fraction. The remaining Zn was distributed among the HF-fraction (25 %), HCl_{1M}-fraction (20 %) and HNO_3-fraction (10 %). At St. 9 (750 m), most Zn was present in the HF-fraction (40 %). With the exception of Station 9, Cd was almost exclusively contained in the $HCl_{0.5M}$-fraction (95 %).

The combined HCl- and the HNO_3-extractions are plotted against TS and POC contents to help further constrain whether TMs in these host phases are likely to be associated with organic matter or sulphide minerals, respectively (Fig. III.6). The data showed a negative correlation at the shelf stations (St. 1 to 6, 75 to 245 m) between POC and Mn, Co and Zn in the HCl-fraction (R^2 = 0.61, 0.56 and 0.36 respectively) and in the case of Mn also in the HNO_3-fraction (R^2 = 0.68) ($p < 0.001$). At the shelf stations, a positive correlation with POC was found for Ni in the HCl- and HNO_3-fractions (R^2 = 0.74 and 0.63 respectively, $p < 0.001$). A positive correlation of POC with Cu was also observed at the shelf stations in the HNO_3-fraction (R^2 = 0.75) and for Cd in the HCl-fraction (R^2 = 0.57) ($p < 0.001$). Most TMs showed no clear correlation with TS considering all shelf station data. However, in the HCl-fraction of the deeper Stations 5 to 9 (195 to 750 m), Cd, Ni, and Cu (R^2 = 0.93, 0.83 and 0.82 respectively, $p < 0.001$) and to a lesser extent Zn (R^2 = 0.46, $p = 0.001$) correlated with TS. If only

St. 1 and 9 are considered, Co and Mn would fall on a line of linear regression in the HCl- (R^2 = 0.94 and 0.92 respectively) and in the HNO_3-fraction (R^2 = 0.77 and 0.71 respectively) ($p < 0.001$). If all stations are considered, Co still positively correlated with TS in the HNO_3-fraction (R^2 = 0.61, $p < 0.001$).

III.4 Discussion

III.4.1 Sedimentary depletion of manganese and cobalt

In line with other studies (Böning et al., 2004; Scholz et al., 2011; Little et al., 2015), our data showed depletion of Mn and Co in sediments on the Peruvian margin (Fig. III.6). Excess fluxes of both TMs displayed a similar pattern of decreasing depletion along the transect and with distance from the coast (Mn: -1161 to -100 µmol m^{-2} y^{-1}, Co: -123 to -3.5 µmol m^{-2} y^{-1}) (Fig. III.7). The depletion must be caused by a transfer of TMs from the solid phase to the dissolved phase and transport away from the study area. In anoxic sediments, Mn is commonly released from the solid phase to the sediment pore water through the reductive dissolution of Mn-oxides coupled to the remineralisation of organic matter (Canfield and Thamdrup, 2009). The sedimentary cycling of Mn and Co is often coupled, whereby Co delivery is generally associated with Mn-oxides. Dissolution of Mn-oxides thus also releases Co to pore waters under reducing conditions (Heggie and Lewis, 1984; Gendron et al., 1986; Sundby et al., 1986; Scholz and Neumann, 2007; van de Velde et al., 2020). However, our data are only partly consistent with a close coupling between the cycling of Mn and Co on the Peruvian shelf because the contribution of diffusive benthic efflux to the sedimentary depletion differs between the two TMs.

The diffusive Mn effluxes from the sediment pore water into the bottom water of 26 to 551 µmol m^{-2} y^{-1} determined from our sampling campaign may vary temporally as function of bottom water oxygen concentrations. The fluxes are remarkably similar to 5 to 460 µmol m^{-2} y^{-1} determined off Peru at 11°S in 2008 (Scholz et al., 2011), but orders-of-magnitude lower than values observed in less reducing continental margin systems (McManus et al., 2012) and restricted basins (Pakhomova et al., 2007; van de

Velde et al., 2020). The diffusive fluxes agreed well with the overall sedimentary depletion at St. 4 (145 m) and 6 (245 m) (Fig. III.7), demonstrating that loss by diffusion across the sediment-water interface can account for Mn depletion at these sites. At St. 1 (75 m), 3 (130 m) and 5 (195 m) only half of the depletion can be related to benthic efflux. Following previous studies (Landing and Bruland, 1987; Johnson et al., 1996; Noble et al., 2012), we argue that the remaining Mn dissolution takes place in the anoxic water column. Efficient offshore transport of the dissolved Mn liberated from particles in the water column and sediments (Vedamati et al., 2014a) can explain sedimentary Mn depletion and generally low benthic Mn fluxes compared to other marine systems. At the slope station with oxic bottom water (St. 9, 750 m), Mn depletion may be related to the particular sediment composition (phosphorite, glauconite and lag sediment that generally contain less Mn) or to downslope transport of Mn-depleted shelf sediment that has undergone extensive leaching prior to deposition on the slope.

Few studies have reported diffusive benthic Co fluxes from sediments. The effluxes of Co observed in our study were similar to those reported for sediments from underneath oxygen-deficient bottom waters in the Santa Monica basin (around -4 µmol m^{-2} y^{-1}) (Johnson et al., 1988). In contrast to Mn, however, these are far too low to account for a substantial portion of the total depletion from the solid phase (up to -123 µmol m^{-2} y^{-1}). Particularly at St. 1 (75 m) and St. 3 (130 m), the diffusive efflux accounted for less than 10 % of the total depletion (Fig. III.7). As for Mn at St. 1, 3 and 5, this implies that the bulk of particle-associated Co must have already dissolved in the water column before reaching the seafloor.

The release of Co from particles in oxygen-deficient upwelling regions is believed to play an important role in the Co budget of the upper ocean (Saito et al., 2004; Noble et al., 2012). Model results suggest that the main external input flux of dissolved Co to the ocean derives from sediments at continental margins, two thirds of which is derived from sediments underneath oxygen-deficient bottom waters (Tagliabue et al., 2018). By comparing Co:Al ratios in sediments off Peru to the ratio of the lithogenic background, Hawco et al. (2016) calculated that around half of the land-derived particulate Co is dissolved, which leads to the formation of a large Co plume observed in the water column off Peru. This estimate agrees well with sedimentary Co:Al ratios in our study. For comparison, Mn:Al ratios indicate that only 10 – 40 % of

land derived particulate Mn is ultimately lost from the sediments. Modelling studies estimated Co fluxes from sediments off Peru of 25 µmol m^{-2} y^{-1} (Tagliabue et al., 2018). The total depletion at the shelf stations 3, 4 and 5 (-27 to -12 µmol m^{-2} y^{-1}) is in good agreement with this estimate. However, our findings reveal that < 5 µmol m^{-2} y^{-1} is released from the sediments by diffusion whereas the majority of the Co is dissolved in the water column.

The spatial decoupling between the release of Co and Mn may be explained by a scenario where Co desorption from Mn oxide surfaces (Murray, 1975; Shaw et al., 1990) happens more readily and prior to Mn oxide dissolution itself. An alternate explanation could be that upon release, Co chiefly remains in the dissolved phase whereas Mn undergoes partial re-precipitation in the water column and deposition at the seafloor. This mechanism may be particularly relevant at the shallow shelf (St. 1, 75 m) where the relative depletion of Co compared to Mn is higher (Co_{xs}:Mn_{xs} = 0.1) than further offshore (Co_{xs}:Mn_{xs} = 0.04) due to decreasing Mn:Al ratios (derived from Fig. III.5). Consistent with this scenario, Mn oxidation has been shown to be faster than Co oxidation (Landing and Bruland, 1987; Tebo, 1991; Thamdrup et al., 1994; Moffett and Ho, 1996; Noble et al., 2012). Therefore, once released into the water column, there is little Co scavenging or removal (Noble et al., 2012; Hawco et al., 2016). Instead, Co concentrations in the water column are primarily controlled by phytoplankton uptake rather than co-precipitation with Mn (Saito et al., 2004).

Within the sediment pore water, a decoupling was observed between Mn and Co since dissolved Co:Mn ratios exceeded crustal and phytoplankton ratios and increased in a downcore direction (Fig. III.8). Increasing Co:Mn ratios in pore water were related to decreasing Mn concentrations below a shallow maximum, which is attributed to the precipitation of Mn carbonate or Mn adsorption onto calcite (Middelburg et al., 1987; Kuleshov, 2017). Consistent with this notion, reactive Mn is mainly present in the HCl soluble fraction, which contains Mn carbonates, oxides and potentially some Mn bound to silicate minerals. In contrast to Mn, a significant proportion of sedimentary Co (7 to 21 %) was extracted with HNO_3 and Co concentrations within this fraction covaried with TS, which is mainly present as pyrite (Suits and Arthur, 2000; Scholz et al., 2014b). This observation suggests that authigenic pyrite is an important burial phase for Co in Peru margin sediments. Overall, preferential precipitation and retention of Mn relative to Co in sediments on the shallow

shelf is likely to contribute to increasing sedimentary Co to Mn contents along the transect (Fig. III.4).

III.4.2 Sedimentary enrichment of nickel, copper, zinc and cadmium

The TMs Ni, Cu, Zn and Cd are enriched in sediments throughout the study area. Zinc is the only TM where diffusion across the sediment-water interface can explain the majority of TM accumulation (Fig. III.7). By contrast, Ni, Cu and Cd must primarily be supplied by particles. Nickel displays a negative diffusive flux out of the sediment indicating that a fraction of the particulate TM delivered is solubilised within the sediment and recycled into the bottom water. The various TM delivery pathways are discussed in the following sections.

III.4.2.1. Diffusive delivery of Zn

Based on a covariation between Zn enrichment factors and POC concentrations in sediments and elevated Zn concentrations in plankton, prior studies concluded that biological uptake and deposition of organic material represents the main delivery pathway of Zn to sediments on the Peruvian margin (Böning et al., 2004; Little et al., 2015). In contrast, our flux data reveal that this mechanism can only explain 10 to 20 % of the Zn accumulation on the shelf (60 to 2230 µmol m^{-2} y^{-1}) (Fig. III.7). We find that molecular diffusion of Zn is the main process of Zn delivery to the sediments on the Peruvian margin. The diffusive flux of Zn into the sediment equals the total enrichment flux at St.1 (75 m) (around 2000 µmol m^{-2} y^{-}1) and the fluxes at the other shelf stations are high enough or even exceed the fluxes required to account for the excess Zn accumulation.

A steep Zn concentration gradient between the bottom water just above the sediment surface and pore waters was the driver for high diffusive fluxes (Fig. III.3). Water column studies report Zn concentrations of only a few nanomoles (maximum10 nM) in open ocean waters (Bruland and Lohan, 2006; Tim M Conway and John, 2014; Conway and John, 2015a; Janssen and Cullen, 2015; Sieber et al., 2020) including those within the Peruvian OMZ (John et al., 2018b; Rapp et al., 2020). However, only

a few Zn concentration data for bottom waters are available. In bottom waters from benthic chamber incubations in productive coastal environments, Zn concentrations can reach several hundred nanomoles (Westerlund et al., 1986; Ciceri et al., 1992; Turetta et al., 2005), which is similar to the bottom water concentrations found in our study (23 to 780 nM) (Fig. III.3). We suggest that the high Zn concentrations in bottom water are due to Zn release from labile organic matter within the benthic fluff layer overlying the sediment. In that case, organic material could still play a role in the delivery of easily dissolvable Zn to the seafloor. However, any Zn bound to organic material is unlikely to originate through direct uptake from the photic zone as this flux is far lower compared to the diffusive flux. Instead, Zn scavenging by downward sinking organic material or Zn incorporation by pelagic microbial communities could be a viable mechanisms by which Zn is bound to organic molecules (Sheng et al., 2004; Vijayaraghavan et al., 2005; Ohnemus et al., 2017).

III.4.2.2 Particulate supply of Ni, Cu and Cd by organic matter or metal oxides

Particulate supply with phytoplankton-derived organic matter may contribute to the accumulation of Ni, Cu, and Cd in Peru margin sediments to a significant extent (Fig. III.7). This is particularly the case for Ni, where uptake by phytoplankton and delivery to the seafloor could explain between 100 % (St. 1, 75 m) and 20 % (St. 5, 195 m) of the excess Ni accumulation at the shelf stations (87 to 180 µmol m^{-2} y^{-1}). A correlation between Ni and POC is typically found in sediments below OMZs in upwelling regions, including the sediments off Peru (Böning et al., 2015; Ciscato et al., 2018a). It has been argued based on a correlation between concentrations of Ni and chlorine (an intermediate degradation product of chlorophyll pigments) in surface sediments off Peru that excess Ni is ultimately derived from enzymes within diatoms (Böning et al., 2015). A coupled supply of Ni and organic matter to the sediment is also supported by our sediment data. The station with the highest sedimentary Ni contents also showed the highest POC content (St. 6, 245 m) (Table III.S.4) and sequential extraction data of Ni correlated with POC contents in the HNO_3-fraction (Fig. III.6).

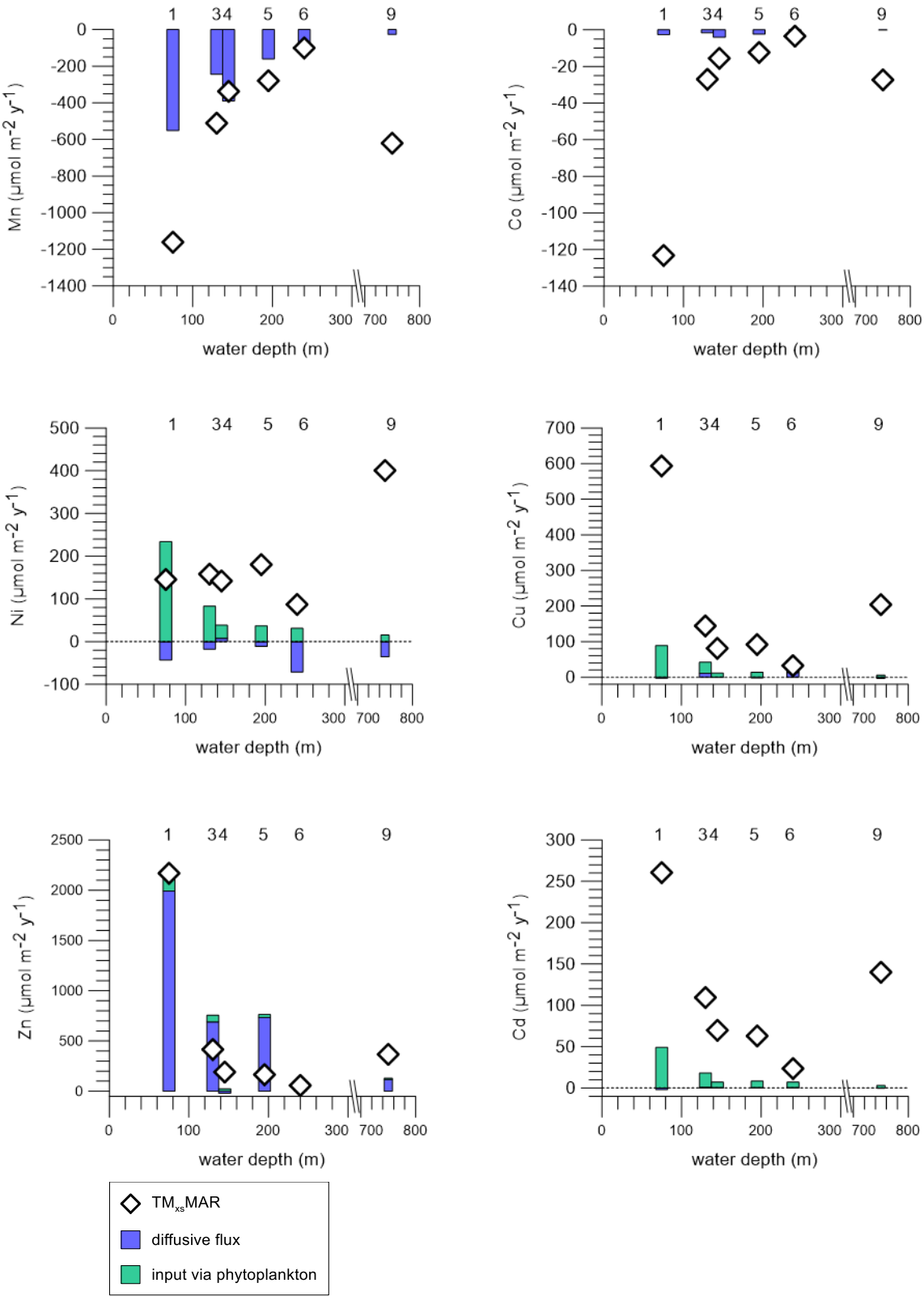

Figure III.7: Sedimentary trace metal excess accumulation or loss ($TM_{xs}MAR$) (diamonds) and the contribution of trace metal delivery to or removal from the sediment via different pathways; diffusion across the sediment-water interface (blue) and trace metal incorporation by phytoplankton and delivery to the sediment with organic matter (green) (displayed is the maximum value, see Methods). Positive values represent fluxes into the sediment whereas negative values represent fluxes out of the sediment. Numbers in the upper panel depict station numbers.

Table III.1: Sedimentary trace metal excess accumulation ($TM_{xs}MAR$) and the contribution of trace metal delivery to the sediment by diffusion and via incorporation by phytoplankton and deposition of organic particles (see section III.2.4 for a detailed description how these fluxes were calculated).

Station	Diffusive flux (µmol m^{-2} y^{-1})						Input via phytoplankton [1] (µmol m^{-2} y^{-1})						Excess accumulation [2] (µmol m^{-2} y^{-1})					
	Mn	Co	Ni	Cu	Zn	Cd	Mn	Co	Ni	Cu	Zn	Cd	Mn	Co	Ni	Cu	Zn	Cd
1	-551	-2.57	-43.2	-2.82	1993	-1.84	112/ 656	7.55/ 44.4	39.8/ 234	15.1/ 88.8	32.3/ 190	8.34/ 49.0	-1160	-123	145	594	2170	261
3	-244	-1.66	-17.6	10.6	688	0.83	65.1/ 233	4.41/ 15.8	23.2/ 83.0	8.82/ 31.5	18.9/ 67.3	4.87/ 17.4	-511	-27.0	158	144	415	110
4	-390	-4.05	7.63	-0.40	-20.3	0.54	20.8/ 86.6	1.41/ 5.86	7.41/ 30.9	2.81/ 11.7	6.02/ 25.1	1.56/ 6.48	-386	-18.3	117	61.5	212	63.0
5	-160	-2.33	-11.5	-1.94	733	0.63	76.3/ 103	5.17/ 7.00	27.2/ 36.8	10.3/ 14.0	22.1/ 29.8	5.71/ 7.71	-279	-11.0	180	91.8	165	63.0
6	-128	-3.96	-71.3	12.7	20.9	0.55	48.1/ 87.4	3.26/ 5.92	17.2/ 31.2	6.51/ 11.8	13.9/ 25.3	3.60/ 6.54	-100	-3.44	87.0	32.5	57.8	23.6
9	-26.4	-0.13	-35.7	-3.47	117	0.30	19.7/ 42.9	1.34/ 2.90	7.04/ 15.3	2.67/ 5.81	5.71/ 12.4	1.48/ 3.21	-880	-33.3	249	168	356	5.78

[1]multiplying the TM:C ratio in average phytoplankton (Moore et al., 2013) with particulate organic carbon rain rates (maximum values) and organic carbon accumulation rates (minimum values) for each site (data from Dale et al. (2015b)).

[2]Excess accumulation was calculated from Eq. III.2 by multiplying the trace metal excess (calculated after Brumsack (2006) (Eq. III.1) with the sediment mass accumulation rate for each site (Dale et al., 2020).

In potential conflict with the above discussion, other studies have estimated that direct Ni uptake by phytoplankton and organic matter export can contribute only a fraction of the Ni_{xs} in Peru margin sediments (Little et al., 2015; Ciscato et al., 2018a). This conclusion is based on a mismatch between the Ni enrichment factor and POC contents in Peruvian sediments compared to sediments below other oxygen depleted regions and higher Ni_{xs}:Zn_{xs} compared to plankton ratios (Little et al., 2015). Furthermore, Ciscato et al. (2018) found a mismatch between Ni:C and Ni:Si ratios in diatoms and Peru margin sediments. However, the Ni:C of sinking diatoms may be increased by preferential dissolution of POC or by Ni incorporation in reducing microniches within sinking organic matter, both of which would obscure Ni supply by diatom remains (Ciscato et al., 2018a). Furthermore, sedimentary organic carbon is subject to degradation (Dale et al., 2015b), biogenic silica undergoes dissolution (Dale et al., 2020) and Zn is delivered by molecular diffusion (see Section III.4.2.1). Therefore, a match between Ni:C, Ni:Si and Ni:Zn in diatoms or plankton and sediments is not expected. We compensate for the mismatch between organic carbon delivery and sedimentary POC by considering POC rain rates rather than POC burial rates.

Our estimate of Ni delivery with organic material is still dependent on the Ni:C ratio within fresh biomass, which is applied in our calculations ($8.06 \cdot 10^{-6}$). Using a regional Ni:C ratio for diatoms ($3.7 \cdot 10^{-6}$) (Twining et al., 2011), POC-associated excess Ni would decrease by ~50 %. In contrast, applying the regional bulk plankton maximum ratio ($11.9 \cdot 0^{-6}$) (Twining et al., 2011), the excess delivery would increase by ~50 %. Another regional bulk plankton (mostly zooplankton) Ni:C ratio estimate ($9.15 \cdot 10^{-6}$) (Collier and Edmond, 1984) is similar to the value used in our calculation. Using the Ni:C ratio from particulate data off Peru ($3.71 \cdot 10^{-5}$), organic matter could supply between 80 to 100 % of Ni excess on the shelf. However, this ratio is derived from particles that are likely enriched in TMs by prokaryotic communities (Ohnemus et al., 2017). The Ni:POC ratio measured in bulk sediments off Peru (average $16 \cdot 10^{-5}$) were generally higher than the plankton ratios reported above (Fig. III.9). However, the ratios in the uppermost surface sediment sample were closer to phytoplankton ratios than sedimentary ratios further downcore (surface Ni:POC = $8 \cdot 10^{-5}$ to $10 \cdot 10^{-5}$ at St. 3 to 6). This observation suggests that Ni is progressively enriched relative to C during degradation of organic matter and early diagenesis. Overall, our estimates suggest that biological Ni uptake and delivery with organic material make an important

contribution to Ni accumulation in Peru margin sediments. However, determining the TM:C ratio in fresh local phytoplankton and zooplankton before alteration and in sinking biogenic particles near the seafloor would help to reduce the uncertainty of TM fluxes associated with organic matter on the Peruvian margin.

Some of the mismatch between Ni supply with organic matter and total Ni accumulation could be related to the delivery of other Ni-containing particulate phases such Mn- and Fe-oxides, which are known to scavenge Ni from the water column (Shaw et al., 1990; Audry et al., 2006; Little et al., 2015; Olson et al., 2017). The Ni content of the Mn-oxide birnessite has been shown to be as high as 40 mg g^{-1} (Peacock and Sherman, 2007). Especially at the deeper shelf stations, where Ni delivery with organic material is less important (20 to 50 %), Ni delivery by Mn- and Fe-oxides could be important. Such a scenario is also supported by increasing Ni concentrations within the pore water of surface sediments, which coincides with the initial accumulation of dissolved Mn (and also of Fe) (Plass et al., 2020).

Only 16 to 36 % of the excess Cu accumulation (33 to 594 µmol m^{-2} y^{-1}) can be explained as direct uptake by phytoplankton (Fig. III.7). The remainder must be delivered by another particulate phase. Pore water profiles of Cu and Cd (Fig. III.3) do not provide evidence for major recycling processes within the surface sediment, which is why release of these elements from Mn- and Fe-oxides appears to be unlikely. However, it is known that Cu is quite reactive towards biogenic particles and scavenging by sinking biogenic material has been argued to be an important vector for Cu transfer from the water column to the sediment (Fischer et al., 1986; Johnson et al., 1988; Shaw et al., 1990; Sheng et al., 2004; Vance et al., 2008; Roshan and Wu, 2015; Little et al., 2017). Furthermore, the binding of Cu to organic matter is very stable and a decrease in bottom water oxygen concentrations has been shown to increase the association of Cu with organic matter (Fischer et al., 1986; Chakraborty et al., 2015; Chakraborty et al., 2016). It therefore seems likely that the positive correlation between POC and Cu in the HNO_3-fraction (Fig. III.6) is due to Cu association with organic matter, either in the water column or during early diagenesis. In suspended particles off Peru, Cu:C ratios ($2.9 \cdot 10^{-5}$) are elevated compared to phytoplankton and particulate Cu concentrations increase with water depth (Ohnemus et al., 2017; Lee et al., 2018). Using this elevated Cu:C ratio to calculate Cu delivery with organic matter yields a maximum estimate, which could explain the total Cu excess accumulation in

shelf sediments. However, this ratio does not represent surface to mixed layer phytoplankton uptake (Ohnemus et al., 2017; Lee et al., 2018) but rather reflects the affinity of Cu to associate with sinking particles.

III.4.2.3 Precipitation of TM sulphide minerals within the water column or sediment

The TMs Cu, Zn and Cd are known to form their own sulphide minerals rather than to become incorporated into Fe sulphides such as mackinawite (FeS) and pyrite (FeS_2). Furthermore, their solubility in sulphidic water is low compared to Mn, Co and Ni (Morse and Luther, 1999; Audry et al., 2006). It is thus likely that interaction with H_2S, either within the sediment or during sulphidic events in the water column, affects the mobility of Cu, Zn and Cd to some extent.

Cadmium sulphide (greenockite) has the lowest solubility among the TM sulphides that are relevant to this study. In the marine environment, greenockite precipitates at the presence of trace amounts of H_2S (Davies-Colley et al., 1985; Rosenthal et al., 1995). In a previous study, Plass et al. (2020) demonstrated based on benthic chamber incubation data that Cd sulphide precipitation in near bottom waters can quantitatively account for the majority (up to 60 %) of excess Cd accumulation on the Peruvian margin (24 to 260 µmol m^{-2} y^{-1}). Our new sequential extraction data provide additional evidence for the importance of Cd sulphide as a delivery and burial phase of Cd. At the shelf stations, Cd was exclusively present in the HCl-fraction at all sediment depths (Fig. III.4) and Cd in the HCl-fraction correlated with TS (Fig. III.5).

The behaviour of Cu in sulphidic environments is complex since multiple different Cu sulphide minerals, which may be dissolved in either HCl or HNO_3, exist (Morse and Luther, 1999). Furthermore, Cu may occur as Cu(I) or Cu(II) in these minerals and the conditions under which Cu reduction takes place is matter of debate (Pattrick et al., 1997; Theberge et al., 1997; Al-Farawati and van den Berg, 1999; Ehrlich et al., 2004; Goh et al., 2006). Copper forms sulphide complexes in anoxic waters, which are quite stable compared to other TM sulphide complexes (Dyrssen, 1988; Pattrick et al., 1997; Theberge et al., 1997; Al-Farawati and van den Berg, 1999). Experimental studies demonstrated that Cu sulphide complexes can be precipitated

as covellite (CuS) from aqueous solutions (Luther et al., 2002). Therefore, a particulate Cu input via sulphide precipitation may contribute to the Cu enrichment in Peruvian sediments (cf. Ciscato et al., 2019). In particular at St. 1 (75 m), where the contribution of organic matter is rather low (< 3%) and pore waters were highly sulphidic, a possible release of H_2S into bottom water may have favoured Cu sulphide precipitation, in a similar manner as suggested for Cd. Ciscato et al. (2019) hypothesized that Cu sulphide precipitation in the water column and sediment is the main control on Cu delivery and retention in the Peru margin sediments. We cannot clearly distinguish between Cu bound to sulphide minerals or organic matter with our sequential extraction data. Given that we observed a positive correlation of Cu extracted with HNO_3 and POC, Cu in this phase is likely related to organic matter rather than sulphide. However, Cu sulphides may be present within the HCl phase, in which a positive correlation with TS was observed (Fig. III.6).

Unlike Cd (and maybe Cu), the precipitation of Zn sulphides (e.g., sphalerite) in the water column is not an important mechanism of Zn delivery to the seafloor. However, Zn sulphide precipitation within the sediment (Morse and Luther, 1999) is likely to be the ultimate reason for low Zn concentrations in pore water (< 5 nM) and downward diffusion of Zn from the bottom water. This notion is supported by our sequential extraction data showing that the majority of Zn in shelf sediments is present in the HCl-fraction (60 %), which contains ZnS (Fig. III.4). By contrast, on the slope at St. 9 (750 m), where no H_2S was detected, Zn concentrations in pore waters are higher (up to 18 nM) and only 30 % of Zn is present in the HCl-fraction. Zinc removal from the anoxic water column has also been ascribed to Zn sulphide precipitation in particle microenvironments (Conway and John, 2015a; Janssen and Cullen, 2015). However, according to our data such a mechanism is not required to explain excess Zn accumulation in the sediment.

In contrast to Cu, Zn and Cd, Ni is unlikely to be delivered and/or buried as sulphide mineral on the Peruvian margin. In sulphidic marine environments, Ni is co-precipitated with pyrite and does not form its own sulphide minerals (Morse and Luther, 1999). Furthermore, Ni does not become precipitated from anoxic-sulphidic water columns (Tankéré et al., 2001). In agreement with a subordinate role of sulphides as a host phase for Ni in the sediment, Ni in both the HCl-fraction and the HNO_3-fraction correlated with POC rather than TS (Fig. III.6).

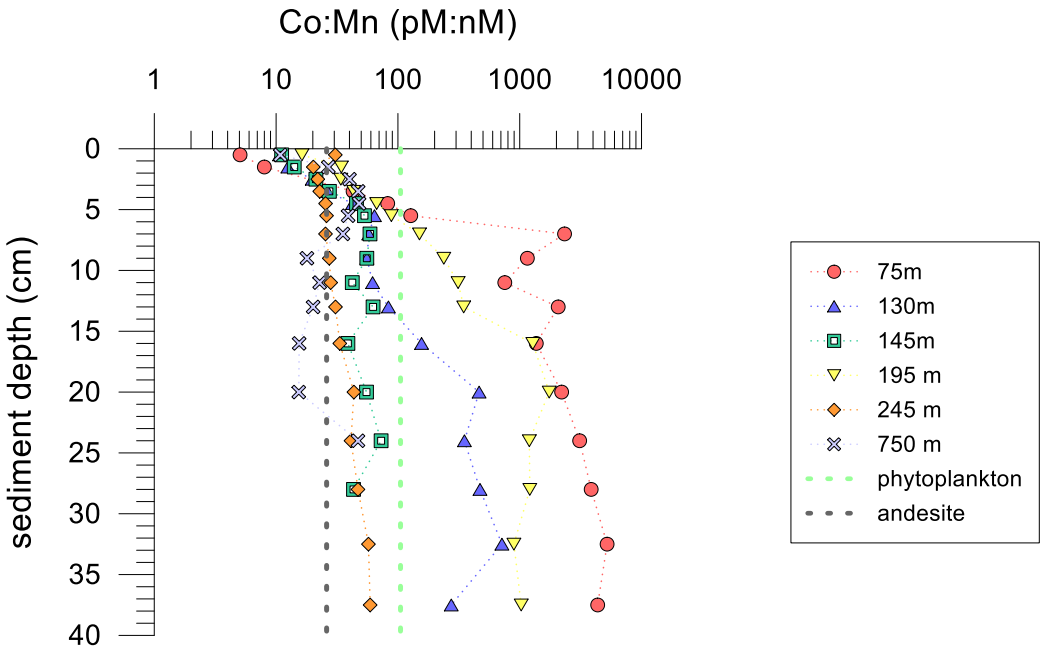

Figure III.8: Cobalt to manganese ratio (Co:Mn) in sediment pore waters, average phytoplankton (Moore et al., 2013) and andesitic crust (Taylor and McLennan, 1995).

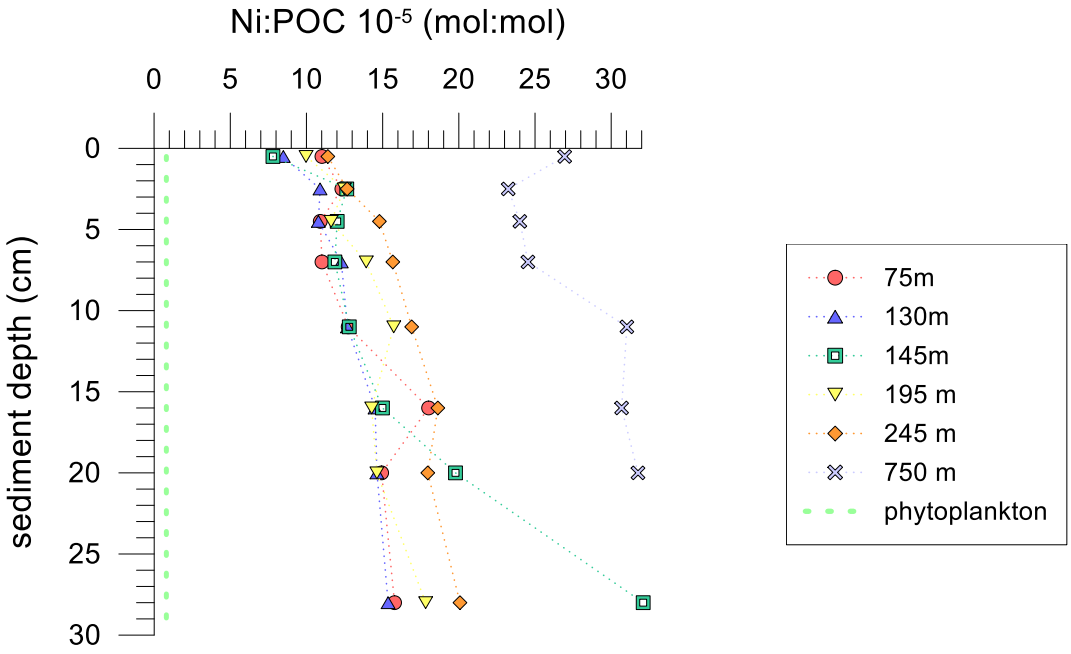

Figure III.9: Nickel to particulate organic carbon ratio (Ni:POC) within bulk sediments and average phytoplankton (Moore et al., 2013).

III.5 Summary and conclusions

We presented TM data for sediments and pore waters along a latitudinal transect across the OMZ off Peru. Consistent with previous studies, our data reveal that sediments on the Peruvian shelf are a source of dissolved Mn and Co to the water column, whereas they represent a sink for dissolved Ni, Cu, Zn and Cd. We provided mass accumulation rates and diffusive benthic fluxes for each element, which can be used to better constrain trace metal fluxes in models and mass balances. Furthermore, our data provide new insights into the pathways and main processes by which TMs are lost from or delivered to the sediment. Our findings are summarized in a schematic sketch shown in Figure III.10:

1. Manganese and Co show a similar pattern of sedimentary depletion across the transect but the location where dissolution and liberation from particles takes place is different. While Mn is mostly solubilised in the sediment and lost to the water column by molecular diffusion across the sediment-water interface, the vast majority of Co is already liberated in the water column. Moreover, partial Mn retention in the sediment as Mn carbonates contributes to the decoupling of Mn and Co accumulation in Peruvian margin sediments.

2. Delivery of Ni to the sediment seems to be mostly mediated via Ni uptake by phytoplankton and downward sinking of organic material. In addition, scavenging of Ni by metal oxides in the water column may contribute to Ni accumulation in the sediment and some Ni recycling across the sediment-water interface as a result of metal oxide reduction.

3. Direct uptake of Cu, Zn and Cd by phytoplankton can explain only a minor fraction of the sedimentary accumulation of these TMs. Instead, Cu and Zn may become passively scavenged by organic material during downward sinking though the water column.

4. The majority of Zn accumulation is mediated by Zn sulphide precipitation in the sediment coupled to molecular diffusion of Zn across the sediment-water interface. High benthic Zn fluxes are primarily driven by high Zn concentrations in bottom waters, which are attributed to Zn liberation from labile organic matter within the fluffy layer overlying the sediment surface.

5. Cadmium delivery to the sediment surface is mediated by sulphide precipitation in the near-bottom water. A similar process may contribute to the particulate delivery of Cu to the sediment.

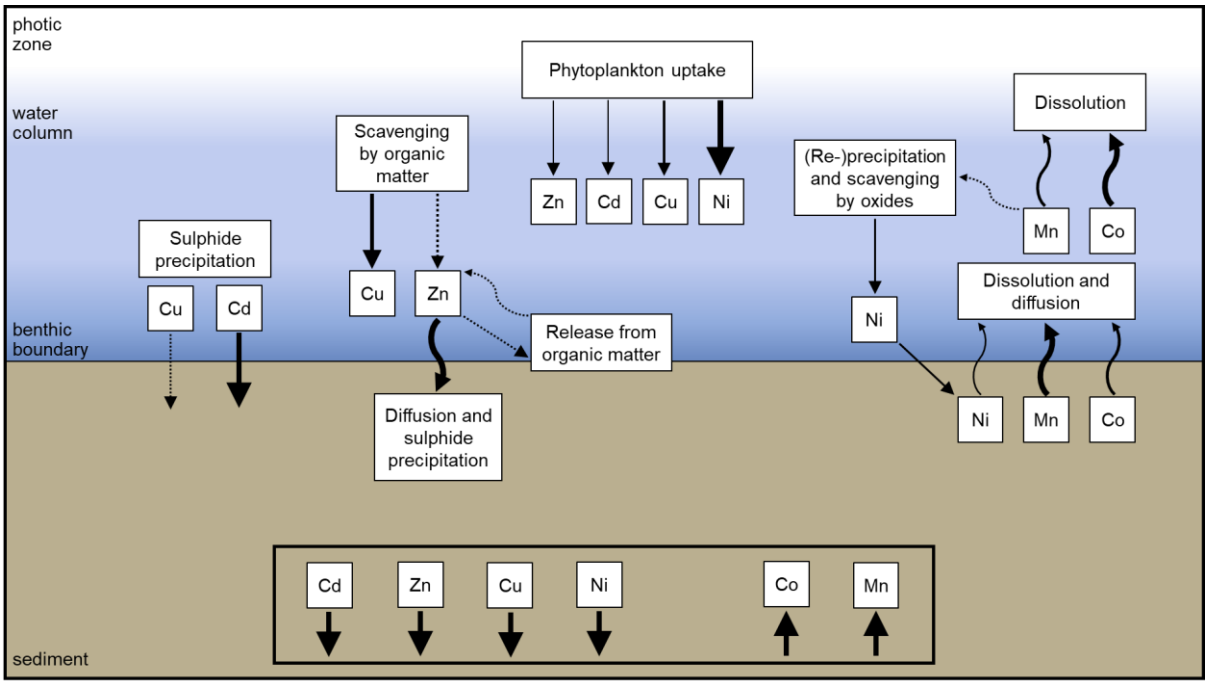

Figure III.10: Schematic sketch illustrating the main pathways and processes by which TMs are lost from or delivered to Peru margin sediments. Straight arrows represent solid phase transport, curved arrows represent dissolved transport. Dashed arrows denote possible transport and precipitation processes that are uncertain but can be potentially important. The arrow size depicts the relative magnitude of the flux. The lower pannel illustrates net-depletion (upward directed arrow) or net-enrichment (downward directed arrow) of the different trace metals in the sediment.

Our results demonstrate that bio-essential TMs are characterized by a complex and divergent behaviour under low-oxygen conditions. A decline in oceanic oxygen concentrations and an expansion of OMZs has been observed over the last decades (Stramma et al., 2010; Helm et al., 2011; Schmidtko et al., 2017) and is predicted to continue in the future (Bopp et al., 2002; Oschlies et al., 2008; Keeling et al., 2010). According to our findings, TMs will respond differently to declining oxygen

concentrations and the associated expansion of sulphidic conditions in surface sediments and bottom waters. While some TMs may be become increasingly released from particles or from the sediment into the water column (e.g. Mn, Co), others may be removed or retained in the sediments more efficiently (e.g. Ni, Cu, Zn, Cd). Ultimately, such different behaviour can modify the TM stoichiometry in upwelling water masses and potentially affect TM-dependent ecosystems in the surface ocean.

Acknowledgements

We are grateful for the support of the crew of RV Meteor during the fieldwork. For their technical and analytical assistance, we thank A. Bleyer, B. Domeyer, D. Jasinski, T. Steffens, and R. Surberg. This study was supported by the German Research Foundation through the Emmy Noether Nachwuchsforschergruppe ICONOX (Iron Cycling in Continental Margin Sediments and the Nutrient and Oxygen Balance of the Ocean) and Sonderforschungsbereich 754 (Climate-Biogeochemistry Interactions in the Tropical Ocean). We would also like to thank S. H. Little and one anonymous reviewer for their constructive comments and thoughtful questions which helped to improve this manuscript, as well as T. S. Bianchi and P. H. Santschi for the editorial handling.

References

Aguirre, L., 1988. Chemical mobility during low-grade metamorphism of a Jurassic lava flow: Río Grande Formation, Peru. J. South Am. Earth Sci. 1, 343–361. https://doi.org/10.1016/0895-9811(88)90022-3

Al-Farawati, R., van den Berg, C.M.G., 1999. Metal–sulfide complexation in seawater. Mar. Chem. 63, 331–352. https://doi.org/10.1016/S0304-4203(98)00056-5

Algeo, T.J., Liu, J., 2020. A re-assessment of elemental proxies for paleoredox analysis. Chem. Geol. 540, 119549. https://doi.org/10.1016/j.chemgeo.2020.119549

Archer, C., Vance, D., Milne, A., Lohan, M.C., 2020. The oceanic biogeochemistry of nickel and its isotopes: New data from the South Atlantic and the Southern Ocean biogeochemical divide. Earth Planet. Sci. Lett. 535, 116118. https://doi.org/10.1016/j.epsl.2020.116118

Audry, S., Blanc, G., Schäfer, J., Chaillou, G., Robert, S., 2006. Early diagenesis of trace metals (Cd, Cu, Co, Ni, U, Mo, and V) in the freshwater reaches of a macrotidal estuary. Geochim. Cosmochim. Acta 70, 2264–2282. https://doi.org/10.1016/j.gca.2006.02.001

Baeyens, W., Monteny, F., Leermakers, M., Bouillon, S., 2003. Evalution of sequential extractions on dry and wet sediments. Anal. Bioanal. Chem. 376, 890–901. https://doi.org/10.1007/s00216-003-2005-z

Böning, P., Brumsack, H.J., Böttcher, M.E., Schnetger, B., Kriete, C., Kallmeyer, J., Borchers, S.L., 2004. Geochemistry of Peruvian near-surface sediments. Geochim. Cosmochim. Acta 68, 4429–4451. https://doi.org/10.1016/j.gca.2004.04.027

Böning, P., Brumsack, H.J., Schnetger, B., Grunwald, M., 2009. Trace element signatures of Chilean upwelling sediments at ~ 36°S. Mar. Geol. 259, 112–121. https://doi.org/10.1016/j.margeo.2009.01.004

Böning, P., Shaw, T., Pahnke, K., Brumsack, H.-J., 2015. Nickel as indicator of fresh organic matter in upwelling sediments. Geochim. Cosmochim. Acta 162, 99–108. https://doi.org/10.1016/j.gca.2015.04.027

Bopp, L., Le Quéré, C., Heimann, M., Manning, A.C., Monfray, P., 2002. Climate-induced oceanic oxygen fluxes: Implications for the contemporary carbon budget. Global Biogeochem. Cycles 16, 6-1-6–13. https://doi.org/10.1029/2001GB001445

Borchers, S.L., Schnetger, B., Böning, P., Brumsack, H.-J., 2005. Geochemical signatures of the Namibian diatom belt: Perennial upwelling and intermittent anoxia. Geochemistry, Geophys. Geosystems 6. https://doi.org/10.1029/2004GC000886

Boudreau, B.P., 1997. Diagenetic Models and Their Implementation. Springer. https://doi.org/10.1007/978-3-642-60421-8

Bruland, K.W., Lohan, M.C., 2006. Controls of Trace Metals in Seawater, in: Elderfield, H. (Ed.), The Oceans and Marine Geochemistry, Treatise on Geochemistry. Elsevier, pp. 23–47.

Brumsack, H.J., 2006. The trace metal content of recent organic carbon-rich sediments: Implications for Cretaceous black shale formation. Palaeogeogr. Palaeoclimatol. Palaeoecol. 232, 344–361. https://doi.org/10.1016/j.palaeo.2005.05.011

Canfield, D.E., Thamdrup, B., 2009. Towards a consistent classification scheme for geochemical environments, or, why we wish the term “suboxic” would go away: Editorial. Geobiology 7, 385–392. https://doi.org/10.1111/j.1472-4669.2009.00214.x

Chakraborty, P., Ramteke, D., Chakraborty, S., 2015. Geochemical partitioning of Cu and Ni in mangrove sediments: Relationships with their bioavailability. Mar. Pollut. Bull. 93, 194–201. https://doi.org/10.1016/j.marpolbul.2015.01.016

Chakraborty, P., Chakraborty, S., Jayachandran, S., Madan, R., Sarkar, A., Linsy, P., Nath, B.N., 2016. Effects of bottom water dissolved oxygen variability on copper and lead fractionation in the sediments across the oxygen minimum zone, western continental margin of India. Sci. Total Environ. 566–567, 1052–1061. https://doi.org/10.1016/j.scitotenv.2016.05.125

Ciceri, G., Maran, C., Martinotti, W., Queirazza, G., 1992. Geochemical cycling of heavy metals in a marine coastal area: benthic flux determination from pore water profiles and in situ measurements using benthic chambers. Hydrobiologia 235–236, 501–517. https://doi.org/10.1007/BF00026238

Ciscato, E.R., Bontognali, T.R.R., Vance, D., 2018. Nickel and its isotopes in organic-rich sediments: implications for oceanic budgets and a potential record of ancient seawater. Earth Planet. Sci. Lett. 494, 239–250. https://doi.org/10.1016/j.epsl.2018.04.061

Ciscato, E.R., Bontognali, T.R.R., Poulton, S.W., Vance, D., 2019. Copper and its Isotopes in Organic-Rich Sediments: From the Modern Peru Margin to Archean Shales. Geosciences 9, 325. https://doi.org/10.3390/geosciences9080325

Collier, R., Edmond, J., 1984. The trace element geochemistry of marine biogenic

particulate matter. Prog. Oceanogr. 13, 113–199. https://doi.org/10.1016/0079-6611(84)90008-9

Conway, T.M., John, S.G., 2014. The biogeochemical cycling of zinc and zinc isotopes in the North Atlantic Ocean. Global Biogeochem. Cycles 28, 1111–1128. https://doi.org/10.1002/2014GB004862

Conway, T.M., John, S.G., 2015a. Biogeochemical cycling of cadmium isotopes along a high-resolution section through the North Atlantic Ocean. Geochim. Cosmochim. Acta 148, 269–283. https://doi.org/10.1016/j.gca.2014.09.032

Conway, T.M., John, S.G., 2015b. The cycling of iron, zinc and cadmium in the North East Pacific Ocean - Insights from stable isotopes. Geochim. Cosmochim. Acta 164, 262–283. https://doi.org/10.1016/j.gca.2015.05.023

Dale, A.W., Nickelsen, L., Scholz, F., Hensen, C., Oschlies, A., Wallmann, K., 2015a. A revised global estimate of dissolved iron fluxes from marine sediments. Global Biogeochem. Cycles 29, 691–707. https://doi.org/10.1002/2014GB005017

Dale, A.W., Sommer, S., Lomnitz, U., Montes, I., Treude, T., Liebetrau, V., Gier, J., Hensen, C., Dengler, M., Stolpovsky, K., Bryant, L.D., Wallmann, K., 2015b. Organic carbon production, mineralisation and preservation on the Peruvian margin. Biogeosciences 12, 1537–1559. https://doi.org/10.5194/bg-12-1537-2015

Dale, A.W., Paul, M., Clemens, D., Scholz, F., Schroller-Lomnitz, U., Wallmann, K., Geilert, S., Hensen, C., Plass, A., Liebetrau, V., Grasse, P., Sommer, S., 2020. Recycling and burial of biogenic silica in an open margin oxygen minimum zone. Global Biogeochem. Cycles. https://doi.org/10.1029/2020GB006583

Davies-Colley, R.J., Nelson, P.O., Williamson, K.J., 1985. Sulfide control of cadmium and copper concentrations in anaerobic estuarine sediments. Mar. Chem. 16, 173–186. https://doi.org/10.1016/0304-4203(85)90021-0

Dyrssen, D., 1988. Sulfide complexation in surface seawater. Mar. Chem. 24, 143–153. https://doi.org/10.1016/0304-4203(88)90045-X

Echevin, V., Aumont, O., Ledesma, J., Flores, G., 2008. The seasonal cycle of surface chlorophyll in the Peruvian upwelling system: A modelling study. Prog. Oceanogr. 79, 167–176. https://doi.org/10.1016/j.pocean.2008.10.026

Ehrlich, S., Butler, I., Halicz, L., Rickard, D., Oldroyd, A., Matthews, A., 2004. Experimental study of the copper isotope fractionation between aqueous Cu(II) and covellite, CuS. Chem. Geol. 209, 259–269. https://doi.org/10.1016/j.chemgeo.2004.06.010

Fischer, K., Dymond, J., Lyle, M., Soutar, A., Rau, S., 1986. The benthic cycle of copper: Evidence from sediment trap experiments in the eastern tropical North Pacific Ocean. Geochim. Cosmochim. Acta 50, 1535–1543. https://doi.org/10.1016/0016-7037(86)90327-3

Freund, M., 2020. Dispersion of a Tracer in the Eastern Tropical South Pacific - an Investigation of Interactions from the Benthic Boundary Layer to the Ocean Interior -. Dr. Diss.

Froelich, P.., Arthur, M.., Burnett, W.., Deakin, M., Hensley, V., Jahnke, R., Kaul, L., Kim, K.-H., Roe, K., Soutar, A., Vathakanon, C., 1988. Early diagenesis of organic matter in Peru continental margin sediments: Phosphorite precipitation. Mar. Geol. 80, 309–343. https://doi.org/10.1016/0025-3227(88)90095-3

Gendron, A., Silverberg, N., Sundby, B., Lebel, J., 1986. Early diagenesis of cadmium and cobalt in sediments of the Laurentian Trough. Geochim. Cosmochim. Acta 50, 741–747. https://doi.org/10.1016/j.ijmachtools.2007.10.013

Goh, S.W., Buckley, A.N., Lamb, R.N., 2006. Copper(II) sulfide? Miner. Eng. 19, 204–208. https://doi.org/10.1016/j.mineng.2005.09.003

Grasshoff, M., Erhardt, M., Kremling, K., 1999. Methods of seawater analysis. Wiley-VCH, Weinheim. https://doi.org/10.1002/ange.19770890738

Gutiérrez, D., Enríquez, E., Purca, S., Quipúzcoa, L., Marquina, R., Flores, G., Graco, M., 2008. Oxygenation episodes on the continental shelf of central Peru: Remote forcing and benthic ecosystem response. Prog. Oceanogr. 79, 177–189. https://doi.org/10.1016/j.pocean.2008.10.025

Hawco, N.J., Ohnemus, D.C., Resing, J.A., Twining, B.S., Saito, M.A., 2016. A dissolved cobalt plume in the oxygen minimum zone of the eastern tropical South Pacific. Biogeosciences 13, 5697–5717. https://doi.org/10.5194/bg-13-5697-2016

Heggie, D., Lewis, T., 1984. Cobalt in pore waters of marine sediments. Nature 311, 453–455. https://doi.org/10.1038/311453a0

Helm, K.P., Bindoff, N.L., Church, J.A., 2011. Observed decreases in oxygen content of the global ocean. Geophys. Res. Lett. 38, 1–6. https://doi.org/10.1029/2011GL049513

Ho, T.-Y., Quigg, A., Finkel, Z. V., Milligan, A.J., Wyman, K., Falkowski, P.G., Morel, F.M.M., 2003. THE ELEMENTAL COMPOSITION OF SOME MARINE PHYTOPLANKTON1. J. Phycol. 39, 1145–1159. https://doi.org/10.1111/j.0022-3646.2003.03-090.x

Homoky, W.B., Weber, T., Berelson, W.M., Conway, T.M., Henderson, G.M., van Hulten, M., Jeandel, C., Severmann, S., Tagliabue, A., 2016. Quantifying trace element and isotope fluxes at the ocean–sediment boundary: a review. Philos. Trans. R. Soc. A Math. Phys. Eng. Sci. 374, 20160246. https://doi.org/10.1098/rsta.2016.0246

Huerta-Diaz, M.A., Morse, J.W., 1990. A quantitative method for determination of trace metal concentrations in sedimentary pyrite. Mar. Chem. 29, 119–144. https://doi.org/10.1016/0304-4203(90)90009-2

Jacobs, L., Emerson, S., Skei, J., 1985. Partitioning and transport of metals across the O2 H2S interface in a permanently anoxic basin: Framvaren Fjord, Norway. Geochim. Cosmochim. Acta 49, 1433–1444. https://doi.org/10.1016/0016-7037(85)90293-5

Janssen, D.J., Conway, T.M., John, S.G., Christian, J.R., Kramer, D.I., Pedersen, T.F., Cullen, J.T., 2014. Undocumented water column sink for cadmium in open ocean oxygen-deficient zones. Proc. Natl. Acad. Sci. 111, 6888–6893. https://doi.org/10.1073/pnas.1402388111

Janssen, D.J., Cullen, J.T., 2015. Decoupling of zinc and silicic acid in the subarctic northeast Pacific interior. Mar. Chem. 177, 124–133. https://doi.org/10.1016/j.marchem.2015.03.014

John, S.G., Helgoe, J., Townsend, E., Weber, T., DeVries, T., Tagliabue, A., Moore, K., Lam, P., Marsay, C.M., Till, C., 2018. Biogeochemical cycling of Fe and Fe stable isotopes in the Eastern Tropical South Pacific. Mar. Chem. 201, 66–76.

https://doi.org/10.1016/j.marchem.2017.06.003

Johnson, K.S., Stout, P.M., Berelson, W.M., Sakamoto-Arnold, C.M., 1988. Cobalt and copper distributions in the waters of Santa Monica Basin, California. Nature 332, 527–530. https://doi.org/10.1038/332527a0

Johnson, K.S., Coale, K.H., Berelson, W.M., Michael Gordon, R., 1996. On the formation of the manganese maximum in the oxygen minimum. Geochim. Cosmochim. Acta 60, 1291–1299. https://doi.org/10.1016/0016-7037(96)00005-1

Karstensen, J., Stramma, L., Visbeck, M., 2008. Oxygen minimum zones in the eastern tropical Atlantic and Pacific oceans. Prog. Oceanogr. 77, 331–350. https://doi.org/10.1016/j.pocean.2007.05.009

Keeling, R.F., Körtzinger, A., Gruber, N., 2010. Ocean Deoxygenation in a Warming World. Ann. Rev. Mar. Sci. 2, 199–229. https://doi.org/10.1146/annurev.marine.010908.163855

Kostka, J.E., Luther, G.W., 1994. Partitioning and speciation of solid phase iron in saltmarsh sediments. Geochim. Cosmochim. Acta 58, 1701–1710. https://doi.org/10.1016/0016-7037(94)90531-2

Kuleshov, V., 2017. Manganese Carbonates in Modern Sediments, in: Isotope Geochemistry. Elsevier, pp. 5–62. https://doi.org/10.1016/B978-0-12-803165-0.00002-1

Landing, W.M., Bruland, K.W., 1987. The contrasting biogeochemistry of iron and manganese in the Pacific Ocean. Geochim. Cosmochim. Acta 51, 29–43. https://doi.org/10.1016/0016-7037(87)90004-4

Lee, J.-M., Heller, M.I., Lam, P.J., 2018. Size distribution of particulate trace elements in the U.S. GEOTRACES Eastern Pacific Zonal Transect (GP16). Mar. Chem. 201, 108–123. https://doi.org/10.1016/j.marchem.2017.09.006

Levin, L., Gutiérrez, D., Rathburn, A., Neira, C., Sellanes, J., Muñoz, P., Gallardo, V., Salamanca, M., 2002. Benthic processes on the Peru margin: a transect across the oxygen minimum zone during the 1997–98 El Niño. Prog. Oceanogr. 53, 1–27. https://doi.org/10.1016/S0079-6611(02)00022-8

Li, Y.-H., Gregory, S., 1974. Diffusion of ions in sea water and in deep-sea sediments. Geochim. Cosmochim. Acta 38, 703–714. https://doi.org/10.1016/0016-7037(74)90145-8

Little, S.H., Vance, D., Lyons, T.W., McManus, J., 2015. Controls on trace metal authigenic enrichment in reducing sediments: Insights from modern oxygen-deficient settings. Am. J. Sci. 315, 77–119. https://doi.org/10.2475/02.2015.01

Little, S.H., Vance, D., McManus, J., Severmann, S., 2016. Key role of continental margin sediments in the oceanic mass balance of Zn and Zn isotopes. Geology 44, 207–210. https://doi.org/10.1130/G37493.1

Little, S.H., Vance, D., McManus, J., Severmann, S., Lyons, T.W., 2017. Copper isotope signatures in modern marine sediments. Geochim. Cosmochim. Acta 212, 253–273. https://doi.org/10.1016/j.gca.2017.06.019

Lohan, M.C., Tagliabue, A., 2018. Oceanic Micronutrients: Trace Metals that are Essential for Marine Life. Elements 14, 385–390. https://doi.org/10.2138/gselements.14.6.385

Lüdke, J., Dengler, M., Sommer, S., Clemens, D., Thomsen, S., Krahmann, G., Dale, A.W., Achterberg, E.P., Visbeck, M., 2020. Influence of intraseasonal eastern boundary circulation variability on hydrography and biogeochemistry off Peru. Ocean Sci. 16, 1347–1366. https://doi.org/10.5194/os-16-1347-2020

Luther, G.W., Theberge, S.M., Rozan, T.F., Rickard, D., Rowlands, C.C., Oldroyd, A., 2002. Aqueous Copper Sulfide Clusters as Intermediates during Copper Sulfide Formation. Environ. Sci. Technol. 36, 394–402. https://doi.org/10.1021/es010906k

McManus, J., Berelson, W.M., Severmann, S., Johnson, K.S., Hammond, D.E., Roy, M., Coale, K.H., 2012. Benthic manganese fluxes along the Oregon–California continental shelf and slope. Cont. Shelf Res. 43, 71–85. https://doi.org/10.1016/j.csr.2012.04.016

Middelburg, J.J., De Lange, G.J., van Der Weijden, C.H., 1987. Manganese solubility control in marine pore waters. Geochim. Cosmochim. Acta 51, 759–763. https://doi.org/10.1016/0016-7037(87)90086-X

Moffett, J.W., Ho, J., 1996. Oxidation of cobalt and manganese in seawater via a

common microbially catalyzed pathway. Geochim. Cosmochim. Acta 60, 3415–3424. https://doi.org/10.1016/0016-7037(96)00176-7

Moore, C.M., Mills, M.M., Arrigo, K.R., Berman-Frank, I., Bopp, L., Boyd, P.W., Galbraith, E.D., Geider, R.J., Guieu, C., Jaccard, S.L., Jickells, T.D., La Roche, J., Lenton, T.M., Mahowald, N.M., Marañón, E., Marinov, I., Moore, J.K., Nakatsuka, T., Oschlies, A., Saito, M.A., Thingstad, T.F., Tsuda, A., Ulloa, O., 2013. Processes and patterns of oceanic nutrient limitation. Nat. Geosci. 6, 701–710. https://doi.org/10.1038/ngeo1765

Morel, F.M.M., Price, N.M., 2003. The Biogeochemical Cycles of Trace Metals in the Oceans. Science (80-.). 300, 944–947. https://doi.org/10.1126/science.1083545

Morel, F.M.M., Milligan, A.J., Saito, M.A., 2014. Marine Bioinorganic Chemistry: The Role of Trace Metals in the Oceanic Cycles of Major Nutrients, in: Treatise on Geochemistry. Elsevier, pp. 123–150. https://doi.org/10.1016/B978-0-08-095975-7.00605-7

Morford, J.L., Emerson, S., 1999. The geochemistry of redox sensitive trace metals in sediments. Geochim. Cosmochim. Acta 63, 1735–1750. https://doi.org/10.1016/S0016-7037(99)00126-X

Morse, J.W., Luther, G.W., 1999. Chemical influences on trace metal-sulfide interactions in anoxic sediments. Geochim. Cosmochim. Acta 63, 3373–3378. https://doi.org/10.1016/S0016-7037(99)00258-6

Muñoz, P., Lange, C.B., Gutiérrez, D., Hebbeln, D., Salamanca, M.A., Dezileau, L., Reyss, J.L., Benninger, L.K., 2004. Recent sedimentation and mass accumulation rates based on 210Pb along the Peru–Chile continental margin. Deep Sea Res. Part II Top. Stud. Oceanogr. 51, 2523–2541. https://doi.org/10.1016/j.dsr2.2004.08.015

Murray, J.W., 1975. The interaction of cobalt with hydrous manganese dioxide. Geochim. Cosmochim. Acta 39, 635–647. https://doi.org/10.1016/0016-7037(75)90007-1

Nameroff, T.J., Balistrieri, L.S., Murray, J.W., 2002. Suboxic trace metal geochemistry in the Eastern Tropical North Pacific. Geochim. Cosmochim. Acta 66, 1139–1158. https://doi.org/10.1016/S0016-7037(01)00843-2

Noble, A.E., Lamborg, C.H., Ohnemus, D.C., Lam, P.J., Goepfert, T.J., Measures, C.I., Frame, C.H., Casciotti, K.L., DiTullio, G.R., Jennings, J., Saito, M.A., 2012. Basin-scale inputs of cobalt, iron, and manganese from the Benguela-Angola front to the South Atlantic Ocean. Limnol. Oceanogr. 57, 989–1010. https://doi.org/10.4319/lo.2012.57.4.0989

Noffke, A., Hensen, C., Sommer, S., Scholz, F., Bohlen, L., Mosch, T., Graco, M., Wallmann, K., 2012. Benthic iron and phosphorus fluxes across the Peruvian oxygen minimum zone. Limnol. Oceanogr. 57, 851–867. https://doi.org/10.4319/lo.2012.57.3.0851

Ohde, T., 2018. Coastal Sulfur Plumes off Peru During El Niño, La Niña, and Neutral Phases. Geophys. Res. Lett. 45, 7075–7083. https://doi.org/10.1029/2018GL077618

Ohnemus, D.C., Rauschenberg, S., Cutter, G.A., Fitzsimmons, J.N., Sherrell, R.M., Twining, B.S., 2017. Elevated trace metal content of prokaryotic communities associated with marine oxygen deficient zones. Limnol. Oceanogr. 62, 3–25. https://doi.org/10.1002/lno.10363

Olson, L., Quinn, K.A., Siebecker, M.G., Luther, G.W., Hastings, D., Morford, J.L., 2017. Trace metal diagenesis in sulfidic sediments: Insights from Chesapeake Bay. Chem. Geol. 452, 47–59. https://doi.org/10.1016/j.chemgeo.2017.01.018

Oschlies, A., Schulz, K.G., Riebesell, U., Schmittner, A., 2008. Simulated 21st century's increase in oceanic suboxia by CO 2-enhanced biotic carbon export. Global Biogeochem. Cycles 22, 1–10. https://doi.org/10.1029/2007GB003147

Pakhomova, S. V., Hall, P.O.J., Kononets, M.Y., Rozanov, A.G., Tengberg, A., Vershinin, A. V., 2007. Fluxes of iron and manganese across the sediment–water interface under various redox conditions. Mar. Chem. 107, 319–331. https://doi.org/10.1016/j.marchem.2007.06.001

Pattrick, R.A.D., Mosselmans, J.F.W., Charnock, J.M., England, K.E.R., Helz, G.R., Garner, C.D., Vaughan, D.J., 1997. The structure of amorphous copper sulfide precipitates: An X-ray absorption study. Geochim. Cosmochim. Acta 61, 2023–2036. https://doi.org/10.1016/S0016-7037(97)00061-6

Peacock, C.L., Sherman, D.M., 2007. Sorption of Ni by birnessite: Equilibrium

controls on Ni in seawater. Chem. Geol. 238, 94–106. https://doi.org/10.1016/j.chemgeo.2006.10.019

Pennington, J.T., Mahoney, K.L., Kuwahara, V.S., Kolber, D.D., Calienes, R., Chavez, F.P., 2006. Primary production in the eastern tropical Pacific: A review. Prog. Oceanogr. 69, 285–317. https://doi.org/10.1016/j.pocean.2006.03.012

Plass, A., Schlosser, C., Sommer, S., Dale, A.W., Achterberg, E.P., Scholz, F., 2020. The control of hydrogen sulfide on benthic iron and cadmium fluxes in the oxygen minimum zone off Peru. Biogeosciences 17, 3685–3704. https://doi.org/10.5194/bg-17-3685-2020

Rapp, I., Schlosser, C., Rusiecka, D., Gledhill, M., Achterberg, E.P., 2017. Automated preconcentration of Fe, Zn, Cu, Ni, Cd, Pb, Co, and Mn in seawater with analysis using high-resolution sector field inductively-coupled plasma mass spectrometry. Anal. Chim. Acta 976, 1–13. https://doi.org/10.1016/j.aca.2017.05.008

Rapp, I., Schlosser, C., Menzel Barraqueta, J.-L., Wenzel, B., Lüdke, J., Scholten, J., Gasser, B., Reichert, P., Gledhill, M., Dengler, M., Achterberg, E.P., 2019. Controls on redox-sensitive trace metals in the Mauritanian oxygen minimum zone. Biogeosciences 16, 4157–4182. https://doi.org/10.5194/bg-16-4157-2019

Rapp, I., Schlosser, C., Browning, T.J., Wolf, F., Le Moigne, F.A.C., Gledhill, M., Achterberg, E.P., 2020. El Niño-Driven Oxygenation Impacts Peruvian Shelf Iron Supply to the South Pacific Ocean. Geophys. Res. Lett. 47. https://doi.org/10.1029/2019GL086631

Reimers, C.E., Suess, E., 1983. Spatial and Temporal Patterns of Organic Matter Accumulation on the Peru Continental Margin. NATO Conf. Ser. 4 Mar. Sci. 10 B, 311–345.

Rigaud, S., Radakovitch, O., Couture, R.M., Deflandre, B., Cossa, D., Garnier, C., Garnier, J.M., 2013. Mobility and fluxes of trace elements and nutrients at the sediment-water interface of a lagoon under contrasting water column oxygenation conditions. Appl. Geochemistry 31, 35–51. https://doi.org/10.1016/j.apgeochem.2012.12.003

Rosenthal, Y., Lam, P., Boyle, E.A., Thomson, J., 1995. Precipitation and

postdepositional mobility. Earth Planet. Sci. Lett. 132, 99–111. https://doi.org/10.1016/0012-821X(95)00056-I

Roshan, S., Wu, J., 2015. The distribution of dissolved copper in the tropical-subtropical north Atlantic across the GEOTRACES GA03 transect. Mar. Chem. 176, 189–198. https://doi.org/10.1016/j.marchem.2015.09.006

Saito, M.A., Moffett, J.W., DiTullio, G.R., 2004. Cobalt and nickel in the Peru upwelling region: A major flux of labile cobalt utilized as a micronutrient. Global Biogeochem. Cycles 18, 1–14. https://doi.org/10.1029/2003GB002216

Saito, M.A., Goepfert, T.J., Ritt, J.T., 2008. Some thoughts on the concept of colimitation: Three definitions and the importance of bioavailability. Limnol. Oceanogr. 53, 276–290. https://doi.org/10.4319/lo.2008.53.1.0276

Sarbas, B., Nohl, U., 2009. The GEOROC database – a decade of “online geochemistry.” Geochim. Cosmochim. Acta 73, Supplement p. A1158.

Schmidtko, S., Stramma, L., Visbeck, M., 2017. Decline in global oceanic oxygen content during the past five decades. Nature 542, 335–339. https://doi.org/10.1038/nature21399

Scholz, F., Neumann, T., 2007. Trace element diagenesis in pyrite-rich sediments of the Achterwasser lagoon, SW Baltic Sea. Mar. Chem. 107, 516–532. https://doi.org/10.1016/j.marchem.2007.08.005

Scholz, F., Hensen, C., Noffke, A., Rohde, A., Liebetrau, V., Wallmann, K., 2011. Early diagenesis of redox-sensitive trace metals in the Peru upwelling area - response to ENSO-related oxygen fluctuations in the water column. Geochim. Cosmochim. Acta 75, 7257–7276. https://doi.org/10.1016/j.gca.2011.08.007

Scholz, F., Severmann, S., McManus, J., Noffke, A., Lomnitz, U., Hensen, C., 2014. On the isotope composition of reactive iron in marine sediments: Redox shuttle versus 45 early diagenesis. Chem. Geol. 389, 48–59. https://doi.org/10.1016/j.chemgeo.2014.09.009

Scholz, F., Löscher, C.R., Fiskal, A., Sommer, S., Hensen, C., Lomnitz, U., Wuttig, K., Göttlicher, J., Kossel, E., Steininger, R., Canfield, D.E., 2016. Nitrate-dependent iron oxidation limits iron transport in anoxic ocean regions. Earth Planet. Sci. Lett. 454, 272–281. https://doi.org/10.1016/j.epsl.2016.09.025

Schunck, H., Lavik, G., Desai, D.K., Großkopf, T., Kalvelage, T., Löscher, C.R., Paulmier, A., Contreras, S., Siegel, H., Holtappels, M., Rosenstiel, P., Schilhabel, M.B., Graco, M., Schmitz, R.A., Kuypers, M.M.M., LaRoche, J., 2013. Giant Hydrogen Sulfide Plume in the Oxygen Minimum Zone off Peru Supports Chemolithoautotrophy. PLoS One 8. https://doi.org/10.1371/journal.pone.0068661

Shaw, T.J., Gieskes, J.M., Jahnke, R.A., 1990. Early diagenesis in differing depositional environments: The response of transition metals in pore water. Geochim. Cosmochim. Acta 54, 1233–1246. https://doi.org/10.1016/0016-7037(90)90149-F

Sheng, P.X., Ting, Y.-P., Chen, J.P., Hong, L., 2004. Sorption of lead, copper, cadmium, zinc, and nickel by marine algal biomass: characterization of biosorptive capacity and investigation of mechanisms. J. Colloid Interface Sci. 275, 131–141. https://doi.org/10.1016/j.jcis.2004.01.036

Sieber, M., Conway, T.M., de Souza, G.F., Hassler, C.S., Ellwood, M.J., Vance, D., 2020. Cycling of zinc and its isotopes across multiple zones of the Southern Ocean: Insights from the Antarctic Circumnavigation Expedition. Geochim. Cosmochim. Acta 268, 310–324. https://doi.org/10.1016/j.gca.2019.09.039

Sommer, S., Gier, J., Treude, T., Lomnitz, U., Dengler, M., Cardich, J., Dale, A.W., 2016. Depletion of oxygen, nitrate and nitrite in the Peruvian oxygen minimum zone cause an imbalance of benthic nitrogen fluxes. Deep. Res. Part I Oceanogr. Res. Pap. 112, 113–122. https://doi.org/10.1016/j.dsr.2016.03.001

Stramma, L., Schmidtko, S., Levin, L.A., Johnson, G.C., 2010. Ocean oxygen minima expansions and their biological impacts. Deep. Res. Part I Oceanogr. Res. Pap. 57, 587–595. https://doi.org/10.1016/j.dsr.2010.01.005

Suess, E., Kulm, L.D., Killingley, J.S., 1987. Coastal upwelling and a history of organic-rich mudstone deposition off Peru. Geol. Soc. London, Spec. Publ. 26, 181–197. https://doi.org/10.1144/GSL.SP.1987.026.01.11

Suits, N.S., Arthur, M.A., 2000. Sulfur diagenesis and partitioning in Holocene Peru shelf and upper slope sediments. Chem. Geol. 163, 219–234. https://doi.org/10.1016/S0009-2541(99)00114-X

Sundby, B., Anderson, L.G., Hall, P.O.J., Iverfeldt, Å., van der Loeff, M.M.R., Westerlund, S.F.G., 1986. The effect of oxygen on release and uptake of cobalt, manganese, iron and phosphate at the sediment-water interface. Geochim. Cosmochim. Acta 50, 1281–1288. https://doi.org/10.1016/0016-7037(86)90411-4

Sweere, T., van den Boorn, S., Dickson, A.J., Reichart, G.-J., 2016. Definition of new trace-metal proxies for the controls on organic matter enrichment in marine sediments based on Mn, Co, Mo and Cd concentrations. Chem. Geol. 441, 235–245. https://doi.org/10.1016/j.chemgeo.2016.08.028

Tagliabue, A., Hawco, N.J., Bundy, R.M., Landing, W.M., Milne, A., Morton, P.L., Saito, M.A., 2018. The Role of External Inputs and Internal Cycling in Shaping the Global Ocean Cobalt Distribution: Insights From the First Cobalt Biogeochemical Model. Global Biogeochem. Cycles 32, 594–616. https://doi.org/10.1002/2017GB005830

Tankéré, S.P.., Muller, F.L.., Burton, J.., Statham, P.., Guieu, C., Martin, J.-M., 2001. Trace metal distributions in shelf waters of the northwestern Black Sea. Cont. Shelf Res. 21, 1501–1532. https://doi.org/10.1016/S0278-4343(01)00013-9

Taylor, S.R., McLennan, S.M., 1995. The geochemical evolution of the continental crust. Rev. Geophys. 33, 241. https://doi.org/10.1029/95RG00262

Tebo, B.M., 1991. Manganese(II) oxidation in the suboxic zone of the Black Sea. Deep Sea Res. Part A. Oceanogr. Res. Pap. 38, S883–S905. https://doi.org/10.1016/S0198-0149(10)80015-9

Thamdrup, B., Glud, R.N., Hansen, J.W., 1994. Manganese oxidation and in situ manganese fluxes from a coastal sediment. Geochim. Cosmochim. Acta 58, 2563–2570. https://doi.org/10.1016/0016-7037(94)90032-9

Thamdrup, B., Dalsgaard, T., Revsbech, N.P., 2012. Widespread functional anoxia in the oxygen minimum zone of the Eastern South Pacific. Deep Sea Res. Part I Oceanogr. Res. Pap. 65, 36–45. https://doi.org/10.1016/j.dsr.2012.03.001

Theberge, M., Luther, G.W., Farrenkopf, A.M., 1997. On the existence of free and metal complexed sulfide in the Arabian Sea and its oxygen minimum zone 44, 1381–1390. https://doi.org/10.1016/S0967-0645(97)00012-X

Tribovillard, N., Algeo, T.J., Lyons, T., Riboulleau, A., 2006. Trace metals as paleoredox and paleoproductivity proxies: An update. Chem. Geol. 232, 12–32. https://doi.org/10.1016/j.chemgeo.2006.02.012

Turetta, C., Capodaglio, G., Cairns, W., Rabar, S., Cescon, P., 2005. Benthic fluxes of trace metals in the lagoon of Venice. Microchem. J. 79, 149–158. https://doi.org/10.1016/j.microc.2004.06.003

Twining, B.S., Baines, S.B., Bozard, J.B., Vogt, S., Walker, E.A., Nelson, D.M., 2011. Metal quotas of plankton in the equatorial Pacific Ocean. Deep Sea Res. Part II Top. Stud. Oceanogr. 58, 325–341. https://doi.org/10.1016/j.dsr2.2010.08.018

Ulloa, O., Escribano, R., Hormazabal, S., Quiñones, R.A., González, R.R., Ramos, M., 2001. Evolution and biological effects of the 1997-98 El Niño in the upwelling ecosystem off northern Chile. Geophys. Res. Lett. 28, 1591–1594. https://doi.org/10.1029/2000GL011548

van de Velde, S.J., Hylén, A., Kononets, M., Marzocchi, U., Leermakers, M., Choumiline, K., Hall, P.O.J., Meysman, F.J.R., 2020. Elevated sedimentary removal of Fe, Mn, and trace elements following a transient oxygenation event in the Eastern Gotland Basin, central Baltic Sea. Geochim. Cosmochim. Acta 271, 16–32. https://doi.org/10.1016/j.gca.2019.11.034

Vance, D., Archer, C., Bermin, J., Perkins, J., Statham, P.J., Lohan, M.C., Ellwood, M.J., Mills, R.A., 2008. The copper isotope geochemistry of rivers and the oceans. Earth Planet. Sci. Lett. 274, 204–213. https://doi.org/10.1016/j.epsl.2008.07.026

Vance, D., Little, S.H., Archer, C., Cameron, V., Andersen, M.B., Rijkenberg, M.J.A., Lyons, T.W., 2016. The oceanic budgets of nickel and zinc isotopes: the importance of sulfidic environments as illustrated by the Black Sea. Philos. Trans. R. Soc. A Math. Phys. Eng. Sci. 374, 20150294. https://doi.org/10.1098/rsta.2015.0294

Vedamati, J., Chan, C., Moffett, J.W., 2014. Distribution of dissolved manganese in the Peruvian Upwelling and Oxygen Minimum Zone. Geochim. Cosmochim. Acta 156, 222–240. https://doi.org/10.1016/j.gca.2014.10.026

Vijayaraghavan, K., Jegan, J., Palanivelu, K., Velan, M., 2005. Biosorption of copper,

cobalt and nickel by marine green alga Ulva reticulata in a packed column. Chemosphere 60, 419–426. https://doi.org/10.1016/j.chemosphere.2004.12.016

Westerlund, S.F.G., Anderson, L.G., Hall, P.O.J., Iverfeldt, Å., Van Der Loeff, M.M.R., Sundby, B., 1986. Benthic fluxes of cadmium, copper, nickel, zinc and lead in the coastal environment. Geochim. Cosmochim. Acta 50, 1289–1296. https://doi.org/10.1016/0016-7037(86)90412-6

Xie, R.C., Rehkämper, M., Grasse, P., van de Flierdt, T., Frank, M., Xue, Z., 2019. Isotopic evidence for complex biogeochemical cycling of Cd in the eastern tropical South Pacific. Earth Planet. Sci. Lett. 512, 134–146. https://doi.org/10.1016/j.epsl.2019.02.001

Zimmerman, A.J., Weindorf, D.C., 2010. Heavy Metal and Trace Metal Analysis in Soil by Sequential Extraction: A Review of Procedures. Int. J. Anal. Chem. 2010, 1–7. https://doi.org/10.1155/2010/387803

Supplement

Table III.S.1: Station coordinates and water depth.

Station	Water depth (m)	Latitude	Longitude
1	75	12°13.519' S	77°10.793' W
3	130	12°16.678' S	77°14.954' W
4	145	12°18.709' S	77°17.796' W
5	195	12°21.504' S	77°21.699' W
6	245	12°23.301' S	77°24.182' W
9	750	12°34.896' S	77°35.013' W

Table III.S.2: Accuracy of replicate ICP-MS measurements (n = 7) of certified reference seawater standards NASS-7 and CASS-6.

	NASS-7 certified value	NASS-7 measured value	CASS-6 certified value	CASS-6 measured value
Mn (µg l^{-1})	0.75 ± 0.06	0.83 ± 0.11	2.22 ± 0.12	2.22 ± 0.40
Co (µg l^{-1})	0.146 ± 0.0014	0.146 ± 0.0054	0.0627 ± 0.0052	0.0630 ± 0.0105
Ni (µg l^{-1})	0.248 ± 0.018	0.247 ± 0.039	0.418 ± 0.040	0.438 ±0.050
Cu (µg l^{-1})	0.199 ± 0.014	0.216 ± 0.012	0.530 ± 0.032	0.521 ± 0.051
Zn (µg l^{-1})	0.42 ± 0.08	0.43 ± 0.08	1.27 ± 0.018	1.29 ± 0.092
Cd (µg l^{-1})	0.0161 ± 0.0016	0.0162 ± 0,0024	0.0217 ± 0.0018	0.0216 ± 0.0016

Table III.S.3: Trace metal contents of in-house reference standard (OMZ 2) from total digestions and the total trace metal content from sequential extractions (n = 3). Reference values of trace metal contents in the certified standard MESS-3 and trace metal contents from total digestions and the sum content of the sequential extractions (n = 17).

	Mn ($\mu g\ g^{-1}$)	**Co ($\mu g\ g^{-1}$)**	**Ni ($\mu g\ g^{-1}$)**	**Cu ($\mu g\ g^{-1}$)**	**Zn ($\mu g\ g^{-1}$)**	**Cd ($\mu g\ g^{-1}$)**	**Al ($\mu g\ g^{-1}$)**
OMZ 2 Reference value (total digestion)	253.3 ± 2.8	6.3 ± 0.1	49.8 ± 1.0	35.3 ± 0.5	98.3 ± 8.8	26.5 ± 0.3	-
OMZ 2 sequential extractions	251.6 ± 3.3	5.7 ± 0.0	47.2 ± 2.7	28.0 ± 0.5	82.3 ± 3.1	27.2 ± 0.5	-
MESS-3 Reference value	324 ± 12	14.4 ± 2.0	46.9 ± 2.2	33.9 ± 1.6	159 ± 8	0.24 ± 0.01	8.59 ± 0.23
MESS-3 total digestion	323 ± 5	14.2 ± 0.3	46.45 ± 0.1	33.1 ± 1.5	156 ± 5	0.24 ± 0.01	8.59 ± 0.11
MESS-3 sequential extractions	311 ± 1	12.2 ± 0.3	20.7 ± 3.5	28.3 ± 8.4	148 ± 2	0.96 ± 0.38	-

Table III.S.4: Average trace metal and particulate organic carbon content in sediments of all samples over each core.

Station	Water depth (m)	Trace metal content (µg g^{-1})							Particulate organic carbon content (mg g^{-1})	Total sulphur content (mg g^{-1})
		Mn	Co	Ni	Cu	Zn	Cd	Al		
1	75	386	7.89	23.3	57.6	176	25.8	54533	36.4	13.3
3	130	275	6.50	46.8	53.8	142	44.4	46424	73.8	14.8
4	145	234	4.93	56.2	44.7	130	44.8	44605	90.4	14.1
5	195	161	4.27	76.6	51.5	99.1	45.2	31966	112	12.0
6	245	156	4.61	109	54.9	105	51.8	32555	134	14.7
9	750	130	3.12	57.5	45.4	98.2	1.96	33190	42.1	3.81

Table III.S.5a: Input data for diffusive flux calculations (Eq. III.3 in main text).

Station	Water depth (m)	Bottom water concentration (nM)						Concentration at sediment surface (nM)					
		Mn	Co	Ni	Cu	Zn	Cd	Mn	Co	Ni	Cu	Zn	Cd
1	75	63.7	0.42	4.96	2.35	775	0.22	276	1.40	21.9	3.37	36.1	0.90
3	130	0.16	0.37	9.92	8.97	294	0.81	93.0	0.99	16.1	5.17	42.7	0.65
4	145	5.60	0.19	5.97	3.57	23.2	0.66	151	1.67	3.09	3.71	30.6	0.47
5	195	5.43	0.22	0.50	5.47	276	0.68	68.0	1.11	5.02	6.18	22.0	0.44
6	245	0	0	8.04	11.9	66.3	0.76	50.1	1.53	36.4	7.18	58.4	0.55
9	750	2.74	0.17	10.8	2.29	131	0.99	26.6	0.29	43.4	5.23	29.5	1.25

Table III.S.5b: Molecular diffusion coefficients in seawater (Li and Gregory, 1974), adjusted to in-situ temperature, pressure and salinity, used for diffusive flux calculations (Eq. III.3 in main text).

Station	Molecular diffusion coefficients 10^{-6} (cm^2 s^{-1})					
	Mn	Co	Ni	Cu	Zn	Cd
1	4.42	4.49	4.36	4.71	4.59	4.60
3	4.38	4.45	4.33	4.67	4.56	4.57
4	4.42	4.49	4.36	4.71	4.50	4.61
5	4.26	4.33	4.20	4.54	4.79	4.44
6	4.24	4.31	4.19	4.52	4.41	4.42
9	2.36	2.40	2.33	2.52	2.46	2.46

Table III.S.5c: Porosity used for diffusive flux calculations (Eq. II.3 in main text) and in-situ temperature, pressure and salinity data used to adjust molecular diffusion coefficients (Table III.S.5b).

Station	Water depth	Porosity	Temperature (°C)	Pressure (bar)	Salinity
1	75	0.93	16.2	8.77	35.1
3	130	0.95	14.0	13.9	35.0
4	145	0.96	14.0	15.4	35.0
5	195	0.96	13.2	20.4	34.9
6	245	0.95	13.3	25.6	34.9
9	750	0.74	6.28	75.0	34.6

IV. A novel device for trace-metal clean sampling of bottom water and suspended particles at the ocean's lower boundary: the Benthic Trace Profiler

Anna Plass[1], Anna-Kathrin Retschko[1], Matthias Türk[1], Florian Scholz[1]

[1]GEOMAR Helmholtz Centre for Ocean Research Kiel, Wischhofstraße 1-3, 24148 Kiel, Germany

Submitted to Limnology and Oceanography: Methods

Abstract

The benthic boundary layer plays a crucial role in the exchange of trace metals between surface sediments and the water column. So far it has been difficult to study dissolved-particulate interactions of trace metals in this highly reactive interface layer due to the lack of suited sampling methods. We developed a new device, called Benthic Trace Profiler, which enables simultaneous sampling of near-bottom water and suspended particles in high resolution within the first three meters above the seafloor. The device was successfully tested in the Baltic Sea. The concentrations of several trace metals (Co, Ni, Cu, Zn and Cd) in the collected bottom waters overlapped with concentrations in water column samples above, which proves the sampling device and method to be trace metal clean. Other trace metals like Fe and Mn showed concentration gradients within the benthic boundary layer. This observation is consistent with a diffusive benthic flux of these trace metals across the sediment-water interface, which was independently verified using pore water profiles. Suspended particles collected by in-line filtration can be used to study precipitation processes and to determine the carrier phases of trace metals. The benthic trace profiler fulfilled all the intended requirements as it allowed a simultaneous, uncontaminating and oxygen-

free sampling of seawater and suspended particles to gather high-resolution profiles of dissolved and particulate trace metal concentrations above the seafloor. The device closes the gap between water column and sediment sampling and helps to understand trace metal exchange processes across the ocean's lower boundary.

IV.1 Introduction

Several trace metals (TM) are essential micronutrients required for marine life. They are part of many enzymes, which catalyse important biological functions such as photosynthesis (Fe, Mn, Cu) and carbon fixation (Co, Zn, Cd). Due to generally low concentrations in the surface ocean the availability of TMs can regulate and (co-)limit primary productivity (Morel, 2003; Saito et al., 2008; Moore et al., 2013; Morel et al., 2014; Lohan and Tagliabue, 2018). Furthermore, sedimentary TM signatures can be used as proxies to infer marine biogeochemical cycling and redox conditions in the geological past (Brumsack, 2006; Tribovillard et al., 2006; Sweere et al., 2016; Algeo and Liu, 2020).

Trace metal fluxes across the sediment-water interface at ocean boundaries play an important role in regulating oceanic TM concentrations. In particular sediments underlying oxygen minimum zones are a source for Fe, Mn and Co and a sink for Ni, Cu, Zn and Cd (Brumsack, 2006; Böning et al., 2009; Little et al., 2015; Plass et al., 2021). However, the processes that are involved in benthic TM cycling are not fully understood. The benthic boundary layer may play a key role in modulating TMs fluxes. This layer is characterised by high chemical reactivity and high exchange and concentrations of dissolved and particulate matter between the water column and the seafloor (Boudreau and Jorgensen, 2001). Depending on the prevailing redox conditions TM precipitation can take place. For example, when dissolved Mn is released from anoxic sediments it can reprecipitate in the bottom water through oxidation processes and therefore be returned to the sediment (Sundby and Silverberg, 1985; Pakhomova et al., 2007). Similarly, after release from the sediments reduced Fe can be oxidised to insoluble Fe(III) by oxygen, nitrate or nitrite (Scholz et al., 2016; Heller et al., 2017; Schlosser et al., 2018). Furthermore, when hydrogen sulphide escapes the sediment, TM removal from bottom water through sulphide

precipitation can take place (especially CdS, which has a very low solubility) (Jacobs et al., 1985; Sundby et al., 1986; Plass et al., 2020). Sampling of suspended particles at the benthic boundary is required to constrain these precipitation reactions and also to determine by which carrier phase TMs are delivered from the water column to the sediment surface. The respective importance of different carrier phases is in many cases poorly constrained. For example, TM sequestration by phytoplankton and delivery with fresh organic material, TM scavenging by inorganic particles (e.g. metal oxides) or refractory organic material and TM sulphide precipitation can contribute to the particulate supply of TMs to the sediment (Böning et al., 2004; Audry et al., 2006; Rigaud et al., 2013; Little et al., 2015; Ciscato et al., 2018b). Furthermore, the biogeochemical conditions leading to TM stabilisation or precipitation in near-bottom waters need to be evaluated in order to gain further insights into benthic TM cycling and fluxes. This can ultimately help to better solve the oceanic mass balances of TMs and to predict how environmental conditions impact the availability of TMs to marine organisms in the surface ocean.

Devices and procedures for TM sampling of the water column are well established, in particular by the GEOTRACES program (Scor Working Group, 2007; Cutter and Bruland, 2012). However, the conventional sampling methods by GO-FLO bottles fail to sample the benthic boundary, as they cannot reach close enough to the seafloor. These bottles are commonly lowered only to a maximum of 5 m above the seafloor to avoid damage to and contamination of the bottle due to touching the seafloor and sampling of artificially re-suspended particles. Furthermore, as GO-FLO bottles are lowered vertically, the samples represent an integrated signal over the height of the bottle (typically > 1 m), which is an unsatisfying vertical resolution close to the seafloor. On the other side, sampling of seawater right above the seafloor is often conducted by the aid of a multiple corer and by collecting the water overlying the sediment (~ 20 to 30 cm). By this method only a single sample representing the first few centimetres to decimetres above the seafloor can be collected. Furthermore, resuspension of sediments to the bottom water or admixing of oxygen during core retrieval and recovery can lead to mixing of pore water and bottom water and/or artificial TM scavenging. With both methods mentioned it is not possible to capture concentration gradients in the first few meters above the seafloor. To close the gap between water column and sediment sampling, bottom water samplers have been developed (e.g. KUM, MARUM). However, consisting of a metal frame and being

equipped with Niskin bottles with metal springs in the interior, these instruments do not meet the requirements for contamination free TM sampling. In addition, the sampling bottles are open while the device is lowered to the seafloor so that re-suspended particles rather than naturally suspended particles are collected upon placement at the seafloor. Furthermore, the sampling bottles are generally not suited for in-line filtration under oxygen free conditions.

To overcome these problems a team of engineers and scientists designed and custom-built a new device, which fulfils the following requirements:

1. Close the gap between water column and sediment sampling.
2. Simultaneous sampling of suspended particles and seawater in the benthic boundary layer.
3. Sampling at several depths above the seafloor to resolve vertical gradients.
4. Sampling with a low risk of contamination.
5. Sampling under oxygen-free conditions.

IV.2 Materials and procedures

IV.2.1 Sampling site

The Benthic Trace Profiler was successfully tested during two short cruises of RV Alkor in October 2018 and March 2019. Our sampling location, Boknis Eck (54°31.2' N, 10°02.5' E), is located in the southwestern Baltic Sea at the entrance of Eckernförde Bay (Fig. IV.1). Boknis Eck is a time series station, which has been operated by marine scientists in Kiel for more than 60 years. The site is monitored on a regular basis for physical and chemical water column properties such as temperature, salinity, oxygen, dissolved nutrients and chlorophyll (see https://www.bokniseck.de/de/home for data). Characteristic for this site is a strong seasonal variability of the biogeochemical conditions in the water column. The seasonal phytoplankton bloom in spring is accompanied by intense export production

of organic material. Seasonal stratification during summer and early fall together with organic matter respiration leads to oxygen depletion culminating occasionally in the occurrence of sulfidic conditions within the deepest water layers at Boknis Eck (up to 30 m). In contrast, during the winter period the water column is generally well ventilated and fully oxygenated (Smetacek, 1980; Hansen et al., 1999; Bange et al., 2011; Lennartz et al., 2014). Due to the seasonal changes in oxygen and redox conditions, Boknis Eck is well suited to study how these different biogeochemical conditions impact TM cycling within the benthic boundary layer. Moreover, since the seafloor at Boknis Eck is located within a local bathymetric depression with slow bottom currents and strongly reducing conditions in the sediment, concentration gradients within the near-bottom waters are likely to establish.

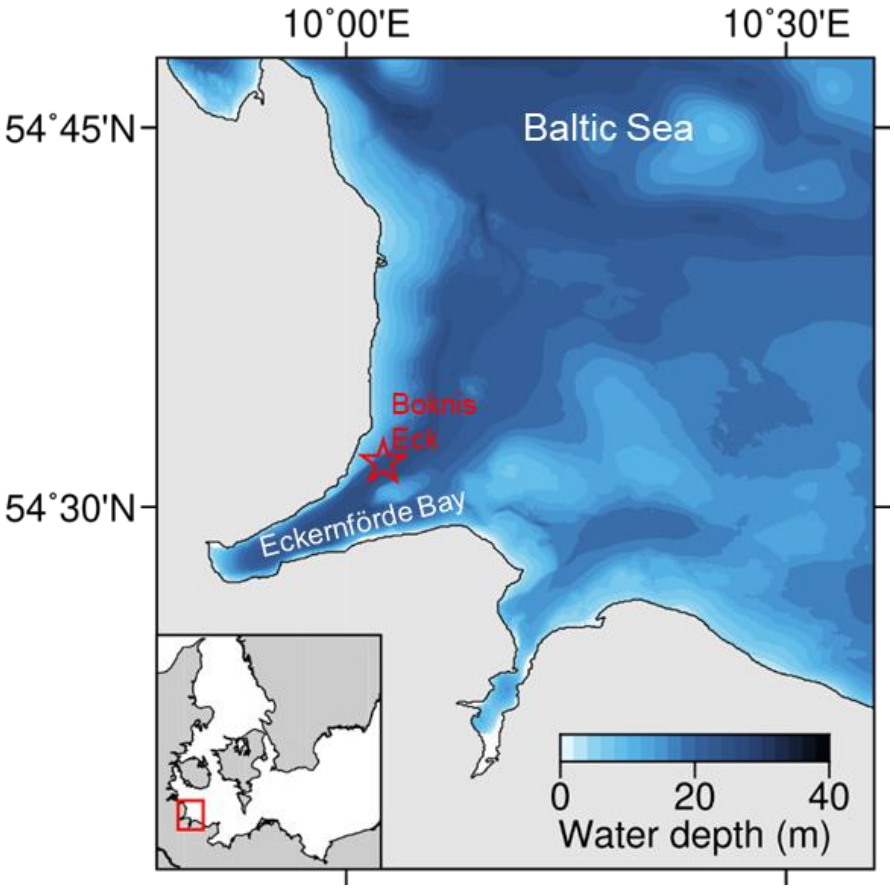

Figure IV.1: Sampling site Boknis Eck in the southwestern Baltic Sea.

IV.2.2 Sampling system and operating mode

All the individual features of the novel bottom water sampler, described in the following, are displayed in technical drawings in Fig. IV.2. The Benthic Trace Profiler consists of a titanium frame with a height of roughly three meters. Five modified GO-FLO bottles (General Oceanics) with a volume of 2.5 litres each are horizontally attached to the frame at adjustable depths (default is 0.3, 0.9, 1.5, 2 and 2.6 m above the seafloor). The sampling bottles are equipped with a plastic gear to their opening mechanism (Fig. IV.3). The gear on the bottles is attached to a gear transmission on the frame, which is controlled by a programmable electric motor (K.U.M. Umwelt- und Meerestechnik Kiel GmbH) that steers the opening and closing of the sampling bottles. The motor is powered by a battery pack (24 x Emmerich NiMH-Akku SUB-C 4000mAh ZLF) within a deep-sea certified pressure housing. Before the sampling bottles are attached to the device they are filled with deionised water (Milli-Q, Millipore) and closed manually to avoid implosion due to the increasing hydrostatic pressure under water. The device is then lowered to the seafloor using the winch and wire of a research vessel. The Profiler is connected to the wire with a rotator shackle and equipped with a fin allowing it to align with the prevailing current. Floats are attached to the wire above the instruments to prevent it from entangling in the Benthic Trace Profiler. The bottom weights (24 x 14 kg) that promote the sinking of the Profiler through the water column are coated with plastic to preclude contamination. A bottom plate prevents the profiler from sinking into the sediment. Once placed on the seafloor, a bottom contact sensor is triggered and after a programmed period of time (e.g., 15 minutes) the sampling bottles are opened by the electric motor and gear transmission. The delay between the placement of the device and the opening of the bottles allows particles that were resuspended to settle down and/or to be transported away by bottom currents. Once the bottles are opened, the deionised water is replaced by denser (saline) near-bottom water including naturally suspended particles. After another programmed period of time (e.g., 5 minutes) the bottles are closed again and the device is heaved back to the ship’s deck. As an alternative to the automatic opening and closing mechanism, the deployment can also be visually monitored and remotely controlled using a deep-sea telemetry. After recovery, the sampling bottles are detached from the frame and taken to the lab, where they are attached to a custom-built rack (Fig. IV.3).

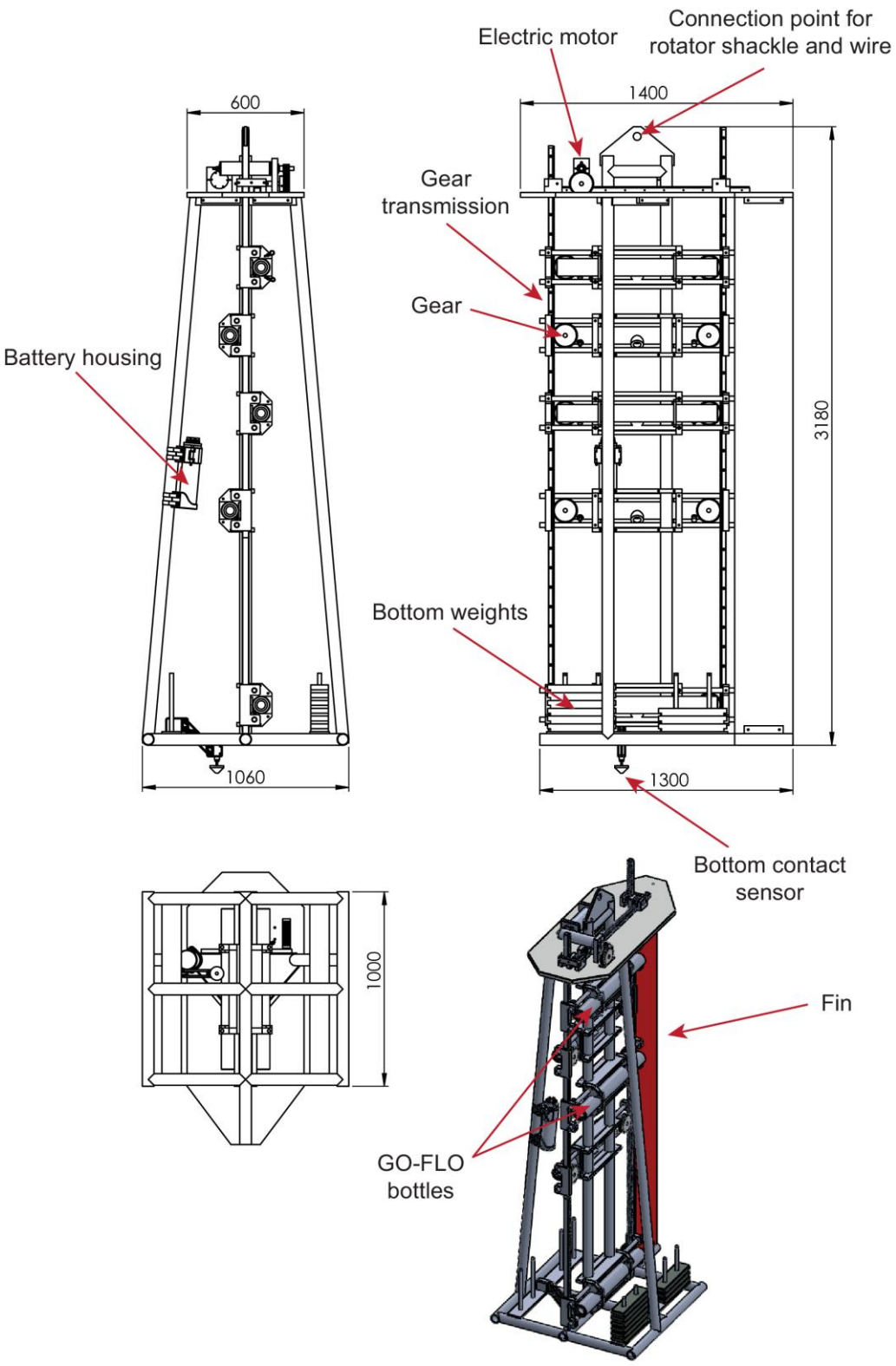

Figure IV.2: Technical drawing of the Benthic Trace Profiler. The different views are displayed to visualise the individual features of the Profiler (upper left: side view, upper rigt: front view, lower left: top view, lower right: trimetric view). Numbers indicate dimensions in millimeters.

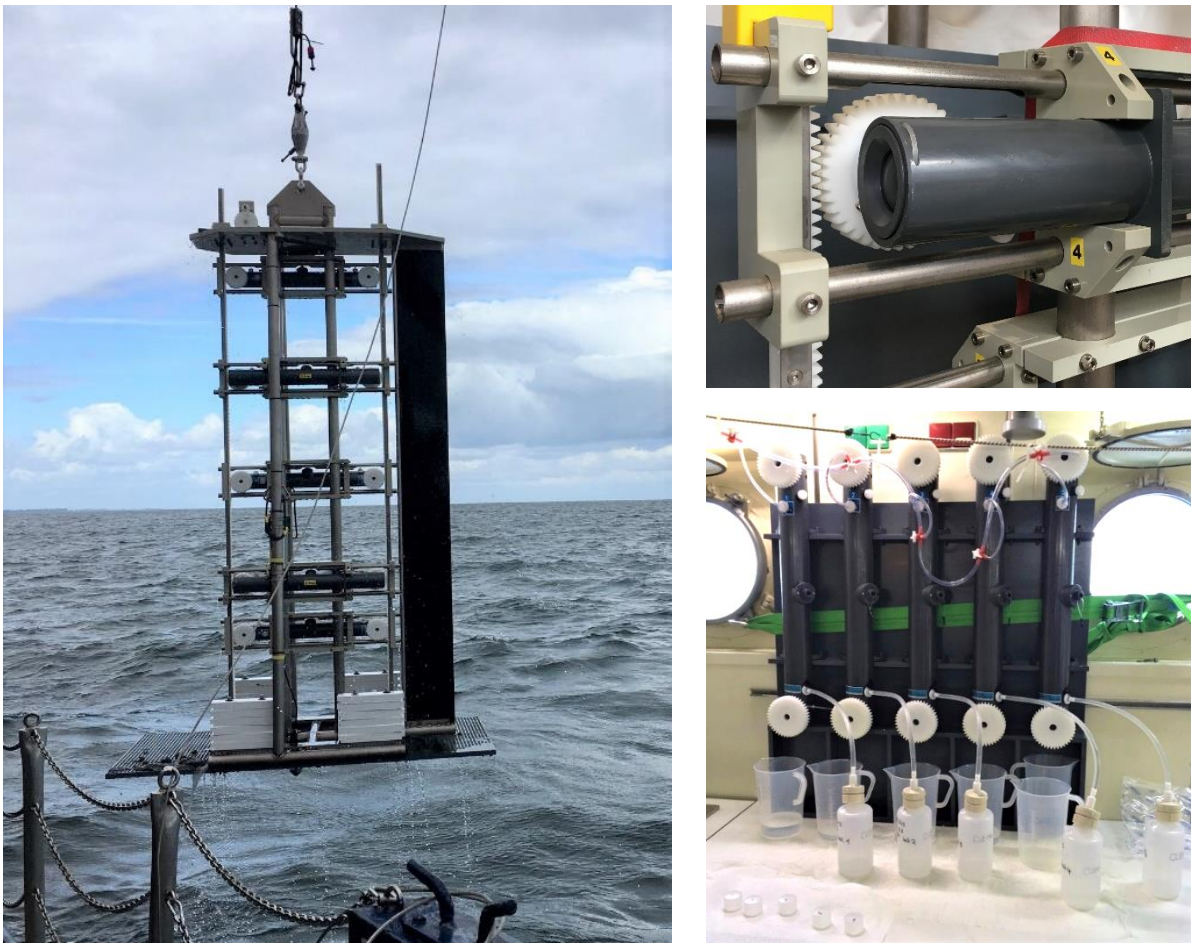

Figure VI.3: Benthic Trace Profiler during deployment in the Baltic Sea (left), close-up of modified sampling bottle and gear transmission mechanism (upper right), in-line filtration of samples in the ship's lab (lower right).

The following sampling procedure corresponds to GEOTRACES standards (Cutter et al., 2010). An inert gas line (argon) is connected to the bottles pressure valve. The gas creates an overpressure (~ 0.2 bar) to collect the water samples and particles under oxygen-free conditions through the sampling spigot. During our test cruises, suspended particles were collected on 0.2 µm polyether sulfone filters (Supor, diameter 47 mm). The near-bottom water was collected in 250 ml low-density polyethylene (LDPE) bottles and acidified to a pH < 2 with subboiled distilled HNO_3. After the near-bottom water was sampled, the filter holder was immediately transferred into a glove bag filled with argon to prevent oxidation reactions. Inside the glove bag the filter holders were opened and the filters containing the suspended particles were collected and stored in analyslides (Pall Laboratory). Subsequently, the filters were

vacuumed and frozen until total digestion or sequential extraction followed by TM analyses or synchrotron radiation-based x-ray analyses. These solid phase analyses and the corresponding interpretation are not the focus of this manuscript and will be presented in a separate publication. All materials used for sampling (sample bottles, tubing and filters) were acid cleaned and rinsed thoroughly with deionised water before usage following GEOTRACES standards (Cutter et al., 2010).

IV.2.3 Ancillary sampling and measurements

General water column properties such as temperature, salinity and oxygen concentrations were determined using a CTD sensor system. To test the TM concentration results obtained by our new sampling method, we additionally took water column samples using a conventional TM clean sampling method following the GEOTRACES protocol (Cutter et al., 2010). For this purpose, GO-FLO bottles were lowered through the water column and triggered at five depths (5, 10, 15, 20 and 25 m). The GO-FLO bottles were always deployed before the Benthic Trace Profiler to avoid water column contamination (which could create an artificial match between both results). In the ship's laboratory the collected water column samples were sampled identically to bottom water samples: an inert gas line (argon) was attached to create an overpressure (0.2 bar), the water sample was collected in low-density polyethylene (LDPE) bottles and acidified to a pH < 2 with subboiled distilled HNO_3.

To identify and quantify benthic diffusive trace metal fluxes across the sediment-water interface, we took short sediment cores (30 cm depth with overlying bottom water) with a multiple corer. The supernatant bottom water was collected and filtered through 0.2 µm cellulose acetate filters (Sartorius) immediately after retrieval. The core was then transferred to a glove bag filled with argon and sliced into vertical sections. These samples were then centrifuged to separate solid sediment and pore water. The supernatant pore water was filtered in another argon filled glove bag and transferred to acid cleaned low-density polyethylene (LDPE) bottles. Pore water and supernatant bottom water samples were acidified to pH < 1 with subboiled distilled HNO_3. Separate non acidified pore water samples were used to measure hydrogen sulphide concentrations (U-2001 Hitachi spectrometer) using a standard photometric technique

(Grasshoff et al., 1999). Additional uncentrifuged sediment samples were collected in pre-weighed plastic cups to determine water content and porosity.

IV.2.4 Trace metal analysis

For TM analysis of water column and near-bottom water samples we followed a preconcentration method using an automated preconcentration device (SeaFAST) (Rapp et al., 2017). Briefly, a 15 ml sample was pH buffered to 6.4 with an ammonium acetate buffer (1.5 M) before it was loaded onto a chelating resin column where the seawater matrix was rinsed off. The TM were then collected by rinsing the column with elution acid (1 M subboiled HNO_3). For the preconcentration of TMs from pore water samples we followed the same procedure but with a half-automated device (Preplab), due the lower volume of sample available. For this method 1 ml of pore water was required and the buffer addition and sample loading was conducted manually.

The pre-concentrated samples were analysed by high resolution inductively coupled plasma mass spectrometry (HR-ICP-MS; Thermo Fisher Element XR). Trace metal concentrations were quantified by standard addition (Mn, Co) and isotope dilution (Ni, Cu, Zn, Cd). Accuracies and detection limits of this method are listed in Plass et al. (2020, 2021). The analytical error was determined through error propagation.

IV.2.5 Diffusive flux calculations

The diffusive fluxes (F_D) of Fe and Mn across the sediment water interface were determined by Fick's first law of diffusion (Boudreau, 1997):

$$F_D = -\phi D_{sed}(dC/dx) \quad \text{(Eq. IV.1)}$$

In this equation, dC/dx is the concentration gradient between the uppermost pore water sample (0 – 1 cm sediment depth) and the bottom water and ϕ represents porosity. The effective molecular diffusion coefficient of a TM in the sediment (D_{sed}) was derived from the diffusion coefficients in seawater (D_{sw}) under standard conditions (Li and

Gregory, 1974) and adjusted to in-situ temperature, pressure and salinity by applying the Stokes-Einstein Equation and by dividing by tortuosity:

$$D_{sed} = D_{sw}/(1 - \ln(\phi^2)) \quad \text{(Eq. IV.2)}$$

A negative flux is directed from the pore water into the bottom water. All input data and diffusive fluxes are listed in Table IV.1.

IV.3. Assessment

During our two sampling campaigns we observed differing physicochemical conditions in the water column (Fig. IV.4) and differing concentration gradients of hydrogen sulphide in the surface sediment (Fig. IV.6). In October 2018, the water column was more stratified and the deep-water was characterized by lower oxygen concentrations (130 µM O_2) compared to the cruise in March 2019 (250 µM O_2). The surface sediment was highly sulphidic during October and hydrogen sulphide concentrations reached up to 3 mM within the first few centimetres of the sediment core. In contrast, during the March campaign no hydrogen sulphide was present at the sediment surface and H_2S concentrations remained below 1 mM within the first few centimetres of the sediment core. As the mobility and cycling of TMs is dependent on redox conditions (Sundby et al., 1986; Morford and Emerson, 1999; Tribovillard et al., 2006; Scholz and Neumann, 2007; Scholz et al., 2011; Rigaud et al., 2013; Rapp et al., 2020), the differing redox-conditions during our test deployments are expected to affect TM gradients close to the seafloor.

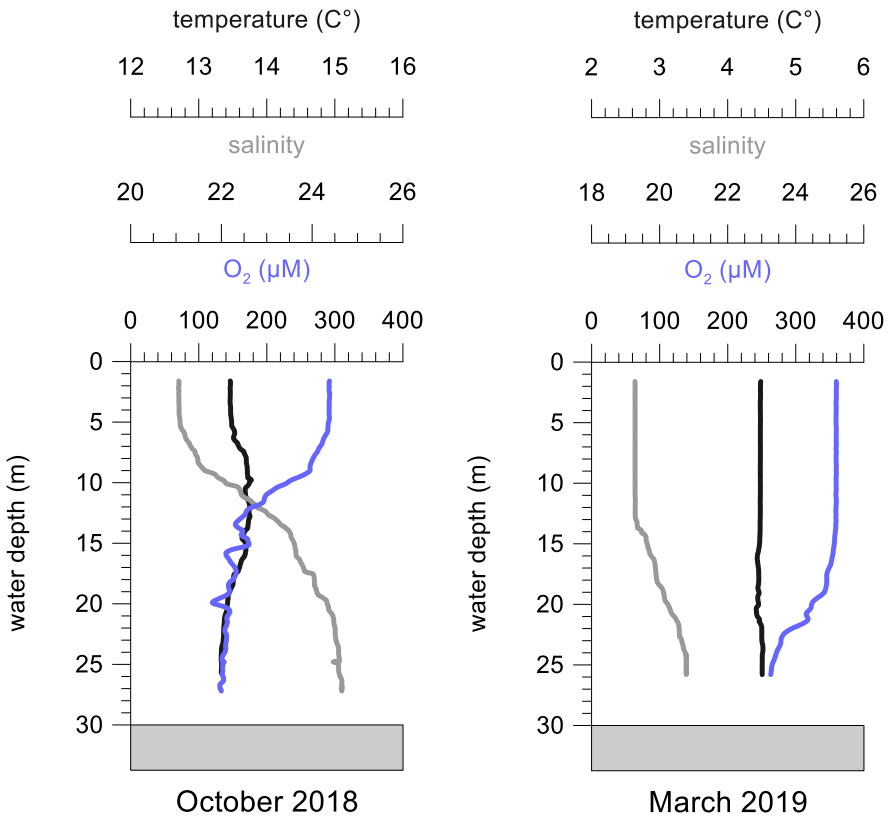

Figure IV.4: Water column temperature, salinity and oxygen profiles during the sampling campaigns in October 2018 (left) and March 2019 (right) at Boknis Eck. The grey shaded area represents the seafloor.

IV.3.1 Comparison of trace metal concentrations in near-bottom water and water column samples

To identify potential contamination of samples obtained by our new sampling device, we compared TM concentrations in samples taken with the Benthic Trace Profiler to concentrations in water column samples taken above with GO-FLO bottles according to the widely applied GEOTRACES protocol (Section IV.2.3). The concentrations show some variability as a function of water depth and season (Fig. IV.5a and IV.5b). However, in general, there is a good agreement between concentrations obtained by the two different sampling methods. Most TM concentrations in near-bottom water are consistent with the range of concentrations observed in the water column above (Table IV.2). Most notably, the concentrations of Zn, a TM that is highly prone to contamination (Cutter and Bruland, 2012), matched well with water column concentrations. Given the generally consistent concentration range in the open water column and near-bottom water, we see no evidence for contamination.

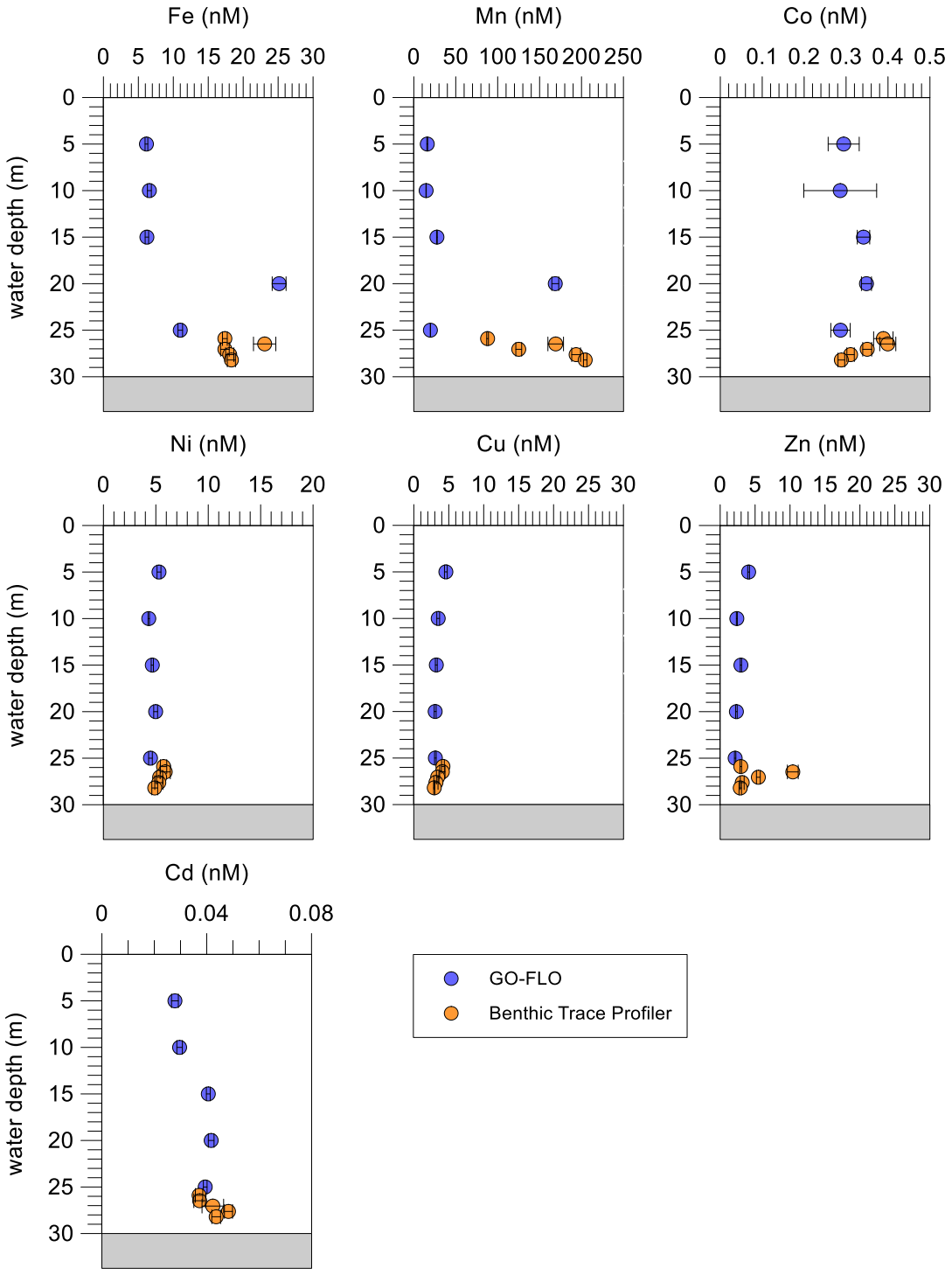

Figure IV.5a: Dissolved trace metal concentrations in the water column (blue) and near-bottom water (orange) at Boknis Eck during the sampling campaign in October 2018. The analytical errors are displayed by the black bars. The grey shaded area represents the seafloor.

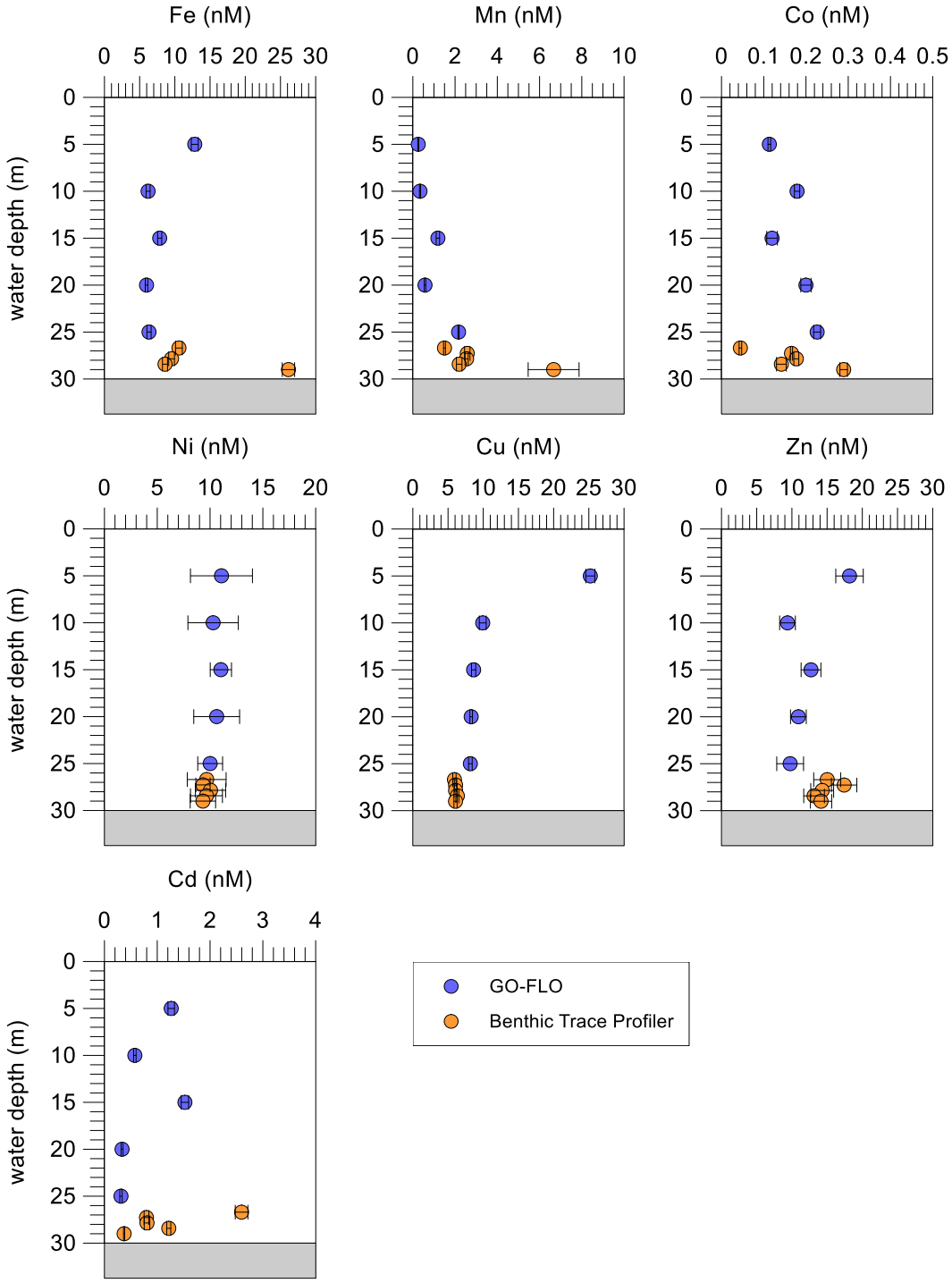

Figure IV.5b: Dissolved trace metal concentrations in the water column (blue) and near-bottom waters (orange) at Boknis Eck during the sampling campaign in March 2019. The analytical errors are displayed by the black bars. The grey shaded area represents the seafloor.

Trace metal concentrations in the water column were variable between sampling campaigns. This seasonal concentration change was also reflected in near-bottom water samples collected with the Benthic Trace Profiler. During October the concentrations of Ni, Cu, Zn and Cd were around half or less than half compared to the March campaign. This observation could be related to enhanced trace metal sequestration by phytoplankton and organic material during and after the productive season (Kremling et al., 1997; Bruland and Lohan, 2006; Noble et al., 2012;). In addition, more reducing and sulphidic conditions in the sediment before and during the October campaign may have led to TM removal into sulphide minerals (Sundby et al., 1986; Brügmann et al., 1998; Pohl and Hennings, 2005; Rigaud et al., 2013).

Some near-bottom water samples were characterised by elevated concentrations of Fe and Mn (> 20 % compared to the water column), which is indicative of a sedimentary source of these elements at our study site (see Section IV.3.2). Concentration maxima of Fe and Mn at 20 m water depth during the October campaign (Fig. IV.5a) could be related to lateral supply from anoxic sediments surrounding the bathymetric depression of Boknis Eck.

Table IV.2: Concentration range of trace metals within the water column and within near-bottom waters.

	October		**March**	
	Water column	**Bottom water**	**Water column**	**Bottom water**
Fe (nM)	6.2 – 25.1	17.4 – 23.1	6.2 - 12.8	8.6 – 10.6
Mn (nM)	14.7 – 168.7	88.0 - 204.4	0.26 – 2.2	1.5 – 6.7
Co (nM)	0.29 – 0.45	0.29 – 0.40	0.11 – 0.23	0.04 – 0.29
Ni (nM)	4.3 – 5.3	4.9 – 5.9	10.0 – 11.0	9.3 – 10.0
Cu (nM)	3.1 - 4.6	2.9 – 4.2	8.2 - 25.2	5.9 – 6.3
Zn (nM)	2.1 – 4.1	2.9 – 10.4	9.4 – 18.2	14.1 – 17.4
Cd (nM)	0.28 – 0.42	0.37 – 0.48	0.31 – 1.52	0.37 – 2.60

IV.3.2 Comparison of concentration gradients in near-bottom waters to benthic fluxes

The Benthic Trace Profiler was designed to detect TM concentration gradients within the benthic boundary layer. In particular Mn showed a clear concentration gradient within the near-bottom waters during the October campaign. The concentration of Mn increased almost linearly from 88.0 to 204 nM within the water layer sampled by the Benthic Trace Profiler. During March, only the sample from immediately above the seafloor (0.3 m) was characterized by elevated Mn (6.7 nM) and Fe (26.1 nM) concentrations compared to the overlying water column (Mn: 1.5 nM, Fe: 8.5 nM). These observations demonstrate that no oxygen contamination took place during sampling as this would have resulted in rapid Fe oxidation and precipitation as Fe (oxyhydr)oxide (Millero et al., 1987). Furthermore, the trend of differing Fe and Mn concentrations in near-bottom water during our two test cruises is consistent with the temporal evolution of pore water profiles and diffusive benthic fluxes. The pore water profiles of Fe and Mn (Fig. IV.6) show an upward directed concentration gradient across the sediment-water interface, which is indicative of a sedimentary Fe and Mn efflux. The diffusive benthic flux of Fe was high during March 2019 (-47.1 mmol m^{-2} y^{-1}), which is consistent with the elevated Fe concentration in the sample taken from immediately above the seafloor (Fig. IV.5b). In contrast to the sediment, the water column was well-oxygenated during the March campaign (Fig. IV.4). Oxidative removal of dissolved Fe is rapid under such conditions, which can explain the lack of an Fe gradient with increasing distance from the seafloor. During October 2018, the diffusive benthic flux of Fe was several orders of magnitude lower (-0.09 mmol m^{-2} y^{-1}), because high concentrations of hydrogen sulphide in surface sediments (up to 3 mM) (Fig. IV.6) and, thus, Fe sulphide precipitation prevented a high sedimentary Fe efflux. Accordingly, Fe concentrations in near-bottom waters were not elevated compared to the water column. This observation confirms that sedimentary Fe fluxes do not linearly increase with decreasing bottom water oxygen concentrations. Instead, hydrogen sulphide accumulation in surface sediments prevents sedimentary Fe release under strongly reducing conditions (Scholz et al., 2014a). The opposite seasonal trend is observed for Mn. Manganese does not form sulphide minerals under strongly sulfidic conditions, which is why the highest diffusive benthic Mn flux (October 2018: -44.2 mmol m^{-2} y^{-1}, March 2019: -38.6 mmol m^{-2} y^{-1}) and the highest Mn concentrations in

near-bottom water (204 nM) were observed during the October campaign, when oxygen concentrations in the water column were lower.

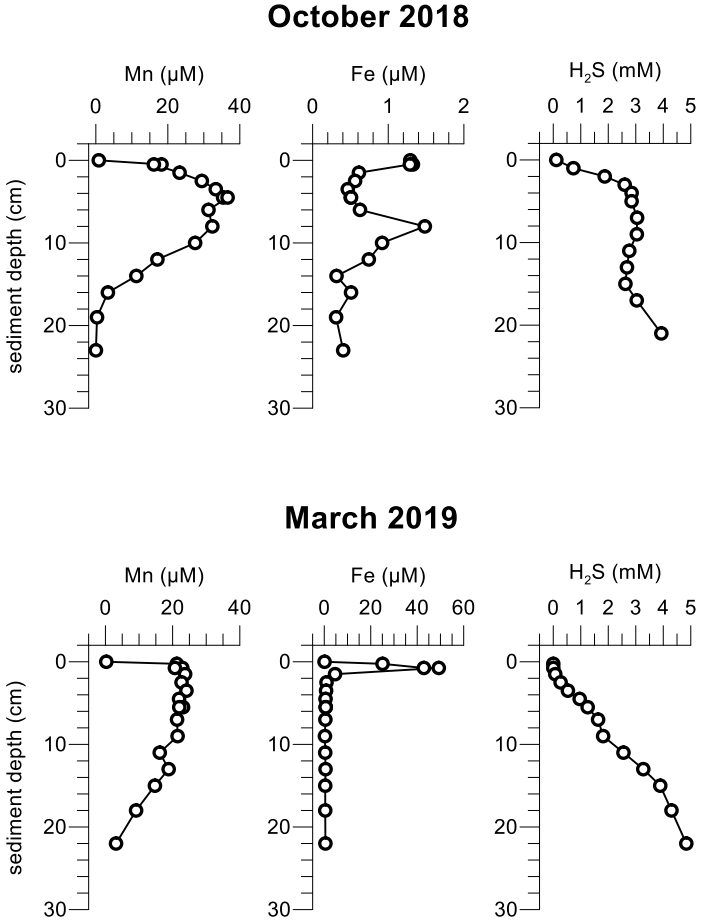

Figure IV.6: Pore water concentrations of iron,manganese and hydrogen sulphide during the sampling campaigns in October 2018 (upper panel) and March 2019 (lower panel). The uppermost point of each profile represents bottom waters sampled with the multiple corer.

Table IV.1: Input data for diffusive flux calculations (section 2.4) and diffusive fluxes of iron and manganese.

Element	Sampling season	Bottom water concentration (µM)	Concentration at sediment surface (µM)	Porosity	Effective molecular diffusion coefficient ($cm^2\ sec^{-1}$)	Diffusive flux ($mmol\ m^{-2}\ y^{-1}$)
Fe	October	1.29	1.33	0.94	4.37×10^{-6}	-0.09
Fe	March	0.13	25.08	0.93	3.22×10^{-6}	-47.10
Mn	October	0.83	18.24	0.94	4.26×10^{-6}	-44.22
Mn	March	0.26	21.22	0.93	3.14×10^{-6}	-38.57

IV.4. Discussion

Our results demonstrate that the benthic trace profiler is well suited for the sampling of TMs that are prone to contamination. The sampling height and distances are suited to detect changes in concentration profiles within near-bottom waters. Furthermore, the height of the sampling bottles above the seafloor is variable and can be adjusted to the requirements of the respective seafloor environment or study.

During our test cruises we were able to detect elevated TM concentrations close to the seafloor (0.3 m) using the Benthic Trace Profiler. A water column sampling campaign based on GO-FLO bottles alone would have failed to detect these gradients, because these sampling devices cannot be lowered this close to the seafloor, thus leaving a blind spot at the benthic boundary. On the other side, when elevated concentrations in bottom waters above the seafloor are derived from measurements of bottom water overlying sediment cores, it is uncertain whether these are natural or due to mixing of pore water and bottom water during core retrieval and recovery. In addition, it is unclear whether elevated concentrations persist at greater distance from the seafloor as revealed here for Mn during the October campaign using the Benthic Trace Profiler. In more general terms, this observation underscores that near-bottom waters are an important transitional environment where TM fluxes are modified. Using the Benthic Trace Profiler, it is possible to determine whether concentration gradients derive from TM precipitation or simple dilution. In this context, it is important to note that the new sampling device can be used without contaminating samples with oxygen. Therefore, it is possible to detect natural concentration gradients that arise from redox-controlled TM precipitation within the near-bottom water.

As the Benthic Trace Profiler has no limit in deployment depth it can not only be deployed in coastal or shelf environments but it is also well-suited for deep-sea research, e.g., in the context of studies on the impact of mining of manganese nodules or on sediment-hosted hydrothermal systems. Another potentially important field of application of the Benthic Trace Profiler are studies on so-called boundary exchange of rare earth elements (REE) (especially neodymium, Nd). It has been suggested that marine sediments represent a major source of Nd to the ocean (Abbott et al., 2015b; Abbott et al., 2015a), which has implications for the applicability of Nd isotopes as a tracer for past ocean circulation. However, the processes by which Nd and other REEs are remobilised and how sedimentary fluxes affect water mass signatures are still

poorly constrained (Haley et al., 2017). The Benthic Trace Profiler is a suitable tool to investigate how water mass and sedimentary REE and Nd isotope signatures are affected by benthic fluxes and interactions with suspended particles close to the seafloor.

Future benthic studies of dissolved TM concentrations (and isotopes) in combination with the analysis of suspended particles will give valuable information about TM fluxes, precipitation processes and carrier phases. Combined with the evaluation of environmental conditions this will help to better understand and quantify TMs cycling and fluxes at the ocean's lower boundary.

Acknowledgements

We would like to thank A. Petersen for crafting the Benthic Trace Profiler as well as our colleagues D. Jasinski, C. Schlosser, T. Steffens and R. Surberg for technical and analytical assistance. We also thanks the crew of RV Alkor for their support during the fieldwork. This study was supported by the German Research Foundation through the Emmy Noether Nachwuchsforschergruppe ICONOX (Iron Cycling in Continental Margin Sediments and the Nutrient and Oxygen Balance of the Ocean).

References

Abbott A. N., Haley B. A. and McManus J. (2015a) Bottoms up: Sedimentary control of the deep North Pacific Ocean's ε Nd signature. *Geology* **43**, 1035–1035. Available at: https://pubs.geoscienceworld.org/geology/article/43/11/1035/131732.

Abbott A. N., Haley B. A., McManus J. and Reimers C. E. (2015b) The sedimentary flux of dissolved rare earth elements to the ocean. *Geochim. Cosmochim. Acta* **154**, 186–200. Available at: http://dx.doi.org/10.1016/j.gca.2015.01.010.

Algeo T. J. and Liu J. (2020) A re-assessment of elemental proxies for paleoredox analysis. *Chem. Geol.* **540**, 119549. Available at:

https://doi.org/10.1016/j.chemgeo.2020.119549.

Audry S., Blanc G., Schäfer J., Chaillou G. and Robert S. (2006) Early diagenesis of trace metals (Cd, Cu, Co, Ni, U, Mo, and V) in the freshwater reaches of a macrotidal estuary. *Geochim. Cosmochim. Acta* **70**, 2264–2282. Available at: https://linkinghub.elsevier.com/retrieve/pii/S0016703706000718.

Bange H. W., Dale A., Hansen H. P., Karstensen J., Malien F., Petereit C., Laß K. and Friederichs G. (2011) LOICZ-Affiliated Activities Boknis Eck Time Series Station (SW Baltic Sea): Measurements from 1957 to 2010. *LOICZ Inprint*, 16–22. Available at: https://oceanrep.geomar.de/12198/.

Böning P., Brumsack H.-J., Böttcher M. E., Schnetger B., Kriete C., Kallmeyer J. and Borchers S. L. (2004) Geochemistry of Peruvian near-surface sediments. *Geochim. Cosmochim. Acta* **68**, 4429–4451. Available at: https://linkinghub.elsevier.com/retrieve/pii/S001670370400403X.

Böning P., Brumsack H.-J., Schnetger B. and Grunwald M. (2009) Trace element signatures of Chilean upwelling sediments at ~36°S. *Mar. Geol.* **259**, 112–121. Available at: http://dx.doi.org/10.1016/j.margeo.2009.01.004.

Boudreau B. P. (1997) *Diagenetic Models and Their Implementation*., Springer. Available at: http://www.ncbi.nlm.nih.gov/pubmed/1163368.

Boudreau B. P. and Jorgensen B. B. (2001) The benthic boundary layer: Transport processes and biogeochemistry. *Oxford Univ. Press* **82**, 658–658. Available at: http://doi.wiley.com/10.1029/01EO00381.

Brügmann L., Hallberg R., Larsson C. and Löffler A. (1998) Trace metal speciation in sea and pore water of the Gotland Deep, Baltic Sea, 1994. *Appl. Geochemistry* **13**, 359–368. Available at: https://linkinghub.elsevier.com/retrieve/pii/S0883292797001054.

Bruland K. W. and Lohan M. C. (2006) Controls of Trace Metals in Seawater. In *The Oceans and Marine Geochemistry, Treatise on Geochemistry* (ed. H. Elderfield). Elsevier. pp. 23–47. Available at: https://linkinghub.elsevier.com/retrieve/pii/B9780080959757006021.

Brumsack H.-J. (2006) The trace metal content of recent organic carbon-rich sediments: Implications for Cretaceous black shale formation. *Palaeogeogr.*

Palaeoclimatol. Palaeoecol. **232**, 344–361. Available at: https://linkinghub.elsevier.com/retrieve/pii/S0031018205002737.

Ciscato E. R., Bontognali T. R. R. and Vance D. (2018) Nickel and its isotopes in organic-rich sediments: implications for oceanic budgets and a potential record of ancient seawater. *Earth Planet. Sci. Lett.* **494**, 239–250. Available at: https://doi.org/10.1016/j.epsl.2018.04.061.

Cutter G. A., Andersson P., Codispoti L., Croot P., Place P., Hoe T., Kingdom U., Francois R., Sciences O., Lohan M., Circus D. and Obata H. (2010) Sampling and Sample-handling Protocols for GEOTRACES Cruises. Available at: https://epic.awi.de/id/eprint/34484/.

Cutter G. A. and Bruland K. W. (2012) Rapid and noncontaminating sampling system for trace elements in global ocean surveys. *Limnol. Oceanogr. Methods* **10**, 425–436. Available at: http://doi.wiley.com/10.4319/lom.2012.10.425.

Grasshoff M., Erhardt M. and Kremling K. (1999) Methods of seawater analysis. *Wiley-VCH, Weinheim*. Available at: http://doi.wiley.com/10.1002/ange.19770890738.

Haley B. A., Du J., Abbott A. N. and McManus J. (2017) The Impact of Benthic Processes on Rare Earth Element and Neodymium Isotope Distributions in the Oceans. *Front. Mar. Sci.* **4**, 1–12. Available at: http://journal.frontiersin.org/article/10.3389/fmars.2017.00426/full.

Hansen H., Giesenhagen H. C. and Behrends G. (1999) Seasonal and long-term control of bottom-water oxygen deficiency in a stratified shallow-water coastal system. *ICES J. Mar. Sci.* **56**, 65–71. Available at: http://icesjms.oxfordjournals.org/cgi/doi/10.1006/jmsc.1999.0629.

Heller M. I., Lam P. J., Moffett J. W., Till C. P., Lee J. M., Toner B. M. and Marcus M. A. (2017) Accumulation of Fe oxyhydroxides in the Peruvian oxygen deficient zone implies non-oxygen dependent Fe oxidation. *Geochim. Cosmochim. Acta* **211**, 174–193. Available at: http://dx.doi.org/10.1016/j.gca.2017.05.019.

Jacobs L., Emerson S. and Skei J. (1985) Partitioning and transport of metals across the interface in a permanently anoxic basin: Framvaren Fjord, Norway. *Geochim. Cosmochim. Acta* **49**, 1433–1444. Available at:

https://linkinghub.elsevier.com/retrieve/pii/0016703785902935.

Kremling K., Tokos J. J. S., Brügmann L. and Hansen H. P. (1997) Variability of dissolved and participate trace metals in the Kiel and Mecklenburg Bights of the Baltic Sea, 1990-1992. *Mar. Pollut. Bull.* **34**, 112–122.

Lennartz S. T., Lehmann A., Herrford J., Malien F., Hansen H. P., Biester H. and Bange H. W. (2014) Long-term trends at the Boknis Eck time series station (Baltic Sea), 1957-2013: Does climate change counteract the decline in eutrophication? *Biogeosciences* **11**, 6323–6339.

Li Y.-H. and Gregory S. (1974) Diffusion of ions in sea water and in deep-sea sediments. *Geochim. Cosmochim. Acta* **38**, 703–714. Available at: http://www.scielo.br/scielo.php?script=sci_arttext&pid=S1414-98932014000401014&lng=pt&tlng=pt.

Little S. H., Vance D., Lyons T. W. and McManus J. (2015) Controls on trace metal authigenic enrichment in reducing sediments: Insights from modern oxygen-deficient settings. *Am. J. Sci.* **315**, 77–119. Available at: http://www.ajsonline.org/cgi/doi/10.2475/02.2015.01.

Lohan M. C. and Tagliabue A. (2018) Oceanic Micronutrients: Trace Metals that are Essential for Marine Life. *Elements* **14**, 385–390. Available at: https://pubs.geoscienceworld.org/msa/elements/article/14/6/385/567322/Oceanic-Micronutrients-Trace-Metals-that-are.

Millero F. J., Sotolongo S. and Izaguirre M. (1987) The oxidation kinetics of Fe(II) in seawater. *Geochim. Cosmochim. Acta* **51**, 793–801. Available at: http://linkinghub.elsevier.com/retrieve/pii/0016703787900937.

Moore C. M., Mills M. M., Arrigo K. R., Berman-Frank I., Bopp L., Boyd P. W., Galbraith E. D., Geider R. J., Guieu C., Jaccard S. L., Jickells T. D., La Roche J., Lenton T. M., Mahowald N. M., Marañón E., Marinov I., Moore J. K., Nakatsuka T., Oschlies A., Saito M. A., Thingstad T. F., Tsuda A. and Ulloa O. (2013) Processes and patterns of oceanic nutrient limitation. *Nat. Geosci.* **6**, 701–710. Available at: http://dx.doi.org/10.1038/ngeo1765.

Morel F. M. M. (2003) The Biogeochemical Cycles of Trace Metals in the Oceans. *Science (80-.).* **300**, 944–947. Available at:

https://www.sciencemag.org/lookup/doi/10.1126/science.1083545.

Morel F. M. M., Milligan A. J. and Saito M. A. (2014) Marine Bioinorganic Chemistry: The Role of Trace Metals in the Oceanic Cycles of Major Nutrients. In *Treatise on Geochemistry* Elsevier. pp. 123–150. Available at: https://linkinghub.elsevier.com/retrieve/pii/B9780080959757006057.

Morford J. L. and Emerson S. (1999) The geochemistry of redox sensitive trace metals in sediments. *Geochim. Cosmochim. Acta* **63**, 1735–1750. Available at: https://linkinghub.elsevier.com/retrieve/pii/S001670379900126X.

Noble A. E., Lamborg C. H., Ohnemus D. C., Lam P. J., Goepfert T. J., Measures C. I., Frame C. H., Casciotti K. L., DiTullio G. R., Jennings J. and Saito M. A. (2012) Basin-scale inputs of cobalt, iron, and manganese from the Benguela-Angola front to the South Atlantic Ocean. *Limnol. Oceanogr.* **57**, 989–1010.

Pakhomova S. V., Hall P. O. J., Kononets M. Y., Rozanov A. G., Tengberg A. and Vershinin A. V. (2007) Fluxes of iron and manganese across the sediment–water interface under various redox conditions. *Mar. Chem.* **107**, 319–331. Available at: https://linkinghub.elsevier.com/retrieve/pii/S0304420307001302.

Plass A., Dale A. W. and Scholz F. (2021) Sedimentary cycling and benthic fluxes of manganese , cobalt , nickel , copper , zinc and cadmium in the Peruvian oxygen minimum zone. *Accept. Publ. Mar. Chem.*

Plass A., Schlosser C., Sommer S., Dale A. W., Achterberg E. P. and Scholz F. (2020) The control of hydrogen sulfide on benthic iron and cadmium fluxes in the oxygen minimum zone off Peru. *Biogeosciences* **17**, 3685–3704. Available at: https://www.biogeosciences.net/17/3685/2020/.

Pohl C. and Hennings U. (2005) The coupling of long-term trace metal trends to internal trace metal fluxes at the oxic–anoxic interface in the Gotland Basin (57°19,20′N; 20°03,00′E) Baltic Sea. *J. Mar. Syst.* **56**, 207–225. Available at: https://linkinghub.elsevier.com/retrieve/pii/S0924796304003033.

Rapp I., Schlosser C., Browning T. J., Wolf F., Le Moigne F. A. C., Gledhill M. and Achterberg E. P. (2020) El Niño-Driven Oxygenation Impacts Peruvian Shelf Iron Supply to the South Pacific Ocean. *Geophys. Res. Lett.* **47**. Available at: https://onlinelibrary.wiley.com/doi/abs/10.1029/2019GL086631.

Rapp I., Schlosser C., Menzel Barraqueta J.-L., Wenzel B., Lüdke J., Scholten J., Gasser B., Reichert P., Gledhill M., Dengler M. and Achterberg E. P. (2019) Controls on redox-sensitive trace metals in the Mauritanian oxygen minimum zone. *Biogeosciences* **16**, 4157–4182. Available at: https://www.biogeosciences.net/16/4157/2019/.

Rapp I., Schlosser C., Rusiecka D., Gledhill M. and Achterberg E. P. (2017) Automated preconcentration of Fe, Zn, Cu, Ni, Cd, Pb, Co, and Mn in seawater with analysis using high-resolution sector field inductively-coupled plasma mass spectrometry. *Anal. Chim. Acta* **976**, 1–13. Available at: http://dx.doi.org/10.1016/j.aca.2017.05.008.

Rigaud S., Radakovitch O., Couture R. M., Deflandre B., Cossa D., Garnier C. and Garnier J. M. (2013) Mobility and fluxes of trace elements and nutrients at the sediment-water interface of a lagoon under contrasting water column oxygenation conditions. *Appl. Geochemistry* **31**, 35–51. Available at: http://dx.doi.org/10.1016/j.apgeochem.2012.12.003.

Saito M. A., Goepfert T. J. and Ritt J. T. (2008) Some thoughts on the concept of colimitation: Three definitions and the importance of bioavailability. *Limnol. Oceanogr.* **53**, 276–290. Available at: http://doi.wiley.com/10.4319/lo.2008.53.1.0276.

Schlosser C., Streu P., Frank M., Lavik G., Croot P. L., Dengler M. and Achterberg E. P. (2018) H2S events in the Peruvian oxygen minimum zone facilitate enhanced dissolved Fe concentrations. *Sci. Rep.* **8**, 12642. Available at: http://www.nature.com/articles/s41598-018-30580-w.

Scholz F., Hensen C., Noffke A., Rohde A., Liebetrau V. and Wallmann K. (2011) Early diagenesis of redox-sensitive trace metals in the Peru upwelling area - response to ENSO-related oxygen fluctuations in the water column. *Geochim. Cosmochim. Acta* **75**, 7257–7276. Available at: http://dx.doi.org/10.1016/j.gca.2011.08.007.

Scholz F., Löscher C. R., Fiskal A., Sommer S., Hensen C., Lomnitz U., Wuttig K., Göttlicher J., Kossel E., Steininger R. and Canfield D. E. (2016) Nitrate-dependent iron oxidation limits iron transport in anoxic ocean regions. *Earth Planet. Sci. Lett.* **454**, 272–281. Available at:

http://dx.doi.org/10.1016/j.epsl.2016.09.025.

Scholz F., Mcmanus J., Mix A. C., Hensen C. and Schneider R. R. (2014) The impact of ocean deoxygenation on iron release from continental margin sediments. *Nat. Geosci.* **7**, 433–437.

Scholz F. and Neumann T. (2007) Trace element diagenesis in pyrite-rich sediments of the Achterwasser lagoon, SW Baltic Sea. *Mar. Chem.* **107**, 516–532. Available at: https://linkinghub.elsevier.com/retrieve/pii/S030442030700196X.

Scor Working Group (2007) GEOTRACES – An international study of the global marine biogeochemical cycles of trace elements and their isotopes. *Geochemistry* **67**, 85–131. Available at: https://linkinghub.elsevier.com/retrieve/pii/S0009281907000050.

Smetacek V. (1980) Annual cycle of sedimentation in relation to plankton ecology in western Kiel Bight. *Ophelia* **Suppl 1**, 65–76. Available at: https://oceanrep.geomar.de/21587/.

Sundby B., Anderson L. G., Hall P. O. J., Iverfeldt Å., van der Loeff M. M. R. and Westerlund S. F. G. (1986) The effect of oxygen on release and uptake of cobalt, manganese, iron and phosphate at the sediment-water interface. *Geochim. Cosmochim. Acta* **50**, 1281–1288. Available at: https://linkinghub.elsevier.com/retrieve/pii/0016703786904114.

Sundby B. and Silverberg N. (1985) Manganese fluxes in the benthic boundary layer 1. *Limnol. Oceanogr.* **30**, 372–381. Available at: http://doi.wiley.com/10.4319/lo.1985.30.2.0372.

Sweere T., van den Boorn S., Dickson A. J. and Reichart G.-J. (2016) Definition of new trace-metal proxies for the controls on organic matter enrichment in marine sediments based on Mn, Co, Mo and Cd concentrations. *Chem. Geol.* **441**, 235–245. Available at: http://dx.doi.org/10.1016/j.chemgeo.2016.08.028.

Tribovillard N., Algeo T. J., Lyons T. and Riboulleau A. (2006) Trace metals as paleoredox and paleoproductivity proxies: An update. *Chem. Geol.* **232**, 12–32. Available at: https://linkinghub.elsevier.com/retrieve/pii/S000925410600132X.

V. Summary, conclusions and future directions

The aim of this thesis was to identify and quantify TM exchange at the ocean's lower boundary and to improve the understanding of parameters and processes that control benthic TM cycling in low-oxygen marine environments. Considering ongoing ocean deoxygenation, the results of this thesis will help to evaluate how TM cycling will respond to future ocean conditions and to understand TM cycling processes in ancient oceans where oxygen-deficient conditions prevailed.

Chapter II compared the benthic fluxes of Fe and Cd, two opposite end-members in terms of sulphide solubility (Fe > Cd). The results showed that the sedimentary Fe release and Cd burial fluxes off Peru covaried with hydrogen sulphide concentrations in surface sediments, controlling the magnitude and direction of their fluxes across the sediment water interface. The spatial and temporal variability of diffuse Fe effluxes is related to partial retention and Fe sulphide precipitation within the sediments at high hydrogen sulphide concentrations. The Cd accumulation within the sediments is mediated by sulphide precipitation at the sediment-water interface or in the water column, which already takes place at trace amounts of hydrogen sulphide.

Chapter III disentangled the different TM pathways that lead to the enrichment of Ni, Cu, Zn and Cd or depletion of Mn and Co within sediments on the Peruvian margin. The majority of Ni enrichment can be ascribed to phytoplankton uptake in the surface ocean and delivery via organic material. Cupper becomes enriched through scavenging by sinking organic matter and maybe partly also due to sulphide precipitation in the bottom water or water column, similar to Cd. The main delivery pathway for Zn is diffusion from the bottom water into the sediment, likely followed by subsequent sulphide precipitation. The sedimentary depletion of Mn is mostly caused by dissolution in the sediment and diffusion into the bottom water, while Co chiefly dissolves already in the water column.

Chapter IV introduces a novel device that fills a gap between water column and sediment sampling of TMs, the Benthic Trace Profiler. The Profiler enables simultaneous, uncontaminating and oxygen-free sampling of dissolved and particulate TMs in high-resolution within in the benthic boundary layer. The application of this device will allow to make an important step forward to solve remaining questions on benthic TM cycling.

The overall finding of this thesis is that the behaviour of the different TMs is very diverse and that the direction and magnitude of different TM fluxes will change individually, dependent on the biogeochemical conditions. The differing TM fluxes across the benthic boundary have the potential to lead to changes in the TM stoichiometry of upwelling water masses and the future ocean, which can ultimately impact marine ecosystems in the surface ocean which have certain TM requirements.

Despite the new insights provided by this thesis some open questions on benthic TM cycling, fluxes and oceanic mass balances remain. The coverage for benthic TM fluxes, especially in open marine systems is still very sparse. To get a comprehensive picture on benthic source and sink fluxes under low-oxygen conditions, further studies at other oxygen depleted sites are required, this should also include less reducing systems. It is important to investigate how TM fluxes vary as a function of regional differences. For example, the magnitude of primary production and the organic carbon flux can regulate the magnitude of TM transport from the surface ocean to the sediment surface via direct phytoplankton uptake or TM scavenging in the water column. Furthermore, the extent of organic matter consumption can regulate the prevailing redox conditions by which TMs are affected. Different sediment types, depending on the source rock and the degree of weathering, can determine how easily TMs can be released from lithogenic material. The corresponding sedimentation rate can determine the supply of dissolvable TMs. The shelf geometry can influence sediment transport processes to deeper sites and determines the sediment area underlaying oxygen depleted waters. Further, the temporal/seasonal variability of TM fluxes should be monitored. The flux magnitude and direction can change depending on different temporal variable factors as productivity and/or biogeochemical conditions.

Another important aspect of future research is how benthic TM fluxes are modulated within the reactive benthic boundary layer, where TM precipitation reactions are likely to take place. The rate of precipitation or threshold values (of either oxygen nitrate, nitrite or hydrogen sulphide) at which sediment-derived Fe, Mn and other TMs are transported or precipitated remain to some extend unclear. The collection of dissolved and particulate samples at the benthic boundary will give insights to this and several other questions on TM particle association. The relative importance of different TM carrier and scavenging phases have been difficult to discern so far, in particular TM association with organic matter or sulphide. In addition, the determination of TM

isotope signatures at the benthic boundary can further contribute to improve the oceanic mass balances of TMs. To answer the remaining questions, future research will largely benefit from samples retrieved by the Benthic Trace Profiler.

Danksagung

Vor allem möchte ich mich bei Florian Scholz bedanken, der es mir ermöglichte diese Doktorarbeit zu schreiben und mir jederzeit mit Rat und Tat zur Seite stand. Du hattest immer eine gute Idee und hast diese Arbeit maßgeblich vorangetrieben.

Ich möchte mich bei Eric Achterberg und Martin Frank für die Ratschläge und die Diskussion meiner Daten bedanken. Ebenso danke ich all meinen Koautoren, die die einzelnen Kapitel dieser Arbeit mit ihrer Hilfe vorangebracht haben.

Vielen Dank an alle, die mich auf See und im Labor unterstützt haben: Antje Beck, Anke Bleyer, Bettina Domeyer, Jutta Heinze, Dominik Jasinsky, Anna-Kathrin Retschko und Tim Steffens.

Weiterhin bedanke ich mich bei Antao, Georgi, Paul, Sümmeya und Yang für die angenehme Atmosphäre in unserem gemeinsamen Büro und für eure Ratschläge. Ebenso bedanke ich mich auch bei meinen anderen lieben Kolleg*innen für die Mittagsausflüge zur Mensa oder die Kaffeepausen an der Kaimauer.

Ein großes Dankeschön geht auch an meine lieben Freunde, die mich in den letzten Jahren unterstützt haben und immer ein offenes Ohr für mich hatten. Danke Alex, Andre, Dominik Stephan, Therese und vor allem Lasse – ich hatte eine gute Zeit mit euch!